Universiteit
Leiden
The Netherlands

GDE transmembrane ecto-enzymes : novel signaling functions through GPI-anchor cleavage

Veen, T.P.M. van

Citation
Veen, T. P. M. van. (2018, September 19). *GDE transmembrane ecto-enzymes : novel signaling functions through GPI-anchor cleavage*. Retrieved from https://hdl.handle.net/1887/65601

Version:	Not Applicable (or Unknown)
License:	Licence agreement concerning inclusion of doctoral thesis in the Institutional Repository of the University of Leiden
Downloaded from:	https://hdl.handle.net/1887/65601

Note: To cite this publication please use the final published version (if applicable).

Cover Page

Universiteit Leiden

The handle http://hdl.handle.net/1887/65601 holds various files of this Leiden University dissertation.

Author: Veen, T.P.M. van
Title: GDE transmembrane ecto-enzymes : novel signaling functions through GPI-anchor cleavage
Issue Date: 2018-09-19

GDE transmembrane ecto-enzymes: novel signaling functions through GPI-anchor cleavage

Thijs Paul Michaël van Veen

ISBN: 978-9-4632329-2-0
Copyright © 2018 by Michiel van Veen
The research described in this th esis was performed at the
Division of Cell Biology of the Netherlands Cancer Institute,
Amsterdam, the Netherlands.

Cover design by Festina Amsterdam.
The illustrations created by Hendrik Thijs van Veen portray the
most distinctive trees growing in the woods of "De Klokkebei", Donkerbroek.

Financial support was provided by the Netherlands Organisation for Scientific Research (NWO) and the Dutch Cancer Society (KWF).

GDE transmembrane ecto-enzymes: novel signaling functions through GPI-anchor cleavage

Proefschrift

ter verkrijging van
de graad van doctor aan de Universiteit Leiden,
op gezag van Rector Magnificus prof.mr. C.J.J.M. Stolker
volgens besluit van het College voor Promoties
te verdedigen op 19 september 2018
klokke 16.15 uur

door

Thijs Paul Michaël van Veen

Geboren te Amsterdam
in 1985

Promotiecommissie

Promotor:	Prof. dr. J.J. Neefjes	
Co-promotor:	Em. prof. dr. W.H. Moolenaar	
Co-promotor:	Dr. E. Matas-Rico	Nederlands Kanker Instituut

Overige Leden:

Prof. dr. A. Perrakis	Universiteit Utrecht
Prof. dr. K. Jalink	Universiteit van Amsterdam
Prof. dr. A. Sonnenberg	
Prof. dr. H. Ovaa	
Dr. A. Haramis	

Table of Contents

Chapter 1	General introduction: The family of GDPD enzymes and their involvement in GPI-anchor cleavage	7
Chapter 2	Negative regulation of urokinase receptor activity by a GPI-specific phospholipase C in breast cancer cells	23
Chapter 3	GDE2 promotes neuroblastoma differentiation through glypican release and is a marker of clinical outcome	49
Addendum	Neuronal differentiation through GPI-anchor cleavage	85
Chapter 4	Glycerophosphodiesterase GDE2/GDPD5 affects pancreas differentiation in zebrafish	93
Chapter 5	GDE2 and GDE3: differences in regulation and substrate recognition	113
Chapter 6	Summary and Discussion	127
Addendum	References	138
	Nederlandse samenvatting voor leken	152
	Curriculum Vitae	156
	List of Publications	157
	Acknowledgements	158

QUERCUS

Chapter 1

General introduction: The family of GDPD enzymes and their involvement in GPI-anchor cleavage

Introduction

After having built some of the earliest microscopes, Robert Hooke first published his observations in his *Micrographia* in 1665 [1]. He described his observation of a common structure present in all organisms which he called "Cells" because of the resemblance to monastic cells. Roughly 200 years later the cell theory was formulated, which states that all living organisms are composed of cells, making them the most basic building block of life [2]. Today this statement is still valid and in addition we now know that all cells come from preexisting cells and carry the heredity information DNA. Although cells are independent units capable of self-replication, communication with their surroundings is vital and enables them to work together to form organs and ultimately the human body. To do so, mechanical or biochemical stimuli from outside the cell are transmitted across the membrane by specialized integral membrane proteins that span the lipid bilayer and activate intracellular signaling cascades. This process is called outside-in signaling. However, from within, cells can also control or adapt their response to extra-cellular stimuli, either by changing the conformation of transmembrane proteins or by pulling the specific protein inside the cell (internalization) to reduce their exposure to extracellular stimuli. But transmembrane proteins are not the only proteins that respond to extracellular stimuli. Another class of peripheral membrane proteins do not cross the membrane but are anchored to the outer leaflet via a lipid tail, so called glycosylphospatidylinositol (GPI) -anchored proteins. About 20% of all membrane proteins are GPI-anchored and play key roles in a wide variety of biological processes. However, because of their very nature, they are incapable of directly signaling inside the cell and thus need to interact with transmembrane co-receptors. Also, because they lack a transmembrane domain, control from within the cell is limited. Therefore, ever since the discovery of this complex protein modification in the 1970s the biological importance of the GPI anchor has been elusive. In this thesis we identify a family of transmembrane enzymes, glycerophosphodiesterases (GDEs), that specifically cleave GPI anchors. By doing so, GDEs release the protein from the membrane to control cell signaling, thereby adding a new role to the GPI-anchor as an enzyme substrate.

GPI-anchored proteins

Since their discovery approximately 40 years ago, we know that proteins can be covalently bound to a phospholipid anchor which is inserted into the outer lipid leaflet[3, 4]. Since then, increasing numbers of GPI-anchored proteins (GPI-APs) have been identified in eukaryotes ranging from fungi to mammals. Today we know that GPI-anchored proteins (predictions vary between 150 to 300 proteins carrying a GPI-anchor [5]) are functionally and structurally diverse, ranging from enzymes (uPAR) to cell-cell adhesion molecules (NCAM) and

complement regulatory factors (CD55). Consequently, proteins carrying a GPI anchor play fundamental roles in various (patho) physiological processes, such as adhesion, cellular differentiation, immune response and general cell signaling [6-11]. The importance of the lipid anchor is further demonstrated by early research showing that complete abrogation of this modification is embryonic lethal [10, 11]. In mammals, mutations in the promotor region of *PIG-M* or in the *PIG-C* gene that are involved in GPI-biosynthesis lead to seizures and are associated with intellectual disability [12, 13]. In addition, in human hematopoietic stem cells, somatic defects in genes involved in GPI-biosynthesis result in paroxysmal nocturnal hemoglobinuria, an acquired life-threatening hemolytic disease [14]. Although these examples clearly demonstrate the importance of GPI-anchored proteins in localization to the membrane, they fail to reveal a physiological role for the GPI anchor itself, which remains an outstanding question. The molecular structure of GPI anchors is complex and includes a phospholipid, a glycan core and a linker group. Although this modification is efficient to anchor proteins to the membrane, it seems too complex to serve only this purpose. Indeed, recent studies have revealed that GPI anchors can be further modified and released by GPI-specific enzymes, showing that the structural complexity of GPI-anchors could have multiple functions beyond simple membrane tethering [15-18].

1. Structure of GPI anchors

The GPI anchor is a C-terminal protein modification with a highly conserved core structure consisting of an ethanolamine phosphate (EtNP) linker region directly attached to the protein, a glycan chain containing a minimum of 3 mannose residues (Man) and a glucosamine (GlcN) group [3]. Finally, an inositol group links the GPI anchor to a phospholipid tail which is inserted into the outer membrane leaflet. Attached to this highly conserved glycan core various additional modifications can be attached, which differ not only within organisms, but also within the protein attached to it. For instance, structural comparisons between the insect life-cycle and bloodstream *T. brucei* VSG (arguably the best charachterized GPI anchor) revealed alterations in carbohydrate side chains. This demonstrates that side chains are constantly modified depending on the cell state or its surroundings[3, 19]. In humans, intra-protein GPI-anchor heterogeneity is also found, as shown by mass spec analysis of CD59 where a fraction of the GPI anchors carry a β-N-acetylgalactosamine group (GalNAc) attached to the 4-position of Man-1 [20]. In general, GPI-anchor modifications include additional EtNP's or various linear or branched glycosyl groups including sialic acid, mannose or galactose (Figure 1)[21]. However, exactly why GPI anchors carry these modifications, to what extent they are reversible and how they are regulated are outstanding questions. Clues from lower eukaryotes suggests that the presence of specific intracellular enzymes together with the tertiary/quarternary structure dictates GPI anchor modifications [5, 22, 23]. Not only the GPI-sugar core is modified, also the inositol phospholipid moiety, typically D-*myo*-inositol-

1-*P*-3(*sn*-1,2-diacylglycerol), can differ between proteins and species. Inositol phospholipid variants can include diacylglycerol (the classic GPI-anchor), *lyso*acyl (in *Trypanosoma cruzi),* ceramide (in *Dictyostelium),* alkenylacyl (bovine) or alkylacylglycerol (in *Leishmania*) [24] (Figure 2). Yet, many of the above modifications are only found in lower eukaryotes. In mammals, only two variations of the inositol phospholipid are described: alkylacylglycerol (Figure 2B) and palmitoylation of the inositol group (erythrocyte AChE) (Figure 2A) [25-28]. The latter modification is especially interesting since it renders GPI-anchor cleavage resistant to bacterial phospholipase C (PLC)(Figure 2) and thus prevents PLC-induced release from the membrane. It is nevertheless unclear if inositol acylation is only present during biosynthesis or also in mature GPI-anchored proteins at the plasma membrane [27, 28]. Furthermore, inositol acylation was only shown in erythrocytes and may represent an exception [29].

2. GPI-anchor biosynthesis

During biosynthesis of GPI-anchored proteins, a C-terminal attachment sequence is recognized and a pre-assembled GPI anchor is then attached to the protein through an irreversible transamidation reaction at the luminal site of the endoplasmic reticulon (ER) [21] (Figure 3). Although the attachment signal is crucial, it is poorly conserved and does not contain a consensus sequence. However, it does contain common features including (i) an ω-site, the lipidation site where the GPI anchor is amine-bonded to the protein; this is generally a small amino acid with small side chains; (ii) two small amino acids in close proximity to the ω-site (ω+1, ω+2), followed by (iii) a short stretch of hydrophilic amino acids (linker region) and (iv), a carboxyl-terminal hydrophobic region [30]. The latter region displays similar properties to a classical transmembrane α-helix, however with marginal hydrophobicity. Consequently, an attachment signal that diffuses between the ER membrane and ER lumen prior to transamidation is thought to be a requisite for proper GPI-anchor attachment [31].

The synthesis of the GPI anchor itself requires at least 10 reactions and over 20 genes are involved in the process [22, 29, 32]. The assembly of the PI moiety occurs at the cytoplasmic side of the ER by stepwise addition of sugars and acylation of the inositol group. The latter modification targets the GPI precursor to the luminal side of the ER by an as yet unknown flippase [29]. Here, the protein is attached to the lipid anchor, which is then modified through removal of a EtNP group at the second Man by PGAP5 and acyl chain removal by PGAP1 [33, 34] (Figure 4). In mice, defective acyl removal through Pgap1 knockout results in normal GPI-AP cell-surface expression, but the mice suffer from severe defects during development and fertilization [9, 33]. One possible explanation for infertility is that acylated GPI-APs accumulate on the membrane because of their resistance to PLC attack. Intriguingly, GPI-anchored cleavage was shown to be essential for sperm maturation, hinting at a possible role

for GPI specific phospholipase [35].

After acyl removal in the ER, only correctly folded GPI-APs are loaded from the ER into Coat protein complex II (COPII) vesicles (Figure 3 and 4). Correctly folded and remodeled GPI-anchors act as an ER exit signal that guide GPI-APs to the Golgi and then to the plasma membrane [36, 37]. When sorted in vesicles, GPI-APs fail to bind cytosolic COPII proteins since they lack a transmembrane domain. Transmembrane adaptor proteins are therefore needed to ensure efficient transport to the plasma membrane. The family of p24 proteins represent such cargo receptors that recycle between the ER and the Golgi [38-40] (Figure 4). These proteins serve as gatekeepers by selectively recognizing GPI-APs modified by PGAP1 and PGAP5 [36, 41].

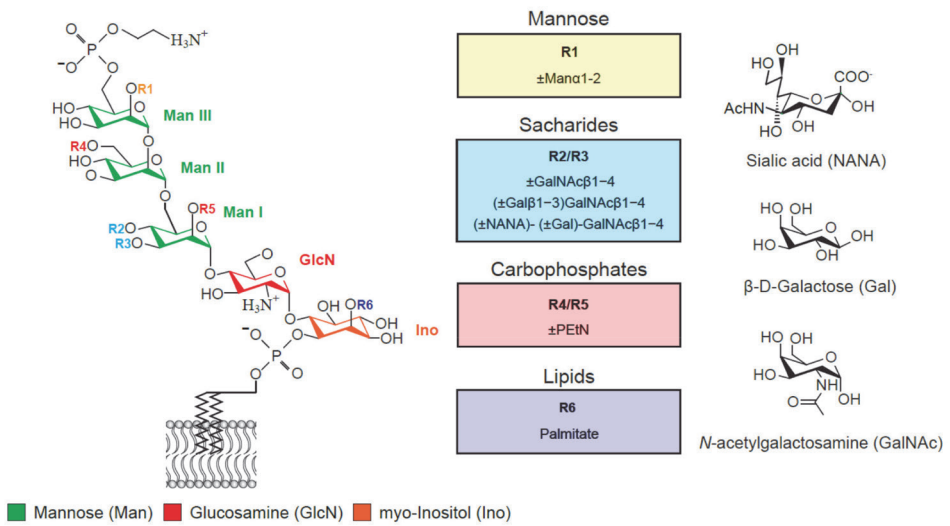

Figure 1. GPI-anchor molecular structure
(left) Minimum GPI-anchor core structure with sites for additional side chain modifications indicated as R^{site}. (right) Depicted modifications as found in human GPI-anchored proteins. PEtN, phosphoethanolamine.

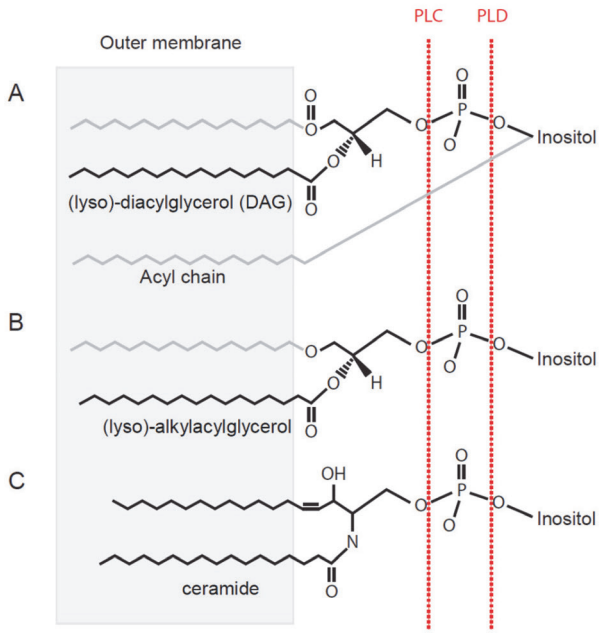

Figure 2. Phospholipid variants present in GPI anchors
Inositol phospholipids with the GPI-PLD and PLC cleavage sites indicated in red. A and B are only found in mammalian GPI anchors. Acylation of the inositol group (indicated in light grey) occurs during biosynthesis and in mature erythrocyte AChE. This modification confers resistance to GPI-PLC activity.

3. GPI membrane localization and recycling

From the Golgi GPI-APs are sorted in the trans-Golgi network (TGN) to so-called detergent resistant microdomains (DRMs) in the plasma membrane [42, 43]. These "rafts" (although their existence has been questioned) are thought to be sorting platforms for the TGN where GPI-anchors form signaling complexes. Through this mechanism, cells target various GPI-APs to the same membrane micro clusters, depending the lipid environment and the actin cytoskeleton [43-46].

In polarized endothelial and neuronal cells, GPI-APs are selectively transported to the apical membrane or axonal region, respectively [42, 47-50]. Although the underlying mechanism is unclear, perturbation of the cholesterol or sphingolipid biosynthesis machinery interrupts GPI-AP-specific sorting. This again demonstrates the importance of the lipid microenvironment [51]. However, lipid composition alone is not sufficient for apical sorting. GPI-AP oligomerization and *N*-glycosylation are also required for correct vesicle sorting [52-54]. While apical sorting is the preferred route for GPI-anchors, they also localize to

basolateral membranes. Fusing the GPI anchor motif from different GPI-APs to a GFP dictates basolateral or apical sorting [48]. In conclusion, it is clear that different mechanisms are in play to sort GPI-APs.

Once on the membrane, GPI-APs can diffuse between heteroclusters in DRMs or as monomers. From here they can recycle through clathrin-independent mechanisms. One such route, the "caveolae pathway", is dependent on dynamin and uses specialized membrane domains (caveolae) [29, 55]. However, most GPI-APs use another clathrin- and dynamin-independent pathway. In this pathway, GPI-APs are internalized by clathrin-independent carriers (CLIC) and transported to a compartment termed "GPI-APs enriched at early endosomal compartment" (GEEC) [56, 57] . From there GPI-APs recycle through early and late endosomes [58, 59] (Figure 4).

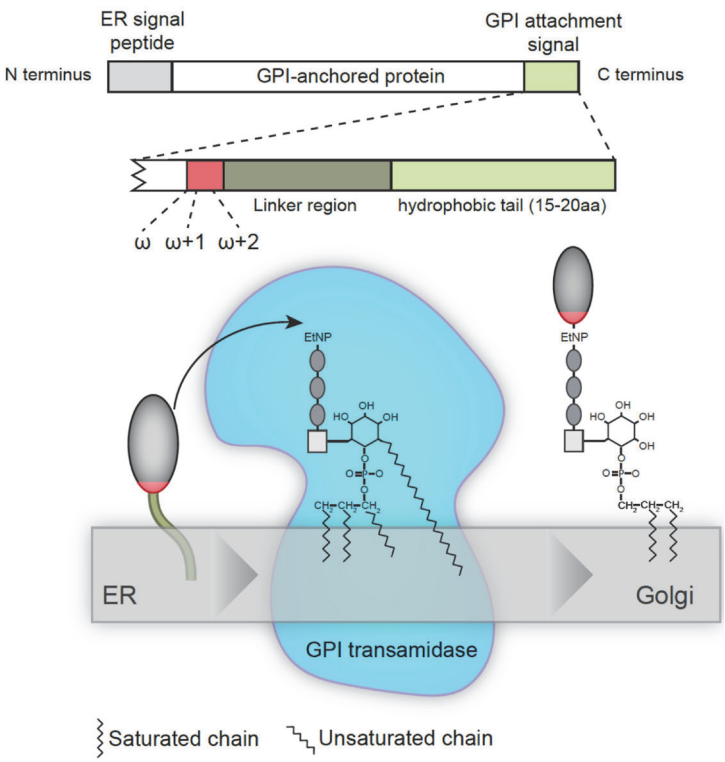

Figure 3: GPI-anchor addition by transamidase
All GPI-anchored proteins have an N-terminal ER signal peptide and a C-terminal GPI attachment signal that consists of a marginal hydrophobic region and a lipidation site (Omega). In the ER, the GPI anchor is preassembled and attached to the protein by transamidases. Thereafter the GPI-AP is transported to the Golgi.

4. GPI-anchor cleavage and release from the membrane

A unique feature of GPI-APs is that they can be cleaved and released from the membrane by phospholipases. Through this mechanism, cells not only regulate cell surface expression, but also generate a soluble protein which in some cases can function as a ligand for neighboring cells and as biomarker of various diseases [35, 60-62]. Of note, cleaving the GPI-anchor can have profound effects on the conformation and hence the function of the attached protein [23, 63]. Early research showed that GPI-APs are efficiently released by a bacterial GPI-specific PLC [64]. In mammals, the release of GPI-APs and its physiological relevance is not understood, however. A GPI-specific phospholipase D (GPI-PLD) was the first characterized enzyme capable of hydrolyzing various GPI-APs in vitro [65-67]. Secreted GPLD1 is able to cleave inositol-acylated GPI-anchors, in contrast to bacterial PI-PLC [68]. However, unlike bacterial PI-PLC, GPI-PLD fails to release GPI-anchors from native membranes, requiring detergents for its activity [4, 69]. Thus, its physiological role remains elusive to date. Another secreted protein, called Notum, was shown to regulate Wnt signaling by cleaving the GPI

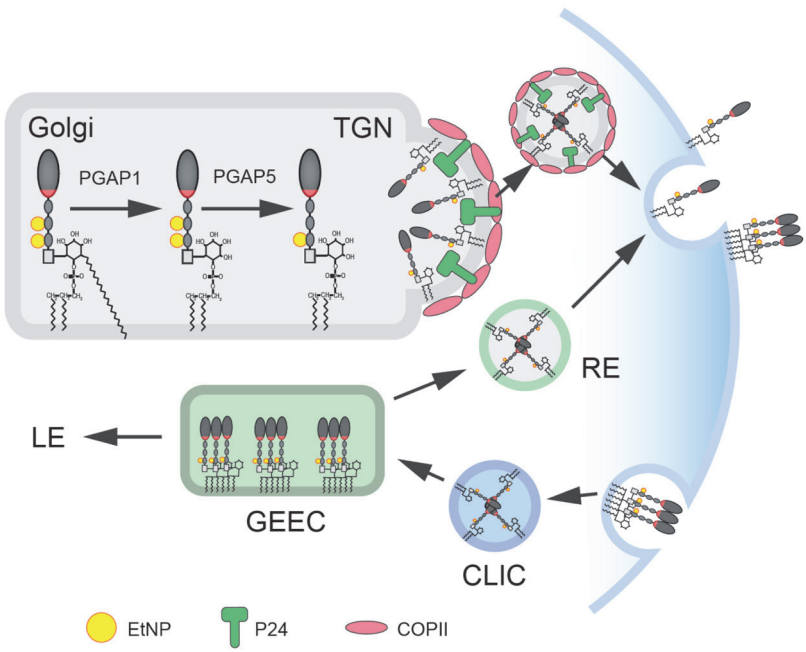

Figure 4: GPI-AP biosynthesis and trafficking

After acyl and EtNP removal in the Golgi, the GPI-AP is sorted and clustered in the TGN into p24- and COPII-positive vesicles. From there, GPI-APs are transported to the membrane where they localize to specific domains. GPI-APs undergo non-clathrin-mediated internalization and recycling following the CLIC-GEEC pathway. RE, recycling endosome; LE, late endosome; TGN, Trans Golgi Network; CLIC, clathrin-independent carrier; GEEC, GPI-AP-enriched early endosomal compartment.

anchor of Dally-like protein in Drosophila [70]. Notum releases multiple GPI-APs from mammalian cells in culture [16]. However, purified Notum was unable to hydrolyze GPI anchors [71]. Instead, recent studies revealed that Notum deacylates the Wnt protein which is required during brain development [15, 71].

During fertilization, spermatozoa express specific GPI-anchored proteins (a.o. TEX101) that are released during transport through the epididymis [72, 73]. Mice lacking germ-cell TEX101 or Angiotensin-converting enzyme (ACE) are subfertile because spermatozoa fail to migrate into the epididymis [74, 75]. Analysis showed that ACE was able to release GPI-anchored TEX101 from HEK293 cells, revealing an in vivo role for GPI-anchor release by ACE [18, 74]. However, caution should be taken when interpreting these results since GPI-releasing activity was weak and could not be reproduced by others [76]

As discussed above, during the last decade, several enzymes capable of releasing GPI-anchored proteins in vitro have been identified. Yet, these enzymes are either secreted or show very limited or even questionable activity. This suggests that more effective GPI-releasing enzymes must exist. Recent research has identified two other attractive candidates; the family of GDPDs and PGAP6.

PGAP6, a GPI-specific phospholipase A2

Bioinformatic analysis in search of PGAP3 (an enzyme involved in GPI-anchor lipid remodeling) family members revealed an uncharacterized gene, termed PGAP6 [77]. This transmembrane protein cleaves the GPI-anchored CRIPTO protein in a phospholipase A2-like manner resulting in a lysophosphatidylinositol-bearing GPI-AP. Although phospholipase A2 cleavage itself does not release GPI-APs into the medium, increased soluble CRIPTO was found in the medium after PGAP6 over-expression, possibly through an unidentified secondary effect. Interestingly, *Pgap6* KO mice exhibit severe defects in the anterior-posterior axis during development, reminiscent of a *Cripto* knockout phenotype.

Family of GDPDs

Glycerophosphodiester phosphodiesterases (GDPDs or GDEs) are a family of proteins present in many organisms, ranging from prokaryotes to protozoa and mammals. Although their primary sequence and catalytic sites are well conserved, their enzymatic features and biological significance are diverse. In *Escherichia coli*, the GDPDs, *GplQ* and *UgpQ* are well characterized and hydrolyze de-acylated glycerophospholipids into glycerol and phosphate [78-80]. Located in the periplasm and cytosol respectively, these enzymes serve a metabolic

function by generating essential building blocks such as choline, ethanolamine, inositol and serine. Likewise, in *H. Influenzae*, a homologue of *GlpQ*, protein D, is localized in the membrane and also hydrolyses deacylated phospholipids [81]. Protein D damages ciliated epithelial cell membranes in a GDPD-dependent manner, thereby contributing to *H. Influenzae* virulence [82]. Because of their high conservation in prokaryotes, the essential role in metabolism and their membrane localization, GDPDs from various organisms are currently exploited to target conjugate vaccines [83-86]. GDPDs isolated from Gram-positive bacteria also generate glycerol-3-phosphate, but in addition have a broad substrate specificity, including teichoic acid and di(glycerophospho)glycerol (deacylated) cardiolipin [87]. Because GDPDs exhibit a broad substrate specificity and can even break down organophosphates, they are also utilized for detoxification of pesticides and nerve agents [88, 89]. Bacterial GDPDs share a common tertiary structure, namely the classical triosephosphate isomerase barrel (TIM barrel) [90]. The general structure of a TIM barrel is composed of alternating α helices and β-strands, together forming a donut shaped (toroid) barrel, where beta strands form the inner lining surrounded by the α helices.

1. Mammalian GDPDs

Bacterial GDPDs have long been studied and although some questions remain to be answered, their function and structure are known. By contrast, the family of mammalian GDPDs is understudied and only recently their role in glycerophospholipid signaling is emerging. The first identified mammalian GDPD, GDE1 (previously MIR16), was isolated from a two-hybrid screen in search of interactors with regulator of G-protein signaling (RGS16) [91, 92]. GDE1 is an integral membrane protein that localizes to internal membranes with the enzymatic domain facing the extracellular space [91] (Figure 5A). Structural modeling and sequence analysis of the enzymatic domain showed a conserved catalytic site with strong sequence and structural similarities to bacterial GDPDs [92, 93]. Consistent with this, GDE1 could hydrolyse glycerophosphoinositol (GroPIns) in a phospholipase D-like manner, producing glycerol-3-phosphate (Gro3P) and inositol (Figure 5B). Its activity was enhanced by magnesium and calcium [91]. MS-based metabolomics of mice lacking GDE1 revealed that GDE1 also hydrolyses GroPSer as well as an anandamide precursor glycerophospho-*N*-arachidonoylethanolamine [91, 94, 95]. A second yeast-two-hybrid screen identified GDE1 as a binding partner of yet another interactor of G-protein coupled signaling (PRAF2) [93], suggesting that GDE1 is involved in or regulated by G-protein signaling. In line with this, GDE1 activity was increased by isoproterenol and inhibited by lysophosphatidic acid (LPA). Taken together, these studies revealed GDE1 as the first mammalian glycerophosphodiester with a potential role in G-protein signaling, although the exact mechanism remains elusive. After GDE1, an additional six mammalian GDEs were cloned that are phylogenetically clustered together with bacterial UgpQ [96, 97] (Figure 5A). Within this family, one branch

is occupied by the six-fold transmembrane members GDE2, GDE3, and GDE6. The second group is formed by GDE4 and GDE7 with two putative trans membrane domains, leaving GDE5 as a unique cytosolic enzyme [96]. GDE5 is mainly expressed by skeletal muscle cells. Overexpression suppressed myogenic differentiation, while knockdown reversed this phenotype [98]. GDE5 selectively hydrolyses GroPCho *in vitro*. Unexpectedly, its myogenic activity was independent of the enzymatic domain, suggesting that other mechanisms are in play during myogenic differentiation [98].

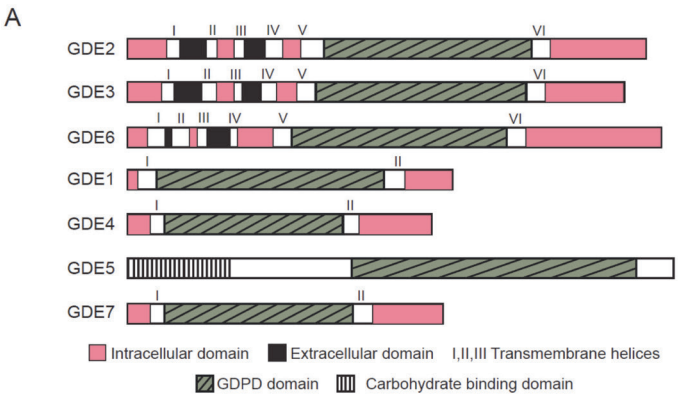

B

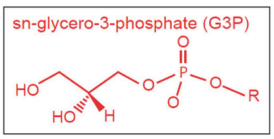

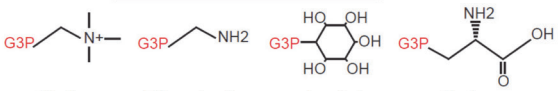

	Choline	Ethanolamine	Inositol	Serine	
GDE1	-	+	+	+	PLD
GDE2/GDPD5	+	N/K	N/K	-	N/K
GDE3/GDPD2	-	N/K	+	N/K	PLC
GDE4/GDPD1	-	-	-	-	LysoPLD
GDE5/GDPD6	+	+/-	-	-	PLD
GDE6/GDPD4	N/K	N/K	N/K	N/K	N/K
GDE7/GDPD3	-	-	-	-	LysoPLD

Figure 5. Mammalian GDPD structure and enzymatic activity
(A) schematic representation of the mammalian GDE/GDPD family. The closest family members GDE2, GDE3 and GDE6 have six transmembrane helices, an extracellular enzymatic domain and intracellular N- and C- termini. **(B)** Table illustrating the enzymatic activity towards various deacylated glycerophosphodiesters by the indicated GDE enzymes. + activity reported; - no activity reported; +/- minor activity; N/K, activity unknown; PLC, phospholipase C; PLD, phospholipase D; lyso-PLD, lyso-phospholipase D [91, 94, 98-101].

2. GDE4 and GDE7, two lyso-phospholipases D

GDE4 and GDE7 are differentially expressed and have a unique function compared to the classical GDPDs. Recent studies showed that the C-terminus of both proteins is conserved with that of *L. laeta* SMaseD, a lysophospholipase D [102]. Following activity studies revealed that both enzymes also have lysoPLD activity without activity towards deacylated phospholipids [101, 103]. Overexpressed GDE4 localizes to perinuclear membranes with no clear phenotypical changes [104]. Both enzymes could generate lysophosphatidic acid (LPA) from lysophosphatidylcholine (LPC) [101]. These studies reveal a novel pathway for LPA production. However, the significance of intracellular LPA production is not understood.

3. Transmembrane ecto-enzymes GDE2, GDE3 and GDE6

GDE2, GDE3 and GDE6 are of special interest because of their six transmembrane helices and enzymatic domain located on the luminal side. The less-studied, and arguably least interesting of the three, GDE6, solely expresses in the testis and localizes to the ER [105] (unpublished data). In contrast, GDE2 and GDE3 localize to the plasma membrane with the enzymatic domain pointing towards the extracellular space. Like other GDPDs, GDE2 and GDE3 hydrolyze deacylated glycerophospholipids GroPCho and GroPIno respectively [99, 100]. However, its physiological significance is ambiguous since GDE2 silencing did not alter choline concentration and had minimal effect on Gro3P levels [106]. Park et al., reported that GDE2 cleaves and releases the GPI anchored protein Reversion-inducing-cysteine-rich *protein* with kazal motifs (RECK). This suggests that these GDEs are the long-sought enzymes that release GPI-APs from the membrane.

GDE2 is a retinoic acid-inducible gene whose expression is sufficient to drive neurite formation *in vitro* [97, 107]. GDE2 is primarily expressed in the developing spinal cord during motor neuron differentiation [108]. Retinoic acid induced GDE2 expression drives differentiation, while GDE2 ablation results in decreased post-mitotic motor neurons, accompanied by increased cell death [108, 109]. The underlying mechanism involves non-cell-autonomous cleavage of RECK by GDE2 [110]. GPI-anchored RECK activates NOTCH signaling by inhibiting metalloprotease-mediate shedding of the NOTCH ligand Delta-like 1 [111, 112]. When expressed in neighboring post-mitotic motor neurons, GDE2 cleaves RECK and thereby inactivates NOTCH signaling in pre-motor neurons, thereby regulating the timing of cortical progenitor differentiation in the developing spinal cord [110]. GDE2 does not cleave GPI-anchored RECK in a classical PLC- or PLD-like manner, suggesting a different attack of the phosphodiester bond compared to bacterial GPI-PLC [100]. Postnatally, GDE2 is continuously expressed and mice lacking GDE2 exhibit slow and progressive neurodegeneration [113]. The observed cellular phenotypes, including vacuolization and lipofuscin depositions, closely resemble human neurodegenerative pathologies, signifying GDE2's role not only in neuronal differentiation but also in neuronal survival.

The GPI-anchored proteins Glypican 4 and 6 were identified as candidate substrates for GDE2, however, a direct role for the release of these GPI-APs in neuronal survival was not shown [113]. Exactly how GDE2 prevents neurodegeneration remains an outstanding question. In chapter 3 we show that Glypican 6 release by GDE2 drives neuroblastoma differentiation [17].

GDE2's closest homologue, GDE3, was isolated in a differential display screen comparing the sequential stages during osteoblast differentiation in culture [114]. GDE3 was highly expressed at the onset of differentiation and remained high thereafter. Tissue GDE3 expression was not only detected in developing bones but also in the spleen, skin and adult brain [115]. *GDE3* overexpression induced osteoblast differentiation [99]. In contrast, GDPD ecto-domain neutralizing antibodies as well as active site mutations reversed this phenotype, suggesting a possible role for the enzymatic domain in glycerophospholipid hydrolysis. Subsequent studies showed that GDE3 specifically hydrolyses GroPIno to glycerol and Ins1*P*. Hence, GDE3 cleaves GroPIno in a PLC dependent manner, unlike other mammalian GDPDs (Figure 5B). It was suggested that GDE3, by cleaving GroPIno, inhibits proliferation and accelerates differentiation. More recent studies demonstrated that GDE3 as well as GDE6 can also cleave GPI-anchors similar to GDE2 [110, 116]. In chapter 2 we show that GDE3 cleaves GPI-anchored uPAR in a phospholipase C-like manner[116]. Altogether these studies reveal a potential role for the serpentine GDE proteins in targeted cleavage and release of GPI-anchored proteins from the membrane.

4. Regulatory mechanisms involved in GDE2 and GDE3 activity

The regulation of GDE enzymatic activity is for the most part unknown. Their secondary structure and variation in intra-cellular N- and C-terminal lengths suggests that GDE2, GDE3 and GDE6 are differentially regulated by intracellular components. In support of this and similar to GDE1 binding to a regulator of G protein signaling, it was shown that the C-terminus of GDE2 binds to Gαi, with unknown consequences [92, 117]. Also, Yan and colleagues identified the antioxidant enzyme peroxiredoxin 1 (Prdx1) as an interactor of GDE2 [118]. They showed that Prdx1 drives motor neuron differentiation by a mechanism that activates GDE2 through the reduction of an intra-cellular disulfide bond, bridging the N- and C- terminus of GDE2. Prdx1 knockdown was reminiscent of GDE2 knockdown and mutant GDE2 variants, deficient in disulfide bond formation, were hyperactive [118]. Later, the same group proposed a second redox dependent mechanism. In this model, Prdx4 dimers in the ER, which are generated after metabolizing H_2O_2, oxidize a disulfide bond in the enzymatic domain of GDE2 [119]. As a consequence, GDE2 trafficking to the plasma membrane is inhibited. Thus, two opposing redox dependent mechanisms that regulate GDE2 cell-surface expression and activity are suggested. Interestingly, the cysteines involved in this process are conserved in other GDE family members. However, their role and the requirements for these thiol-oxidative mechanisms are unknown.

Thesis outline

The studies described in this thesis focus on the role of GDE2 and GDE3 on GPI-anchor hydrolysis to increase our understanding of their physiological functions. **Chapter 1** is a general introduction giving an overview of the current knowledge and progress in GPI-anchored bio-synthesis and signaling, together with an overview of the developing understanding of the mammalian GDPD protein family. **Chapter 2** identifies GDE3 as the first mammalian GPI-specific PLC that selectively cleaves and releases the urokinase receptor (uPAR) from the membrane. By doing so, GDE3 negatively regulates uPAR signaling in breast cancer cells. Its closest family member, GDE2, associates with a positive clinical outcome in neuroblastoma, a childhood disease characterized by defective neuronal differentiation. The molecular mechanism involving neuronal differentiation through selective release of Glypican 6 by GDE2 is presented in **Chapter 3**. **Addendum Chapter 3** comments on the release of GPI-anchored proteins during neuronal differentiation. Next, **Chapter 4** explores the involvement of GDE2 in zebrafish development and describes a potential role for GDE2 in the development of the pancreas. **Chapter 5** compares the enzymatic activity towards specific GPI-anchored proteins and localization of GDE2 and GDE3. In **Chapter 6**, the results presented in this thesis are summarized and discussed.

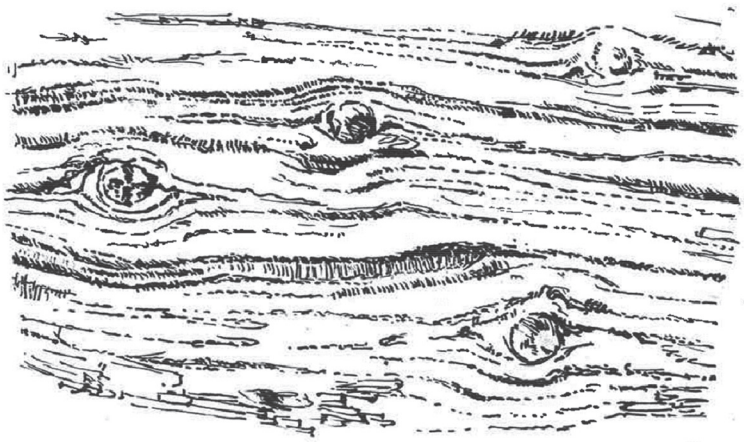

LARIX

Chapter 2

Negative regulation of urokinase receptor activity by a GPI-specific phospholipase C in breast cancer cells

eLife 2017;6:e23649

Michiel van Veen[1&], Elisa Matas-Rico[1&], Koen van de Wetering[2], Daniela Leyton-Puig[1], Katarzyna M. Kedziora[1], Valentina De Lorenzi[3], Yvette Stijf-Bultsma[4], Bram van den Broek[1], Kees Jalink[1], Nicolai Sidenius[3], Anastassis Perrakis[4], Wouter H. Moolenaar[1]

[1] Division of Cell Biology, The Netherlands Cancer Institute, Amsterdam, Netherlands;
[2] Division of Molecular Oncology, The Netherlands Cancer Institute, Amsterdam, Netherlands;
[3] IFOM, The FIRC Institute of Molecular Oncology, Milan, Italy;
[4] Division of Biochemistry, The Netherlands Cancer Institute, Amsterdam, Netherlands
[&] These authors contributed equally

Abstract

The urokinase receptor (uPAR) is a glycosylphosphatidylinositol (GPI)-anchored protein that promotes tissue remodeling, tumor cell adhesion, migration and invasion. uPAR mediates degradation of the extracellular matrix through protease recruitment and enhances cell adhesion, migration and signaling through vitronectin binding and interactions with integrins. Full-length uPAR is released from the cell surface, but the mechanism and significance of uPAR shedding remain obscure. Here we identify transmembrane glycerophosphodiesterase GDE3 as a GPI-specific phospholipase C that cleaves and releases uPAR with consequent loss of function, whereas its homologue GDE2 fails to attack uPAR. GDE3 overexpression depletes uPAR from distinct basolateral membrane domains in breast cancer cells, resulting in a less transformed phenotype, it slows tumor growth in a xenograft model and correlates with prolonged survival in patients. Our results establish GDE3 as a negative regulator of the uPAR signaling network and, furthermore, highlight GPI-anchor hydrolysis as a cell-intrinsic mechanism to alter cell behavior.

Introduction

The urokinase-type plasminogen activator receptor (uPAR) is a central player in a complex signaling network implicated in a variety of remodeling processes, both physiological and pathological, ranging from embryo implantation to wound healing and tumor progression [120-122]. uPAR is a glycosylphosphatidylinositol (GPI)-anchored protein and hence lacks intrinsic signaling capacity. Instead, uPAR acts by binding two major ligands, namely the protease urokinase plasminogen activator (uPA) and the extracellular matrix (ECM) protein vitronectin [120, 121, 123]. Through uPA binding, uPAR localizes plasmin generation to the cell surface and thereby promotes pericellular proteolysis and ECM degradation [120, 121]. In addition, through vitronectin binding and functional interactions with integrins and growth factor receptors, uPAR activates intracellular signaling pathways leading to cytoskeletal reorganization, enhanced cell adhesion and motility and other features of tissue remodeling and cell transformation [120, 123, 124]. As such, uPAR is a master regulator of extracellular proteolysis, cell motility and invasion. uPAR expression is elevated during inflammation and in many human cancers, where it often correlates with poor prognosis, supporting the view that tumor cells hijack the uPAR signaling system to enhance malignancy [120-122]. Increased uPAR expression in solid tumors and the corresponding activated stroma is being evaluated by PET-imaging for patient stratification [125].

It has long been known that full-length uPAR is released from the plasma membrane resulting in a soluble form (suPAR) [126, 127], which is detectable in body fluids and considered a marker of disease severity in cancer and other life-threatening disorders [128-132]. Circulating suPAR is derived from activated immune and inflammatory cells [120, 121], and also from circulating tumor cells [133].

Locally produced suPAR might function as a ligand scavenger to confer negative feedback on uPAR [120]. In addition, both uPAR and suPAR can undergo proteolytic fragmentation by uPA and other proteases, possibly leading to new signaling activities [134]. Yet, despite decades of research, the mechanism of uPAR release and its physiological implications have been elusive. A GPI-specific phospholipase D (GPI-PLD) [135] has often been assumed to mediate the shedding of GPI-anchored proteins, but this unique PLD does not function on native membranes [136].

A possible clue to the mechanism of uPAR release comes from recent studies showing that a member of the glycerophosphodiester phosphodiesterase (GDPD/GDE) family [96], termed GDE2, promotes neuronal differentiation by cleaving select GPI-anchored proteins, notably a Notch ligand regulator and heparan sulfate proteoglycans (glypicans) [110, 137, 138]. GDE2, along with GDE3 and GDE6, belongs to a GDE subfamily characterized by six-transmembrane-domain proteins with a conserved catalytic ectodomain (Figure 1A) [99, 137]. GDE2's close relative, GDE3, accelerates osteoblast differentiation through an unidentified mechanism [99, 115], while the function of GDE6 is unknown.

Here we identify GDE3 as the first mammalian GPI-specific phospholipase C (GPI-PLC) that cleaves and sheds uPAR with consequent loss of uPAR activities in both HEK293 and breast cancer cells.

Results

GDE3, but not GDE2, sheds uPAR from HEK293 cells

We set out to determine whether uPAR can be released by any of the three related GDE family members, GDE2, GDE3 and GDE6. When expressed at relatively low levels in HEK293 cells, human GDE2 and GDE3 (HA-tagged) localized to distinct microdomains at the plasma membrane, possibly representing clustered lipid rafts where GPI-anchored proteins normally reside [139], as well as to filopodia-like extensions [137] (Figure 1 – figure supplement 1A,B). By contrast, human GDE6 was mainly detected in intracellular compartments and therefore was not further tested (Figure 1 – figure supplement 1A).

To assess GDE activity, we generated stable uPAR-expressing HEK293 cells (HEK-uPAR cells), expressed GDE2 and GDE3 and examined the appearance of suPAR in the medium, using bacterial phospholipase C (PI-PLC) as a positive control [137]. Strikingly, uPAR was readily released into the medium by GDE3 and PI-PLC, but not by GDE2 (Figure 1B). GDE3 competed with exogenous PI-PLC to deplete uPAR, since PI-PLC was much less efficient in GDE3-overexpressing than in control HEK-uPAR cells (Figure 1 – figure supplement 1C).

Mutating putative active-site residue H229, corresponding to H233 in GDE2 [137], abolished GDE3 activity without affecting its membrane localization (Figure 1C; Figure 1 – figure supplement 1D). Furthermore, a transmembrane version of uPAR (uPAR-TM) lacking the GPI moiety [140] was resistant to GDE3 attack, consistent with GDE3 acting through GPI-anchor hydrolysis (Figure 1 – figure supplement 1E). Flow cytometry analysis of GDE3-overexpressing cells confirmed decreased uPAR levels in the plasma membrane (Figure 1D), while TIRF microscopy revealed substantial uPAR loss from the ventral cell surface (Figure 1E).

GDE2 versus GDE3: homology modeling

The selectivity of GDE3 versus GDE2 towards uPAR cleavage is striking. In an attempt to understand the structural basis of this selectivity, we constructed homology-based models of the globular α/β barrel GDPD domains, using I-TASSER [141]. We reasoned that the catalytic domains must recognize not only the PI lipid moiety at the membrane-water interface, but also the attached protein. While GDE2 and GDE3 have a similar putative GPI-binding groove leading to the active site, they show striking differences in their surface charge distribution, particularly at the putative substrate interaction surface (Figure 1F). It therefore seems likely that surface properties are a major determinant of selective substrate recognition by GDEs, a notion that should be validated by future structural studies.

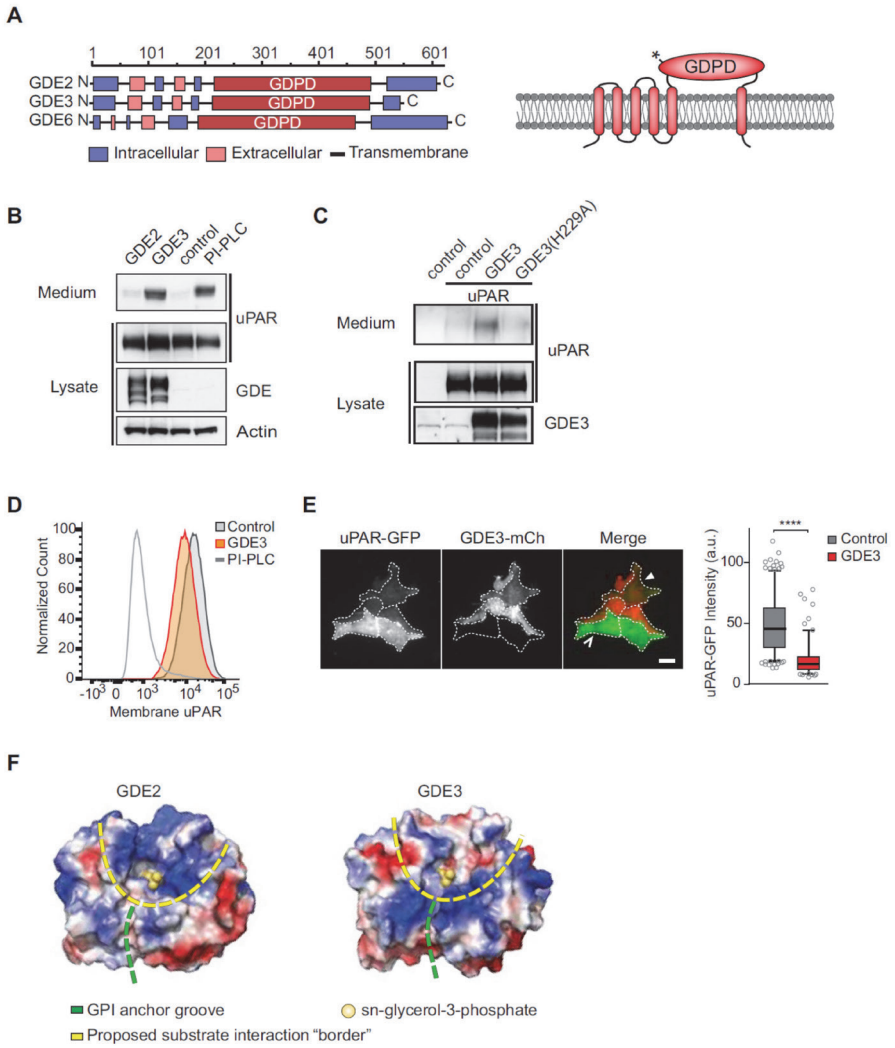

Figure 1. GDE3, but not GDE2, sheds uPAR from HEK293 cells

(**A**) Domain structure of GDE2, GDE3 and GDE6 (left panel), and the transmembrane scheme of GDE3 (right panel). GDPD denotes catalytic glycerophosphodiesterase domain. Asterisk in GDPD domain depicts catalytic His residue in both GDE2 and GDE3. (**B**) Immunoblot analysis of uPAR release into the medium. HEK-uPAR cells transfected with empty vector (control), GDE2 or GDE3. PI-PLC served as positive control. (**C**) Mutant GDE3(H229A) fails to release uPAR. (**D**) Partial loss of uPAR from the plasma membrane by GDE3, as measured by flow cytometry. (**E**) TIRF microscopy reveals loss of uPAR from the basolateral plasma membrane. Box plot shows uPAR-GFP intensity at the ventral membrane (n=3, mean ± SEM ****P<0001). (**F**) Homology modeling of the GDE2 and GDE3 catalytic domains showing surface charge distributions (blue, positive; red, negative; green line, putative GPI-binding groove; yellow line, proposed substrate-binding surface). The active site is indicated by glycerol-3-phosphate located at the template structure.

GDE3 is a GPI-specific phospholipase C that cleaves uPAR in cis

We asked whether GDE3 attacks uPAR in *cis* (same cell) or in *trans* (adjacent cell), or both. By mixing GDE3-expressing cells (lacking uPAR) with uPAR-expressing cells (lacking GDE3), GDE3-expressing cells failed to shed uPAR from the GDE3-deficient cell population (Figure

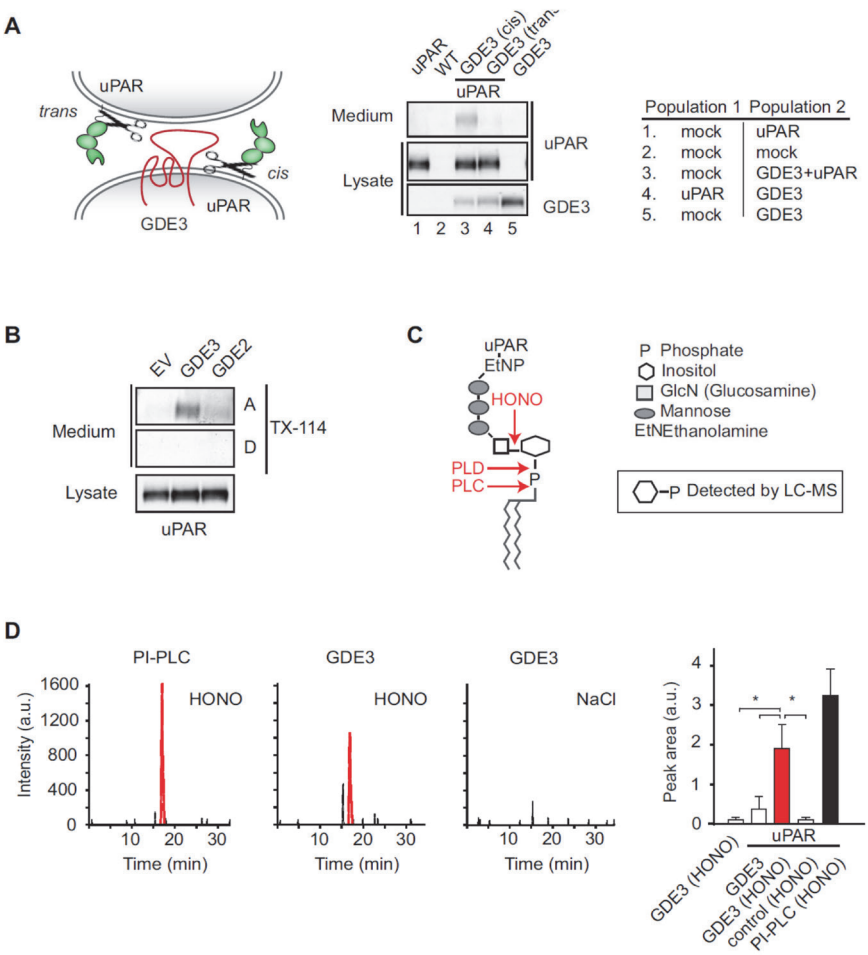

Figure 2. GDE3 is a GPI-specific PLC that cleaves uPAR in cis

(A) (Left) Scheme showing uPAR cleavage in cis or trans. (Right) GDE3-expressing HEK-uPAR cells were mixed with a GDE3-deficient cell population, as indicated. Immunoblot analysis of uPAR in medium and cell lysates indicates that GDE3 acts in cis; mock refers to empty vector-transfected cells. (**B**) GDE3 expression leads to increased GPI-free suPAR. Conditioned medium from HEK-uPAR cells expressing GDE2 or GDE3 was subjected to Triton X-114 phase separation. suPAR in the aqueous (A) and detergent (D) fractions was analyzed by immunoblotting. (**C**) GPI-anchor with phospholipase cleavage sites indicated; HONO, nitrous acid. (**D**) Representative LC-MS ion chromatograms (m/z 259.02-259.03); inositol 1-phosphate peaks in red. HONO-treated suPAR contains inositol 1-phosphate (n=3, mean ± SEM; **P*<0.05).

2A). Thus, GDE3 acts in cis, attacking uPAR on the same plasma membrane, not on adjacent cells. To determine whether GDE3 acts as a phospholipase in GPI-anchor cleavage, we used Triton X-114 partitioning and liquid chromatography-mass spectrometry (LC-MS). Triton X-114 partitioning revealed that suPAR did not contain lipid moieties, as it was not detected in the detergent phase (Figure 2B). Next, suPAR was immunoprecipitated from the medium of GDE3-expressing cells and treated with nitrous acid (HONO) to cleave the glucosamine-inositol linkage in the GPI core (Figure 2C). Subsequent analysis by LC-MS revealed that the acid-treated suPAR samples contained inositol 1-phosphate (Figure 2D). This result defines GDE3 as the first mammalian GPI-specific phospholipase C (GPI-PLC).

GDE3 suppresses the vitronectin-dependent activities of uPAR

When compared to uPAR-deficient cells, HEK-uPAR cells showed markedly increased cell adhesion, loss of intercellular contacts and enhanced spreading with prominent lamellipodia formation on vitronectin, but not on fibronectin (Figure 3A), typical features of a Rac-driven motile phenotype, in agreement with previous studies [123, 142]. Cell spreading coincided with activation of focal adhesion kinase (FAK), indicative of integrin activation (Figure 3B). Strikingly, expression of GDE3 largely abolished the uPAR-induced phenotypes and cellular responses (Figure 3A-F). Catalytically dead GDE3(H229A) had no effect, neither had overexpressed GDE2 (Figure 3F and results not shown). Thus, by releasing uPAR from the plasma membrane, GDE3 suppresses the vitronectin-dependent activities of uPAR. Treatment of diverse cell types with suPAR-enriched conditioned media from HEK293 cells did not evoke detectable cellular responses, supporting the notion that suPAR is biologically inactive, at least under cell culture conditions.

GDE3 locally depletes uPAR and suppresses its activities in breast cancer cells

We next assessed the impact of GDE3 on endogenous uPAR activity in MDA-MB-231 triple-negative breast cancer cells. These cells express relatively high levels of uPAR (Figure 4A) and its ligand uPA [143], thus forming an autocrine signaling loop. Expression of GDE3 (encoded by *GDPD2*) is relatively low in breast cancer lines (n=51), including MDA-MB-231 cells [144] (Figure 4B). GDE3 expression in MDA-MB-231 cells led to a modest loss of uPAR from the plasma membrane as shown by flow cytometry (Figure 4C). To determine how GDE3 expression affects localized uPAR levels at the basolateral plasma membrane, we used confocal and dual-color super-resolution microscopy in TIRF mode. Strikingly, basolateral membrane microdomains containing wild-type GDE3 showed little or no colocalization with endogenous uPAR. In marked contrast, catalytically dead GDE3(H229A) clearly colocalized with uPAR in those membrane domains (Figure 4D). Quantification of co-localization was performed on multiple cells (Figure 4D, right panel). These results strongly suggest that active GDE3 depletes uPAR levels from distinct domains at the basolateral membrane. Consistent

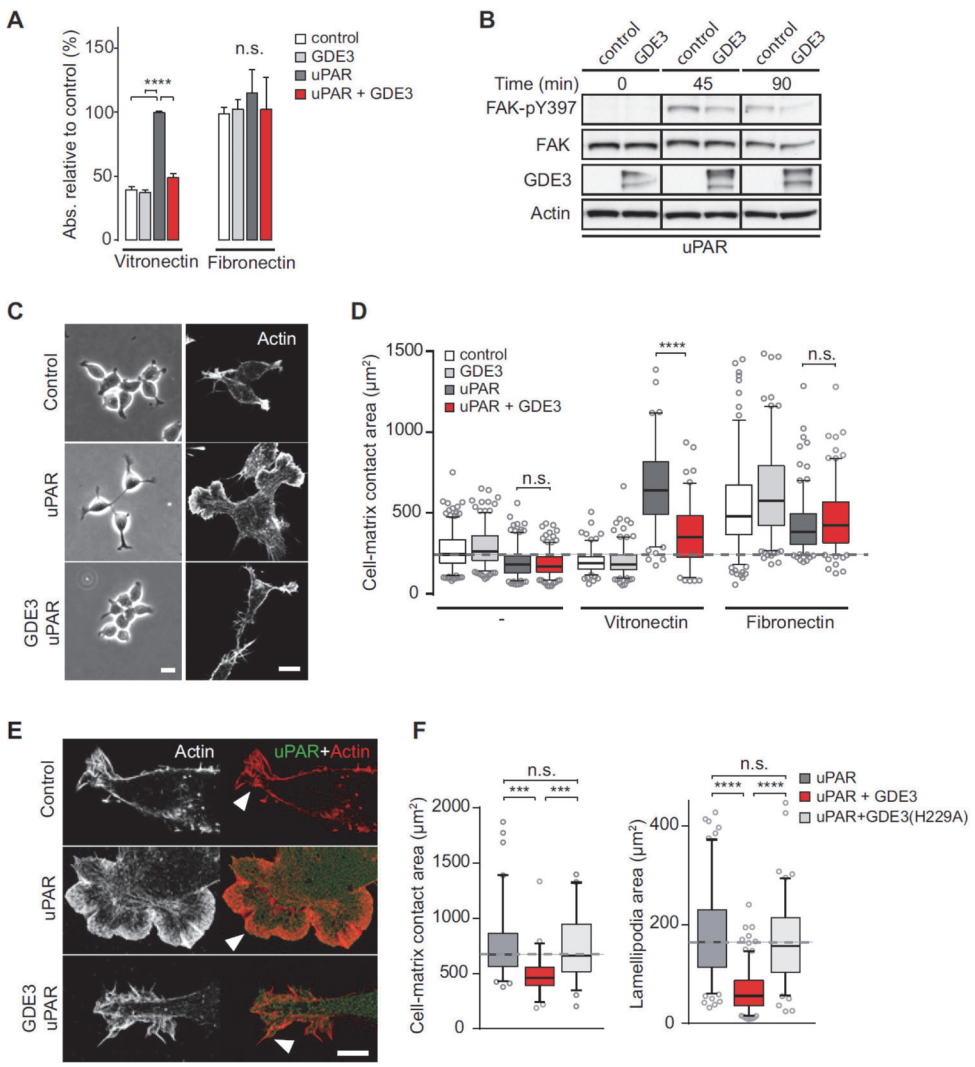

Figure 3. GDE3 suppresses uPAR activity in HEK-uPAR cells

(**A**) uPAR confers increased adhesion to vitronectin, but not fibronectin, which is prevented by GDE3 expression (n=3, mean ± SEM), ****P <0.0001; n.s., not significant. (**B**) GDE3 inhibits FAK activation during cell adhesion. FAK activity was assayed at the indicated times after plating. (**C**) GDE3 inhibits uPAR-induced cell spreading, scattering and lamellipodia formation on vitronectin (bar, 10 µm). (**D**) Cell-matrix contact area of cells expressing the indicated constructs plated on either fibronectin or vitronectin; (-) denotes cells on uncoated cover slips. Box plots show the mean of three independent experiments. Dotted line represents the mean of control cells (n=3, mean ± SEM, ****P<0.0001; n.s., not significant). **(E)** uPAR-induced lamellipodia on vitronectin disappear upon GDE3 expression, as shown by super-resolution microscopy (bar, 5 µm). (**F**) Quantification of cell-matrix contact area in GDE3- and GDE3(H229A)-expressing cells. GDE3(H229A) fails to affect lamellipodia formation (n=3, mean ± SEM ***P<0.001; ****P<0.0001).

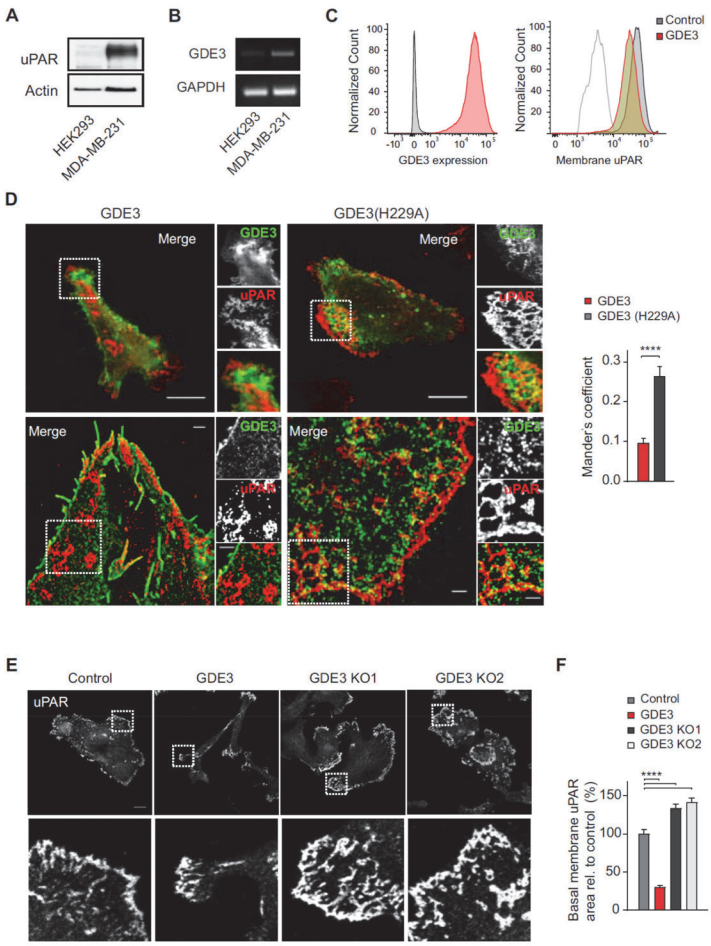

Figure 4. GDE3 depletes uPAR from distinct basolateral membrane domains in MDA-MB-231 breast cancer cells

(**A**) Endogenous uPAR expression in MDA-MB-231 versus HEK293 cells, as determined by immunoblot. **(B)** Endogenous *GDPD2* expression, as determined by qPCR analysis. (**C**) (left) Cell-surface expression of GDE3-mCherry of MDA-MB-231 cells expressing GDE3, as detected by flow cytometry. (Right) Cell-surface expression of uPAR in control (grey) and GDE3-expressing MDA-MB-231 cells (red), as detected by flow cytometry. (**D**) Confocal (top) and dual-color super-resolution microscopy images (bottom) of MDA-MB-231 cells expressing GDE3-GFP or catalytically dead GDE3(H229A)-GFP. Endogenous uPAR was immunostained in red. Merged images show colocalization of uPAR with GDE3(H229A) but not with wild-type GDE3 and uPAR. Scale bars, 10 μm (confocal) and 1 μm (super-resolution). Co-localization analysis (Mander's coefficient) on peripheral uPAR patches in confocal images was done using ImageJ software (n= 30 cells, three independent experiments). (**E**) Endogenous uPAR staining in control, GDE3-overexpressing and GDE3 knockout MDA-MB-231 cells plated on vitronectin. Two distinct GDE3 knockout clones (KO1 and KO2) were examined, as indicated. Scale bar,10 μm. (**F**) Quantification of basolateral uPAR-containing membrane domains referring to the cells in panel (**E**) (n=3, mean ± SEM, ****P<0.0001)

with this, CRISPR-based knockout of GDE3 resulted in increased basolateral uPAR levels when the cells were plated on vitronectin (Figure 4E,F; Figure 4 - Figure supplement 1).

Wild-type MDA-MB-231 cells adopted a motile phenotype on vitronectin, as evidenced by increased cell spreading with marked lamellipodia formation (Figure 5A-C), strongly reminiscent of a uPAR-regulated phenotype. Overexpressed GDE3 abolished the vitronectin-dependent phenotype of MBD-MB-231 cells (Figure 5A-C). Very similar effects of GDE3 overexpression were observed in another uPAR-positive breast cancer cell line (triple-negative Hs578T cells) (Figure 5 – Figure supplement 1). Of note, no effects were observed upon GDE2 overexpression in these cells (data not shown).

To confirm that GDE3 acts through uPAR attack, we expressed non-cleavable uPAR-TM to compete out endogenous uPAR, and found that the GDE3-induced reduction of cell spreading on vitronectin was largely inhibited (Figure 5B). Furthermore, shRNA-mediated knockdown uPAR (Figure 5D) gave rise to the same phenotype as GDE3 overexpression, namely reduced cell adhesion, spreading and lamellipodia formation on vitronectin (Figure 5E,F,G).

GDE3 overexpression attenuates the transformed phenotype, slows tumor growth in vivo and correlates with improved survival in breast cancer

In long-term assays, wild-type MDA-MB-231 cells showed marked scattering, indicative of increased cell motility with loss of intercellular contacts (Figure 6A). Again, GDE3 overexpression mimicked uPAR depletion either in greatly reducing both cell motility and clonogenic potential, using either shRNA-mediated knockdown (Figure 6A,B) or CRISPR-mediated knockout of uPAR (Figure 6 – figure supplement 1).

Having shown that GDE3 suppresses the non-proteolytic activities of uPAR, we next examined how GDE3 affects uPAR-driven proteolytic matrix degradation by MDA-MB-231 cells. Also in this cell system, GDE3 overexpression mimicked uPAR silicencing in inhibiting the degradation of a gelatin matrix (mixed with vitronectin) in the presence of serum (Figure 6C,D) (Figure 6 – figure supplement 1). On the basis of these results, we conclude that GDE3 attenuates the transformed phenotype of uPAR-positive breast cancer cells through loss of functional uPAR.

When injected into the mammary fat pads of female nude mice, GDE3-overexpressing MDA-MB-231 cells showed diminished tumor growth over time, when compared to empty vector-expressing cells (Figure 7A), consistent with the cell-based data. However, the full implications of GDE3 expression on uPAR-dependent tumor growth remain to explored in further detail. Finally, in patients, high expression of *GDPD2* was found to correlate with prolonged relapse-free survival in breast cancer, particularly in triple-negative (basal-like) subtype patients (N=618) (Figure 7B). No such correlation was found for GDE2 (encoded by *GDPD5*; not shown). This suggests that GDE3/GDPD5 may serve as a marker of clinical outcome in breast cancer.

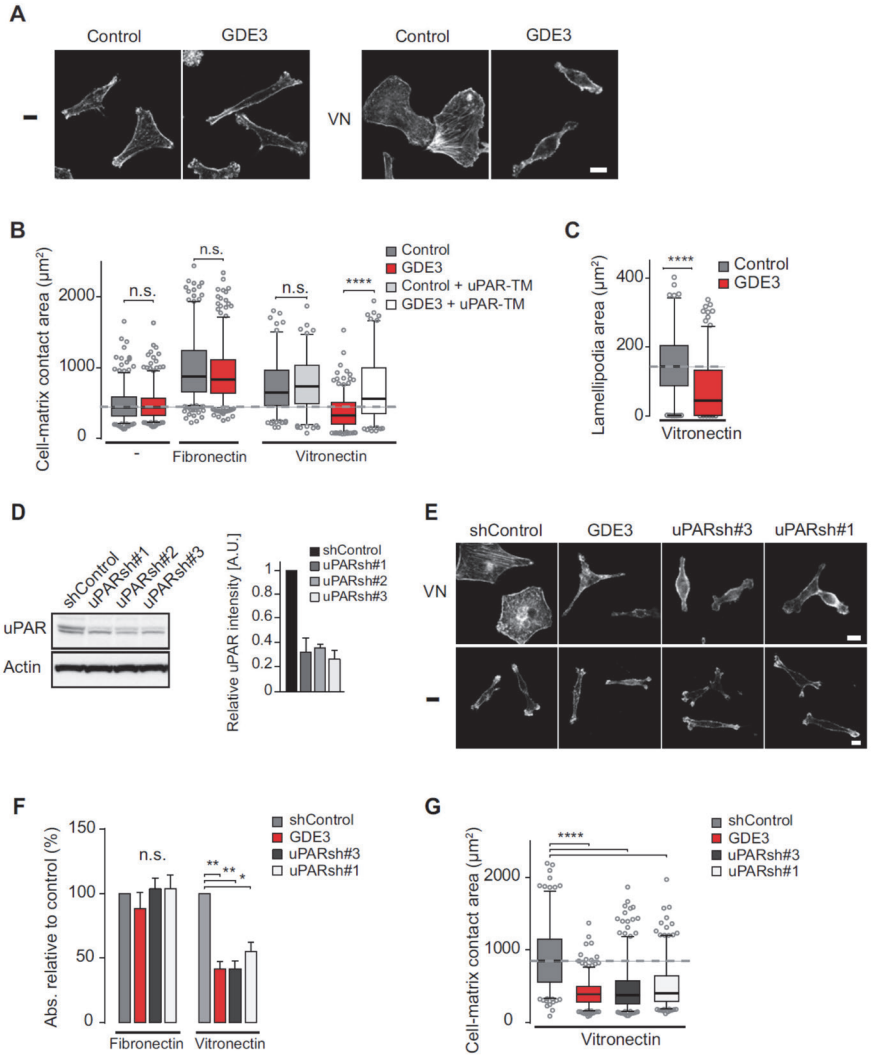

Figure 5. GDE3 suppresses the vitronectin- and uPAR-dependent phenotype of MDA-MB-231 breast cancer cells

(**A**) Confocal images showing that GDE3 prevents cell spreading and lamellipodia formation on vitronectin (VN) but not on uncoated cover slips (-). Bar, 10 µm. (**B**) Quantification of reduced cell spreading on vitronectin by GDE3. Non-cleavable uPAR-TM prevents GDE3 attack. ****P <0.0001; n.s., not significant. (**C**) Quantification of lamellipodia formation on vitronectin. ****P <0.0001. (**D**) Immunoblot analysis of shRNA-mediated uPAR knockdown; maximum knockdown was achieved by small hairpins #1 and #3. The upper protein band represents full-length uPAR, the lower band proteolytically cleaved uPAR(D2+D3) [145]. **(E)** GDE3 overexpression mimics the uPAR knockdown phenotype in cells plated on vitronectin (VN); bar, 10 µm. (-) denotes cells on non-coated cover slips.**(F,G)** Quantification of cell adhesion (**F**; n=3; mean ± SEM) and cell spreading (**G**) induced by GDE3 and uPAR knockdown on the indicated substrates. * P<0.05 ** P<0.001; ****P <0.0001.

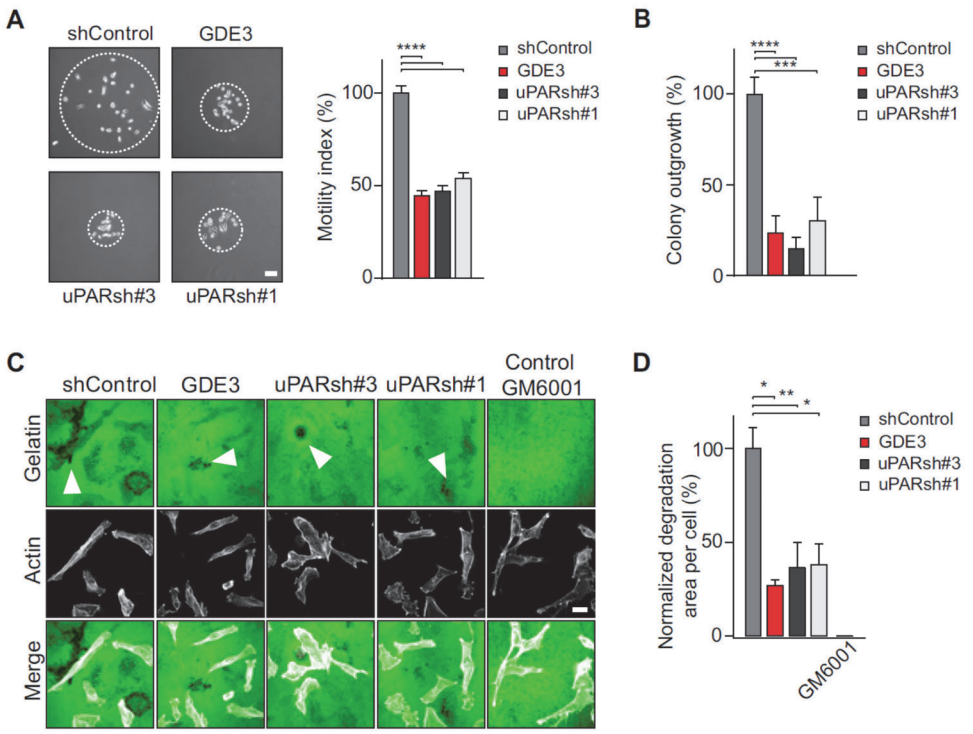

Figure 6. GDE3 overexpression attenuates the uPAR-dependent transformed phenotype of breast cancer cells

(**A**) GDE3 overexpression in MDA-MB-231 cells mimics uPAR knockdown in inhibiting cell scattering. MDA-MB-231 cells grow out as scattered colonies; bar, 100 μm (n=3, mean ±SEM **** P<0.0001). **(B)** GDE3 overexpression mimics uPAR knockdown in suppressing colony formation. colonies were counted after 14 days (n=3, mean ±SEM *** P<0.01; ****P<0.0001. **(C)** Degradation of a gelatin matrix mixed with vitronectin by MDA-MB-231 cells in the presence of serum (bar, 10 μm). Arrows point to black spots where gelatin was degraded. Metalloprotease inhibitor GM6001 was used as a control. (**D**) Quantification of matrix degradation at 20 hrs after plating (mean ± SEM; *P<0.05; ** P<0.001).

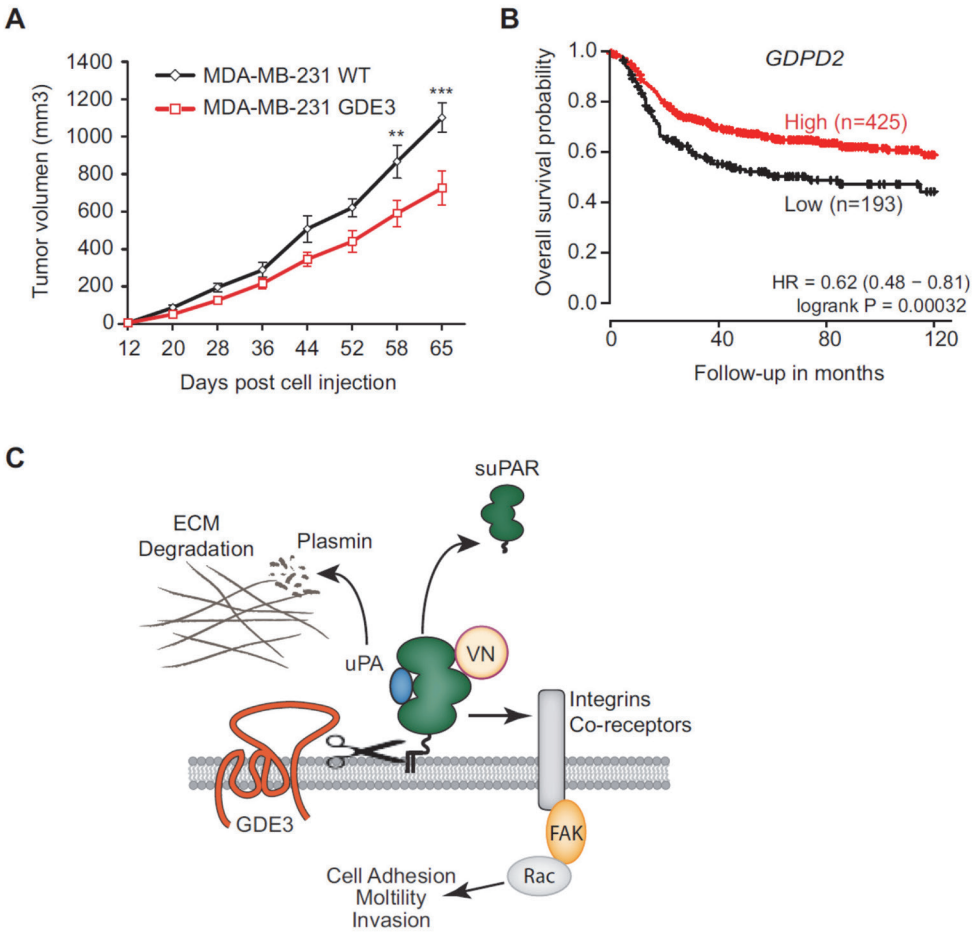

Figure 7. GDE3 overexpression in breast cancer cells slows tumor growth in mice, correlating with higher survival probability in patients

(A) Female nude mice were injected with wild-type and GDE3-overexpessing MDA-MB-231 cells into the mammary fat pad, as described under Materials and Methods. Tumor volume was measured every three days after injection for 9 weeks until the tumor had grown to the appropriated size (data represent the mean ± SEM,$^{***}P<0.001$, t-test corrected for multiple comparison). **(B)** High *GDPD2* expression significantly correlates with higher survival rate in triple-negative (basal-like) subtype breast cancer patients (N=618). HR, hazard ratio with 95% confidence interval indicated. Analysis based on microarray data (www.kmplot.com). **(C)** Schematic model. GDE3 functions as a GPI-PLC that cleaves and sheds uPAR, leading to loss of uPAR function. VN, vitronectin, FAK, focal adhesion kinase, suPAR, soluble uPAR.

Discussion

GPI-anchoring is a compIex post-translational modification that anchors select proteins in the outer leaflet of the plasma membrane. Despite decades of research, the biological significance of GPI anchors has long remained a mystery [146, 147]. Some GPI-anchored proteins are released from their anchor and detected in body fluids, implying involvement of one or more endogenous GPI-specific hydrolases. Recent studies have advanced the field by showing that cleavage and shedding of certain GPI-anchored proteins is mediated by a cell-intrinsic transmembrane glycerophosphodiesterase, termed GDE2 (or GDPD5), thereby promoting neuronal differentiation through multiple signaling pathways [110, 137, 138].

In this study, we focused on the shedding of GPI-anchored uPAR because of its regulatory role in multiple cellular and (patho)physiological activities, while soluble uPAR is considered a biomarker of various human pathologies. Here we report that GDE3 functions as a long-sought GPI-specific PLC that releases uPAR from its anchor. By contrast, its homologue GDE2 failed to release uPAR. As a consequence of GDE3 action, uPAR loses its vitronectin-dependent and matrix-degrading activities, when assayed in HEK293-uPAR and triple-negative breast cancer cells that express both uPAR and uPA. Importantly, loss of uPAR expression by GDE3 was found to be restricted to certain microdomains at the basolateral plasma membrane, where signal transduction is likely to take place. Thus, by acting as a GPI-specific PLC towards uPAR, GDE3 is a negative regulator of the uPAR signaling network (Figure 7C) that includes uPAR's proteolytic and non-proteolytic activities. Consistent with this, GDE3 overexpression in uPA/uPAR-positive MDA-MB-231 breast cancer cells slowed tumor progression in a xenograft mouse model. Although statistically significant, the inhibitory effect of GDE3 overexpression on tumor growth was not dramatic, which should not come as a surprise since MDA-MBA-31 cells express the strongly oncogenic mutant K-RAS protein, which tends to override the regulation of numerous signaling pathways. Yet, this finding adds to the relevance of GPI-specific phospholipases in slowing tumor progression. Furthermore, high GDE3 expression was found to correlate with increased survival probability in triple-negative breast cancer patients. Interestingly, our previous work revealed a similar association between overexpression of GDE2 and positive clinical outcome in neuroblastoma patients, which appears attributable to GDE2-induced glypican shedding[137]. The present patient survival analysis should be interpreted with caution, however, since involvement of uPAR release remains to be formally proven. Furthermore, we cannot rule out that GDE3 may cleave additional GPI-anchored substrates whose functional loss could contribute to positive clinical outcome.

The present results predict that, depending on its expression levels, GDE3 may downregulate normal uPAR-dependent remodeling processes. Indeed, upregulated GDE3 accelerates osteoblast differentiation [99, 115] in a manner resembling the uPAR knockout phenotype [148]. Furthermore, a striking >200-fold upregulation of *GDE3/GDPD2* is observed during

blastocyst formation [149], implicating GDE3 in the invasion of pre-implantation embryos, a process in which the uPA/uPAR signaling network has been implicated [150, 151]. Although correlative, these results support the view that GDE3 is upregulated to downregulate uPAR activity in vivo. The present findings also suggest that circulating full-length suPAR should be regarded as a marker of GDE3 activity, not necessarily reflecting uPAR expression levels.

It will now be important to determine how GDE3 expression and activity are regulated and, furthermore, to explore the substrate selectivity of the respective GDEs in further detail. Homology modeling revealed striking differences in electrostatic surface properties of GDE2 versus GDE3, suggesting that protein-protein interactions may determine substrate recognition by these GDE family members. Specific GPI-anchor modifications [146, 147] could also determine the sensitivity of GPI-anchored proteins to GDE attack.

Finally, when regarded in a broader context, the present and previous findings [110, 137, 138] support the view that vertebrate GDEs, notably GDE2 and GDE3, have evolved to modulate key signaling pathways and alter cell behavior through selective GPI-anchor cleavage.

Experimental Procedures

Cell culture and Materials

HEK293, MDA-MB-231 and Hs578T cells were obtained from the ATCC and grown in Dulbecco's modified Eagle's medium (DMEM) supplemented with 10% fetal bovine serum (FBS) and antibiotics at 37 °C under 5% CO2. Original MDA-MB-231 cells were pathogen tested using the ImpactI test (Idexx Bioresearch, Westbrook, ME, USA) and were negative for all pathogens tested. All cell lines were routinely tested negative for mycoplasma contamination. Antibodies used: anti-mCh and anti-GFP, home-made; anti-Flag, M2, anti-Vinculin and β-Actin (AC-15) from Sigma; anti-uPAR (MAB807) from R&D systems; anti-uPAR (13F6) [152]; anti-FAK(pTyr397) from Thermo Fisher. Vitronectin, fibronectin, inositol 1-phosphate (dipotassium salt) and inositol were purchased from Sigma-Aldrich. *B. cereus* PI-PLC was from Molecular Probes. Phalloidin red (actin-stain™ 647 phalloidin) and green (actin-stain™ 488 phalloidin) were from Cytoskeleton. GM6001 was from Millipore. Research Source Identifiers: MDA-MB-231 cells RRID:CVCL_0062; Hs578T cells RRID:CVL_0332; Antibodies: Flag M2 RRID:AB_259529; Anti Vinculin RRID:AB_10746313; Anti actin RRID:AB_2223210; uPAR RRID:AB_2165463.

Expression vectors

GDE2 cDNA was subcloned as described [137]. GDE3 cDNA was amplified by PCR and subcloned into a pcDNA3-HA plasmid using AflII/HpaI (PCR product) and AflII/EcoRV (plasmid) restriction sites. GDE3 was recloned into a pcDNA3(-mCherry) construct by PCR

amplification with restriction sites PmI1/Xba1, followed by vector digestion using EcoRV/Xba1. GDE6 transcript variant X7 (GDPD4; NCBI: XM_011544834.1) was cloned into pcDNA5_FRT_TO_puro (provided by dr. Geert Kops, University Medical Center Utrecht). All constructs were epitope- tagged on the C-terminus unless otherwise stated. Mutant GDE3(H229A) was generated by amplification with oligos containing the mutation, followed by Dpn1 digestion of the template. The viral plasmids (pBABE-GDE3-mCh, pBABE-uPAR-GFP) were constructed by subcloning the GDE3-pcDNA3 and uPAR-GFP-pEGFP-N1 into a pBABE plasmid. GDE3-mCherry-pcDNA3 was cut using PmeI followed by digestion of the pBABE backbone with SnaBI. uPAR-GFP-pEGFP-N1 was cut with BglII and HpaI and ligated into the pBABE vector, digested with BAMHI and SnaB1. Constructs uPAR-GFP, uPAR-FLAG and non-cleavable uPAR-TM were previously described [140, 153]. Transmembrane-anchored uPAR-TM was constructed by substituting the GPI-anchoring sequence of uPAR (aa 274-313) with the transmembrane region (aa 614-653) of the human epidermal growth factor receptor (EGFR), as described [140].

Transfections and RNA$_i$-mediated knockdown

Cells stably expressing uPAR-GFP or GDE3-mCherry were generated using retroviral transduction and subsequent selection with puromycin. Transient transfections were done using the calcium phosphate protocol or XtremeGene 9 agent (Roche). Stable uPAR knockdown in MDA-MB-231 cells was achieved using shRNAs in a lentiviral pLKO vector; five shRNAs from three RC human shRNA library were tested: TRCN0000052637, TRCN0000052636, TRCN0000052634, TRCN0000052633 and TRCN0000052635. The latter two were used for experiments; sequences: CCGGCCCATGAATCAATGTC TGGTACTCGAGTACCAGACATTGATTCATGGGTTTTTG and CGGGCTTGAAGA TCACCAGCCTTACTCGAGTAAGGCTGGTGATCTTCAAGCTTTTTG, respectively. For virus production, HEK293T cells were transiently transfected using calcium phosphate, and virus particles were collected 48 hr thereafter. uPAR knockdown cells were selected in medium containing 2 μg/ml puromycin.

CRISPR knockout

uPAR and GDE3 knockout cell lines were generated using CRISPR/Cas9 genome editing. CRISPR sequences were designed targeting uPAR (*PLAUR;* exon 2*; 5'-CATGCAGTGTAAGACCAACG-3' and 5'-CCAGGGCGCACTCTTCCACA-3'*) or GDE3 (*GDPD2; exon 2 ; 5'-AGGATGCAAACCAGCAAGG-3')* and cloned into pX330 [154]. MDA-MB-231 cells were transfected with the exon-specific pX330 plasmids in addition to a plasmid containing a guide RNA to the *Danio Rerio* TIA gene (5'- GGTATGTCGGGAACCTCTCC -3') and a cassette of a 2A sequence followed by a BlastR gene, flanked by two TIA target

sites. Co-transfection results in infrequent integration of the BlastR gene at the targeted genomic locus by NHEJ, as previously described [155]. Successful integration of the cassette renders cells resistant to blasticidin. Three days following transfection, the culture medium was supplemented with blasticidin (25 μg/ml). Surviving colonies were clonally expanded, screened for cassette integration and indels into the query gene by PCR (GDE3; 5'- TATGAATCCTGCCCGAAAAG-3' and 5'-AGAGCAGGCCAAACCAGATA-3') or by western blot analysis of the target protein (uPAR).

Liquid chromatography-mass spectrometry (LC-MS)

To determine the inositol phosphate content of cleaved uPAR, suPAR was immuno-precipitated from HEK293 cell conditioned medium using anti-GFP beads (ChromoTek). To remove inositol phosphate from suPAR, the beads were treated with 0.1M acetate buffer (pH 3.5) and subsequently with 0.5M $NaNO_2$ or 0.5M NaCl (Control) for 3 hrs as previously described [156]. Inositol phosphate-containing samples were preprocessed by adding methanol to a final concentration of 70% and shaken at 1000 RPM at room temperature for 10 minutes. Following centrifugation (20,400 x *g* at 4 °C for 10 min), the supernatant was evaporated to dryness in a Speedvac at room temperature. The dried extracts were reconstituted in 50 mM ammonium acetate (pH 8.0), centrifuged (20,400 x *g* at 4 °C for 10 min) and transferred to autosampler vials. Liquid chromatography (LC) was performed using a Dionex Ultimate 3000 RSLCnano system (Thermo Fisher Scientific). A volume of 5 μl was injected on a Zorbax HILIC PLUS column (150 x 0.5 mm, 3.0 μm particles) maintained at 30 °C. Elution was performed using a gradient: (0-5 min, 20% B; 5-45 min 20-100% B; 45-50 min 100% B; 50-50.1 min 20% B; 50.1-60 min 20% B) of 100% acetonitrile (mobile phase A) and 50 mM ammonium acetate adjusted to pH 8.0 with ammonium hydroxide (mobile phase B) at a flow rate of 15 μl/min. Inositol 1-phosphate was detected with an LTQ-Orbitrap Discovery mass spectrometer (Thermo Fisher Scientific) operated in negative ionization mode scanning from *m/z* 258 to 260 with a resolution of 30,000 FWHM. Electrospray ionization was performed with a capillary temperature set at 300 °C and the sheath, auxiliary and sweep gas flow set at 17, 13 and 1 arbitrary units (AU), respectively. Setting for Ion guiding optics were: Source voltage: 2.4 kV, capillary voltage: -18 V, Tube Lens: -83 V, Skimmer Offset: 0 V, Multipole 00 Offset: 5 V, Lens 0: 5 V, Multipole 0 Offset: 5.5 V, Lens 1: 11 V, Gate Lens Offset: 68 V, Multipole 1 Offset: 11.5 V, Front Lens: 5.5 V. Data acquisition was performed using Xcalibur software (Thermo Fisher Scientific). Reference inositol phosphate (Sigma) was used to determine the retention on the Zorbax HILIC plus column. After applying Xcalibur's build-in smoothing algorithm (Boxcar, 7), extracted ion chromatograms (*m/z* 259.02-259.03) were used to semi-quantitatively determine inositol phosphate levels.

Cell adhesion and spreading

48-wells plates were coated overnight at 4°C with fibronectin (10 μg/ml) or vitronectin (5 μg/ml), or left untreated. Thereafter, plates were blocked for 2 hr at 37°C using 0.5% BSA in PBS. Cells were washed and harvested in serum-free DMEM supplemented with 0.1% BSA. Equal numbers of cells were seeded and allowed to adhere for 1 hr. Non-adherent cells were washed away using PBS. Attached cells were fixed with 4% paraformaldehyde (PFA) for 10 min, followed by washing and staining with Crystal violet (5 mg/ml in 2% ethanol) for 10 min. After extensive washing, cells were dried and lysed in 2% SDS for 30 min. Quantification was done by measuring absorbance at 570 nm using a plate reader. For cell-matrix contact area and lamellipodia measurements, coverslips were coated overnight with fibronectin or vitronectin and washed twice with PBS. Cells were trypsinized, washed and resuspended in DMEM and left to adhere and spread for 4 hr. After fixation (4% PFA) and F-actin staining with phalloidin, images were taken using confocal microscopy. Cell and lamellipodia area was quantified using an ImageJ macro.

Cell scattering and colony formation

Cell scattering was determined as described [143]. In brief, single MDA-MB-231 cells were allowed to grow out as colonies, and the area covered by the scattered colonies (colony size) was measured at 6 days after plating. For measuring colony outgrowth, 500 cells were plated and colonies were counted after 14 days.

Matrix degradation

Coverslips were coated with OG-labelled gelatin (InVitrogen) supplemented with vitronectin (5 μg/ml). About 100.000 cells per coverslip were seeded in DMEM with 10% FCS. After 20 hrs, cells were washed, fixed with 4% PFM and stained with phalloidin-Alexa647 (InVitrogen). Gelatin degradation was determined from confocal images of >15 randomly automatically chosen fields of view per coverslip (testing at least two coverslips / condition on two separate days: total four coverslips per condition). The images were randomized and the area of degradation was normalized to the total area of cells or to the number of cells.

RT-qPCRT

Total RNA was isolated using the GeneJET purification kit (Fermentas). cDNA was synthesized by reverse transcription from 2 μg RNA with oligodT15 primers and SSII RT enzyme (Invitrogen). Relative qPCR was measured on a 7500 Fast System (Applied Biosystems) as follows: 95 °C for 2 min followed by 40 cycles at 95 °C for 15 sec followed by 60 °C for 1 min. 200 nM forward and reverse primers, 16 μl SYBR Green Supermix (Applied Biosystems) and diluted cDNA were used in the final reaction mixture. GAPDH was used as reference gene and milliQ was used as negative control. Normalized expression was calculated following the equation NE=2(Ct target-Ct reference). Primers used: GDE3, forward TCAGCAGGACCACGAATGTA, reverse

GCTGCAGCTTCCTCCAATAG; uPAR, forward AATGGCCGCCAGTGTTACAG, reverse CAGGAGACATCAATGTGGTTC; Cyclophilin, forward CATCTGCACTGCCAAGACTGA, reverse TTGCCAAACACCACATGCTT. For RT-PCR 25 ng cDNA was used in a RT-PCR reaction using GoTaq (Promega). Primer sequences GAPDH forward 5'-CCATGTTCGTCATGGGTGT-3', GAPDH reverse 5'-CCAGGGGTGCTAAGCAGTT-3', GDE3 forward 1 5'-TGTTTGAGACTGATGTGATGGTC-3', GDE3 reverse 1 5'-TTCGGGTTGGGAATACAGAG-3'

Western blotting

For Western blotting, cells were washed with cold PBS, lysed in RIPA buffer supplemented with protease inhibitors and spun down. Protein concentration was measured using a BCA protein assay kit (Pierce) and LDS sample buffer (NuPAGE, Invitrogen) was added to the lysate or directly to the medium. Equal amounts were loaded on SDS-PAGE pre-cast gradient gels (4-12% Nu-Page Bis-Tris, Invitrogen) followed by transfer to nitrocellulose membrane. Non-specific protein binding was blocked by 5% skimmed milk in TBST; primary antibodies were incubated overnight at 4° C in TBST with 2% skimmed milk. Secondary antibodies conjugated to horseradish peroxidase (DAKO, Glostrup, Denmark) were incubated for 1 hr at room temperature; proteins were detected using ECL Western blot reagent.

Triton X-114 phase separation

HEK293 cells transiently transfected with GDE2, GDE3 or empty plasmid, were plated on PEI-coated 6-well plates. After 24hrs complete medium was replaced with 1ml serum free medium, 24hrs thereafter the conditioned medium was collected. 2% pre-condensed Triton X-114 was added to ice-cold conditioned medium and phases were separated as previously described [157]. The top aqueous phase and the bottom detergent phase were analyzed by SDS-PAGE and Western blotting.

Microscopy

Cells cultured on 24 mm, #1,5 coverslips were washed and fixed with 4% PFA, permeabilized with 0.1% Triton X-100 and blocked with 2% BSA for 1 hr. Incubation with primary antibodies was done for 1 hr followed by incubation with Alexa-conjugated antibodies or Phalloidin for 45 min at room temperature. For confocal microscopy, cells were washed with PBS, mounted with Immnuno-MountTM (Thermo Scientific) and visualized on a LEICA TCS-SP5 confocal microscopy (63 x objective). Super-resolution imaging was done using a SR-GSD Leica microscope equipped with an oxygen scavenging system, as previously described [137]. In short, 15000 frames were taken in TIRF mode, at 10 ms exposure time. After post image analysis, movies were analyzed and corrected using the ImageJ plugin Thunderstorm (http://imagej.nih.gov/ij/) followed by correction with an ImageJ macro using the plugin Image Stabilizer. For Total Internal Reflection (TIRF) microscopy, HEK293 cells stably expressing

UPAR-GFP and transiently transfected with GDE3-mCherry were imaged using a Leica AM TIRF MC microscope with a HCX PL APO 63x, 1.47 NA oil immersion lens. Excitation was at 488 and 561 nm and detection of fluorescence emission was by a GR filter cube (Leica). Before each experiment, automatic laser alignment was carried out and TIRF penetration depth was set to 200 nm. Data were acquired at 500 ms frame rate. Basolateral uPAR patches were visualized using confocal microscopy and the area was quantified using an ImageJ macro that measured the uPAR patches based on fluorescence intensity.

Flow cytometry

HEK293 cells stably expressing uPAR-GFP were left untreated, treated with PI-PLC or transiently transfected with GDE3-mCherry. MDA-MB-231 cells were stably transfected with GDE3-mCherry. Cells were trypsinized, blocked in 2%BSA and stained with rabbit anti-GFP primary antibody or mouse anti-uPAR (13F6) antibody followed by AlexaFluor-647 coupled anti-rabbit secondary antibody. Cells were analyzed using a BD LSR Fortessa flow cytometer.

Mouse xenograft assay

Equal groups (n=16) of eight-week-old female NMRI nude mice were injected subcutaneously into the mammary fat pads. Prior to injection, GDE3-expressing or control MDA-MB-231 cells (5×105) were suspended in an equal volume of cold phosphate buffered saline and diluted 1:1 with Matrigel. The tumor growth was monitored 3 times a week for 9 weeks by caliper measurements. The tumor volumes were calculated with the formula: 0,5 x length x width¬2 and statistical analysis of the tumor growth was done using a multiple t-test corrected for multiple comparison. A P value < 0.05 was considered statistically different. The mouse experiments were approved by the Animal Ethics Committee of the Netherlands Cancer Institute (protocol number: 30100 2015 407 appendix 1 WP 6061).

Statistical analysis

For all single comparisons, a two-tailed unpaired Student's t-test was used; for multiple comparisons, an ordinary ANOVA with Tukey's test was used. A *P* value <0.05 was considered statistically significant. Error bars shown in the bar diagrams were calculated as the standard error of the mean (SEM); whiskers in the box plots depict 95% confidence intervals.

Acknowledgments

We thank the people from the Preclinical Intervention Unit of the Mouse Clinic for Cancer and Ageing (MCCA) at the NKI for performing the animal experiments. This work was supported by the Netherlands Organisation for Scientific Research (NWO) and the Dutch Cancer Society (KWF).

Supplementary figures

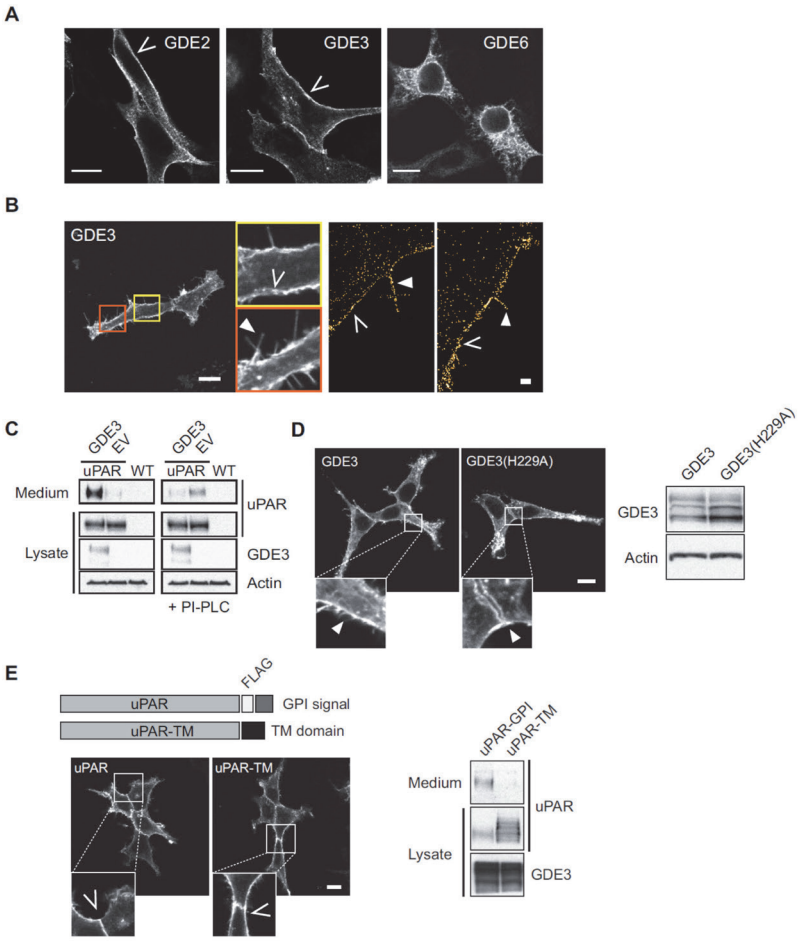

Figure 1. Figure supplement 1. GDE subcellular localization and induction of uPAR release from HEK293-uPAR cells

(**A**) Confocal images of HEK293 cells expressing human GDE2-HA, GDE3-HA or GDE6-HA, as indicated; bar, 10 μm. (**B**) GDE3 localizes to distinct microdomains (yellow square, open arrows) and filopodia-like extensions (orange square, solid arrow), as visualized by confocal and super-resolution microscopy. Bars, 10 μm and 1 μm respectively. (**C**) Immunoblot analysis showing that GDE3 reduces the membrane-anchored uPAR pool and competes with PI-PLC. The medium and lysates of HEK-uPAR cells expressing GDE3 or empty vector (EV) were analyzed without or with PI-PLC treatment (45 min.) of the cells, as indicated (left and right panels, respectively). Right lanes refer to wild-type (WT) HEK293 cells. **(D)** Expression and localization of GDE3 and mutant GDE3(H229A), as measured by immunoblotting and confocal microscopy, respectively, at 24 hrs after transfection. Actin was used as a loading control. (**E**) uPAR-TM containing the transmembrane domain of EGFR is not released by GDE3, as shown by immunoblotting using anti-uPAR antibody, while uPAR-TM is properly expressed at the plasma membrane (bar, 10 μm).

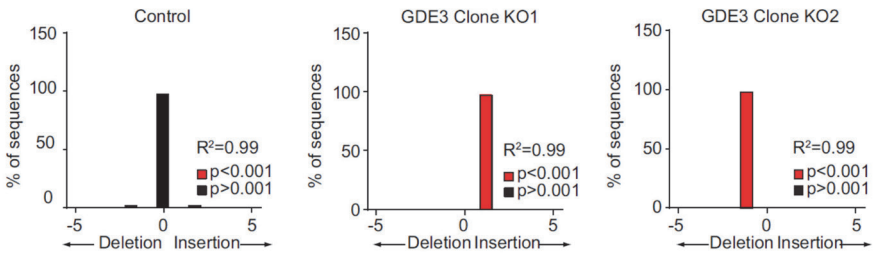

Figure 4. Figure supplement 1. GDE3 knockout validation

GDE3 knockout in MDA-MB231 cells was achieved using CRISPR/Cas9 genome editing. Surviving colonies were screened for cassette integration and indels into the query gene by PCR. Two genetically individual clones (KO1 and KO2) were selected, and knockout was confirmed using Sanger sequencing followed by TIDE deconvolution [158].

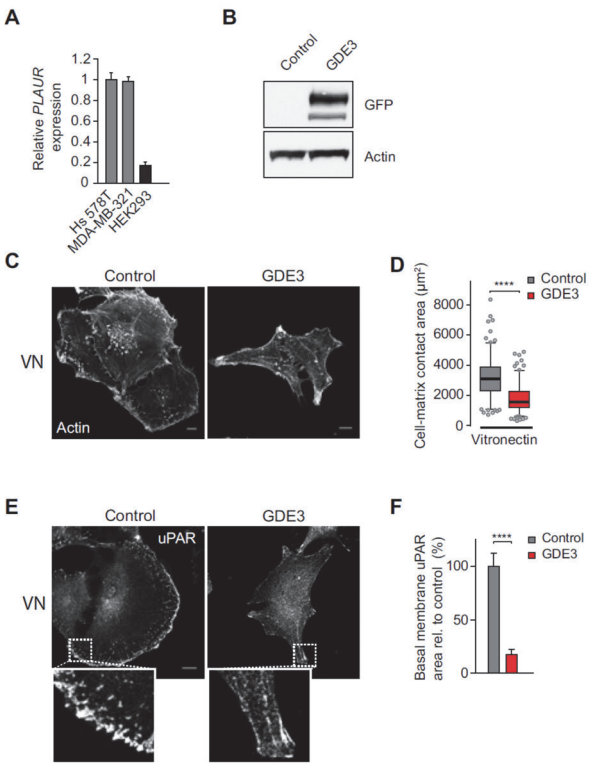

Figure 5. Figure supplement 1. GDE3 overexpression suppresses the uPAR-vitronectin-dependent phenotype in Hs578T breast cancer cells

(**A**) Relative expression of uPAR (encoded by *PLAUR*)) in the indicated cell lines, as determined by qPCR. (**B**) GDE3-GFP expression in Hs578T cells, using anti-GFP antibody. (**C**) Confocal images showing cell morphology (F-actin staining) of GDE3-expressing versus control cells plated on vitronectin (Bar, 10 µm). (**D**) Quantification of cell area of GDE3-expressing versus control Hs578Tcells, plated on vitronectin (n=3, mean ± SEM, ****P <0.0001). (**E**) Hs578T cells with or without stable GDE3-GFP expression were plated on vitronectin and stained for endogenous uPAR. Representative images of the basolateral membrane are depicted. Bar, 10 µm. (**F**) uPAR in the basolateral membrane was quantified in control and GDE3-expressing Hs578T cells plated on vitronectin (n=3, mean ± SEM, ****P <0.0001).

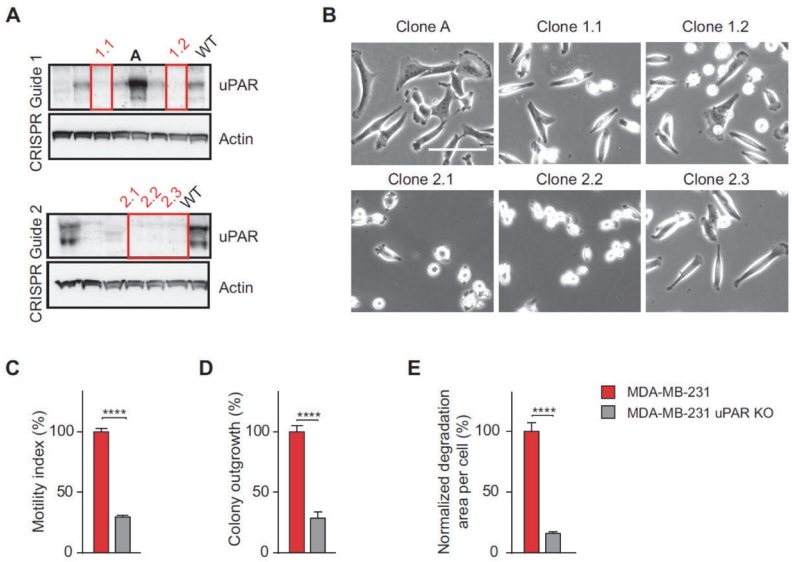

Figure 6. Figure supplement 1. uPAR knockout in MDA-MB-231 cells phenocopies GDE3 overexpression

(**A**) uPAR knockout in MDA-MB-231 cells was achieved using CRISPR/Cas9 genome editing. uPAR knockout was assayed by immunoblot analysis using anti-uPAR antibody. Individual clones were picked and plated on vitronectin. (**B**) uPAR-deficient MDA-MB-231 cells show GDE3 overexpression phenotype. uPAR KO cells show decreased cell spreading and lamellipodia formation on vitronectin. scattering (bar, 100 μm). (**C**) uPAR-deficient MDA-MB-231 cells show reduced cell motility (n=3, mean ±SEM **** $P<0.0001$). (**D**) MDA-MB-231 wild-type or uPAR knockout colonies were counted after 14 days. **** $P<0.001$. (**E**) Gelatin matrix degradation by wild-type and uPAR-deficient MDA-MB-231. Degradation was quantified at 20 hrs after plating (mean ± SEM **** $P<0.0001$).

PINUS SYLVESTRIS

Chapter 3

Glycerophosphodiesterase GDE2 Promotes Neuroblastoma Differentiation through Glypican Release and is a Marker of Clinical Outcome

Cancer Cell 2016;30:548-562.

Elisa Matas-Rico[1], Michiel van Veen[1], Daniela Leyton-Puig[1], Jeroen van den Berg[1], Jan Koster[2], Katarzyna M. Kedziora[1], Bas Molenaar[1], Marjolein J.A. Weerts[1], Iris de Rink[3], René H. Medema[1], Ben N.G. Giepmans[1,5], Anastassis Perrakis[4], Kees Jalink[1], Rogier Versteeg[2], and Wouter H. Moolenaar[1]

[1] Division of Cell Biology, The Netherlands Cancer Institute, Amsterdam, Netherlands
[2] Department of Oncogenomics, Academic Medical Center, University of Amsterdam, Amsterdam, Netherlands
[3] Deep Sequencing Core Facility
[4] Division of Biochemistry, The Netherlands Cancer Institute, Amsterdam, Netherlands
[5] Present address: Department of Cell Biology, University Medical Center Groningen, Groningen, the Netherlands

Abstract

Neuroblastoma is a pediatric embryonal malignancy characterized by impaired neuronal differentiation. A better understanding of neuroblastoma differentiation is essential for developing new therapeutic approaches. GDE2 (encoded by *GDPD5*) is a six-transmembrane-domain glycerophosphodiesterase that promotes embryonic neurogenesis. We find that high *GDPD5* expression is strongly associated with favorable outcome in neuroblastoma. GDE2 induces differentiation of neuroblastoma cells, suppresses cell motility and opposes RhoA-driven neurite retraction. GDE2 alters the Rac-RhoA activity balance and the expression of multiple differentiation-associated genes. Mechanistically, GDE2 acts by cleaving (in *cis*) and releasing glycosylphosphatidylinositol-anchored glypican-6, a putative co-receptor. A single point mutation in the ectodomain abolishes GDE2 function. Our results reveal GDE2 as a cell-autonomous inducer of neuroblastoma differentiation with prognostic significance and potential therapeutic value.

Introduction

Neuroblastoma is a childhood cancer of the developing sympathetic nervous system, and the most common cancer in infancy. It develops from immature neuroblasts in the embryonic neural crest and is characterized by impaired neuronal differentiation [159-161]. It commonly originates in the adrenal gland, but can also develop in nerve tissues elsewhere in the body. Neuroblastoma is a highly heterogeneous disease. In some cases, the tumor undergoes spontaneous regression through mechanisms that remain poorly understood [162]. In many cases, however, neuroblastoma progresses into a high-risk metastatic disease with very poor prognosis. Remarkably, high-risk neuroblastoma is characterized by relatively few recurrent somatic mutations [163, 164]. The paucity of oncogenic mutations, along with an incomplete understanding of neuroblastoma differentiation and regression, hampers the development of new targeted therapies.

In general, overall survival of neuroblastoma patients is largely dependent on the degree of neuronal differentiation and, furthermore, inversely correlated with a motile phenotype [160, 165]. Consistent with this, some high-risk neuroblastomas are associated with mutations in Rac-Rho pathway genes that normally regulate F-actin-based neurite outgrowth and remodeling, as well as tumor cell motility, invasion and metastasis [163]. Unfortunately, treatment options are very limited for high-risk neuroblastoma. One strategy involves differentiation therapy using *cis*-retinoic acid, but this has led to disappointing results [166-168]. Thus, there remains an urgent need to identify new therapeutic targets and develop differentiation-inducing protocols [169]. A better understanding of neuroblastoma differentiation at the molecular level is therefore imperative.

In this study we focus on GDE2 (or GDPD5), a transmembrane ecto-phosphodiesterase that promotes embryonic neurogenesis [108]. GDE2/GDPD5, along with GDE3/GDPD2 and GDE6/GDPD4, belongs to a subfamily of glycerophosphodiester phosphodiesterases (GDEs or GDPDs) characterized by six transmembrane domains and a large catalytic ectodomain [96, 97] (Figure 1A,B). GDE2 promotes the differentiation of postmitotic motor neurons in vivo by inhibiting Notch signaling in adjacent neural progenitors [109]. GDE3 has been implicated in osteoblast differentiation [99, 115], while the function of GDE6 is unknown. Mechanistically, GDE2 acts by cleaving the gycosylphosphatidylinositol (GPI) anchor of RECK, a Notch ligand regulator, leading to RECK release from the cell surface and subsequent induction of differentiation in contacting neuronal cells [110]. Thus, GDE2 promotes neurogenesis in a non-cell-autonomous manner, requiring cell-cell contact, at least in the developing spinal cord.

In view of these findings, we set out to examine a possible role of GDE2 in regulating neuroblastoma differentiation.

Results

GDPD5 Expression Levels Strongly Correlate with Clinical Outcome in Neuroblastoma

We examined how *GDPD5* expression relates to overall survival in neuroblastoma, using mRNA expression data of primary tumor samples from three independent patient cohorts (AMC, Obertheuer and RPM datasets; n=871 patients). *GDPD5* maps to chromosome 11q13, a region often showing loss of heterozygosity in neuroblastoma [159], Kaplan-Meier analysis revealed that high *GDPD5* expression is strongly associated with favorable clinical outcome, while low *GDPD5* expression correlates with poor outcome in all three patient cohorts (Figure 1C). This marks *GDPD5* as a potential tumor suppressor, but no mutations or deletions were detected in tumor samples analyzed by whole genome sequencing [163]. Furthermore, *GDPD5* expression in patients with an 11q deletion was similar to those with a normal chromosome 11, while there was no significant association with *MYCN* amplification (p=0.08) or *ALK* mutation status (p=0.66, Fisher's Exact test; data not shown),

GDE2 promotes neurogenesis through loss of functional RECK [110]; however, we found no significant correlation between *RECK* expression and patient survival (data not shown). Of note, GDE2 family members GDE3 and GDE6 (encoded by *GDPD2* and *GDPD4*, respectively; Figure 1A) were not detectably expressed at the mRNA level in the tumors analyzed, and therefore appear not to have clinical significance in neuroblastoma. These results define high *GDPD5* expression as a favorable prognostic marker in neuroblastoma. We went on to examine how GDE2 affects neuroblastoma cell behavior and to explore its signaling functions and pertinent catalytic activity.

GDE2 Promotes Differentiation of Neuroblastoma Cells in an Autonomous Manner

We used established models of neuroblastoma differentiation, including SH-SY5Y, IMR-32, Neuro-2A and N1E-115 cells; in the latter cells, Rho/Rac signaling and neurite remodeling pathways have been extensively studied. Overexpression of GDE2 in N1E-115 or Neuro-2A cells resulted in prominent cell spreading and neurite outgrowth (Figure 2A-C, Figure S1A). Similarly, expression of doxycycline-inducible GDE2 in either SH-SY5Y or IMR-32 cells led to GDE2 overexpression concomitant with increased neurite outgrowth after doxycycline addition (Figure 2D,E). GDE2-induced neurite outgrowth was accompanied by upregulation of various established neural differentiation genes, including *NEUROD1*, *SNAP25*, *ENO2, TUBB3* and *MAP2* (Figure 2F).

During embryonic development, GDE2 promotes neurogenesis in non-cell-autonomous manner involving contact-dependent Notch signaling [109]. In neuroblastoma cells, however, GDE2-induced cell spreading and neurite formation was observed in both isolated and contacting cells (Figure S1B). Furthermore, conditioned medium from GDE2-overexpressing cells did not affect the morphology of parental cells (results not shown), arguing against the

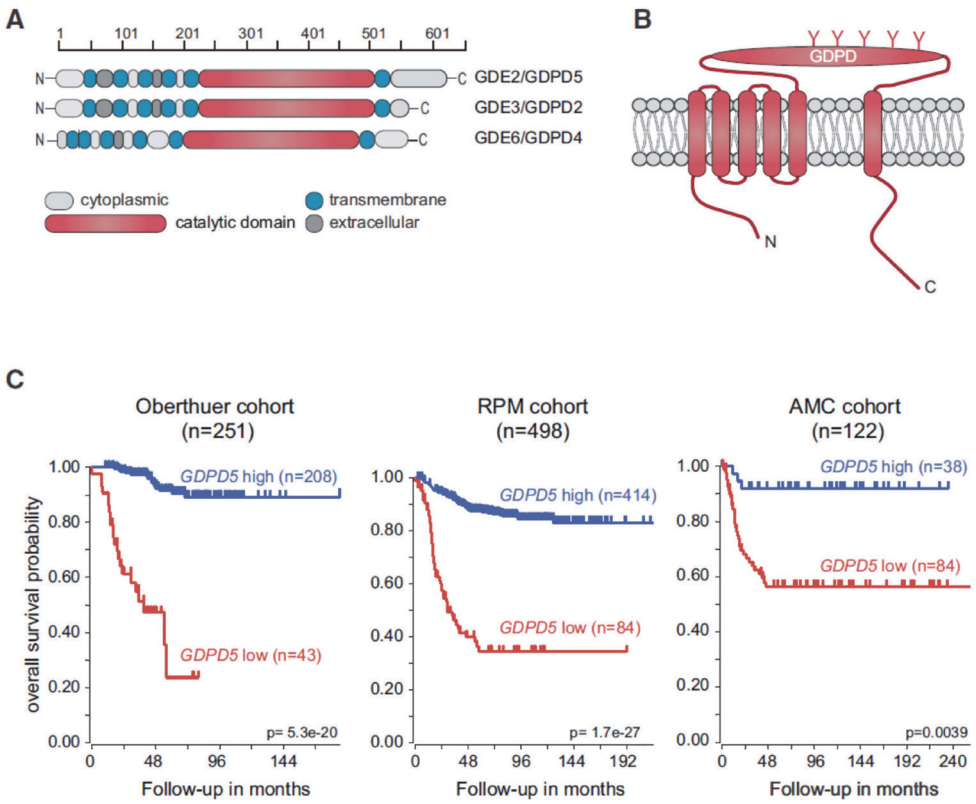

Figure 1. GDE2: its Family Members and Prognostic Significance in Neuroblastoma
(A) GDE2 (or GDPD5) and its close relatives GDE3 (GDPD2) and GDE6 (GDPD4) contain six transmembrane domains and a large catalytic ectodomain, as illustrated. **(B)** Schematic representation of GDE2, with five potential N-glycosylation sites indicated. **(C)** Kaplan-Meier analysis of overall survival in three independent neuroblastoma patient cohorts, as indicated: Oberthuer (n=251; ArrayExpress: E-TABM-38), Neuroblastoma RPM/SEQC (n=498; GEO: GSE62564) and AMC/Versteeg (n=122; GEO: GSE16476 88/122). The graphs depict the p values corrected for the multiple testing (Bonferroni correction) of cut-off levels for *GDPD5*. Family members *GDPD2* and *GDPD4* were not detectably expressed in the tumor samples analyzed.

involvement of a diffusible factor produced by GDE2. It thus appears that GDE2 promotes neuroblastoma differentiation in a cell-autonomous manner, not requiring cell-cell contact.

Various human neuroblastoma cells, including SH-SY5Y, are responsive to retinoic acid (RA), a known inducer of neuronal differentiation that is used as a therapeutic in the clinic [166, 169, 170]. RA upregulates GDE2 expression in the ventricular zone [108] and in Neuro-2A cells [107], but it did not in SH-SY5Y cells (Figure S1C). Upon forced overexpression

in SH-SY5Y cells, GDE2 enhanced the neurite-inducing effect of RA (2 μM) (Figure S1D), strongly suggesting that GDE2 and RA act cooperatively to induce differentiation.

GDE2-overexpresssing SH-SY5Y and IMR-32 cells adhered markedly stronger to extracellular matrix molecules (laminin, fibronectin, collagen) than did the parental cells (Figure 2G). Cell-matrix adhesion is a major determinant of cell motility, and a motile phenotype is associated with increased incidence of metastases and poor prognosis in neuroblastoma [165]. By monitoring the random motility of SH-SY5Y and IMR-32 cells, we established that GDE2 overexpression renders the cells less motile than the wild-type cells (Figure 2H).

When expressed at relatively low levels, GDE2 was detected both at the plasma membrane and in intracellular compartments as revealed by confocal and super-resolution microscopy (Figure S1E,F). Plasma membrane GDE2 localized to distinct microdomains, possibly representing lipid rafts, and was particularly enriched at the tips of neurite-like extensions (Figure S1F). Intracellularly, a relatively large subset of GDE2-containing vesicles was positive for established markers of recycling endosomes, notably Rab11 and the transferrin receptor (TfR) [171, 172] (Figure S1G,H). This suggests that internalized GDE2 follows a Rab11-driven recycling route as a way of regulation. We further note that, once internalized, GDE2 has its catalytic ectodomain exposed to the vesicle lumen and hence cannot act on cytosolic substrates.

⟶ **Figure 2. GDE2 Induces Neuroblastoma Cell Differentiation and Suppresses Cell Motility (A,B)**

Images of N1E-115 cells expressing GDE2-mCh or GDE2-GFP. Note flattened morphology and neurite outgrowth in GDE2-ovexpressing cells (A, black arrows), when compared to non-transfected cells. Bar, 10 μm. In (B), cells were stained with phalloidin to visualize F-actin. Cells transfected with empty vector were used as control. GDE2-GFP in green, F-actin in red. Bar, 10 μm. **(C)** Quantitative analysis of distinct morphologies of GDE2-overexpressing versus empty vector-expressing cells. (Left) Percentage of cells with a round or flattened morphology (assayed in the presence of serum). (Middle) Neurite induction; (Right) Neurite length (three independent experiments; n>300 cells; error bars, mean ± SEM) **** p value < 0.0001 of Fisher's (left, middle) and unpaired t tests (right). **(D)** SH-SY5Y and IMR-32 cells containing doxycyclin (Dox)-inducible GDE2 show longer neurites after Dox (1 μM) addition (bar, 100 μm). Immunoblots (using anti-GDE2 antibody) show Dox-induced GDE2 expression over a 3-72 hr time period. **(E)** Quantification of Dox-induced neurite outgrowth (n = 250 cells; mean ± SEM). **(F)** Dox-induced GDE2 overexpression promotes induction of neural differentiation marker genes *NEUROD1*, *SNAP25*, *ENO2*, *TUBB3* and *MAP2*, but not *NPY* and *GAP43*, as determined by qPCR in SH-SY5Y cells. Error bars represent SEM of triplicate measurements. **(G)** Dox-induced GDE2 overexpression promotes cell-matrix adhesion. At 1 hr after plating, adherent SH-SY5Y and IMR-32 cells were fixed and stained with Crystal Violet for quantification. Error bar represents SD of two independent experiments. **(H)** Random cell motility of individual SH-SY5Y and IMR-32 cells expressing inducible GDE2-mCh (red) or empty vector (black), plated on fibronectin. Tracks were generated from time-lapse movies (12 hr, 10-min. intervals). Graphs show mean migration distances of control versus GDE2-mCh-expressing SH0SY5Y and IMR-32 cells. In panels E-H, * p value < 0.05; ** p value <0.01 *** p value <0.001 **** p value <0.0001 of unpaired t-test. See also Figure S1.

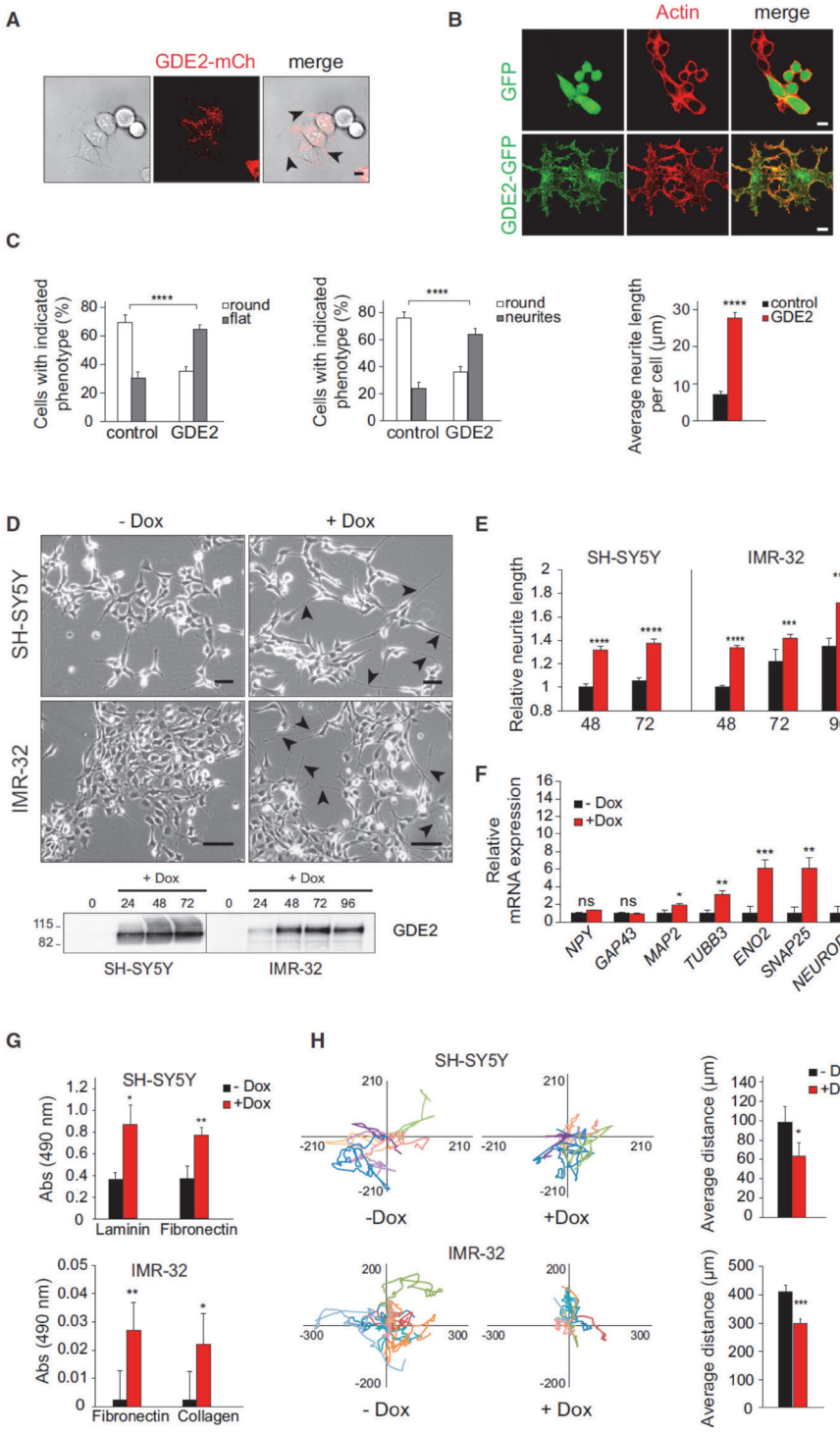
A
GDE2-mCh
merge
B
Actin
merge
GFP
GDE2-GFP
C
Cells with indicated phenotype (%)
round
flat
control
GDE2
round
neurites
Average neurite length per cell (µm)
control
GDE2
D
- Dox
+ Dox
SH-SY5Y
IMR-32
+ Dox
0 24 48 72
0 24 48 72 96
115
82
GDE2
SH-SY5Y
IMR-32
E
SH-SY5Y
IMR-32
- Dox
+Dox
Relative neurite length
48 72 48 72 96 [hr]
F
Relative mRNA expression
- Dox
+Dox
ns
NPY
GAP43
MAP2
TUBB3
ENO2
SNAP25
NEUROD1
G
SH-SY5Y
Abs (490 nm)
Laminin
Fibronectin
IMR-32
Fibronectin
Collagen
H
SH-SY5Y
-Dox
+Dox
IMR-32
- Dox
+ Dox
Average distance (µm)

GDE2 Opposes RhoA-Mediated Neurite Retraction and Activates Rac

Rho GTPases, particularly RhoA, Rac and Cdc42, are key regulators of F-actin-driven processes, including neuronal differentiation, cell adhesion, motility and invasion [173-177]. One hallmark of developing neurites is their susceptibility to acute retraction by RhoA-activating agonists such as lysophosphatidic acid (LPA), a lipid mediator acting on specific G protein-coupled receptors. As such, LPA antagonizes the phenotypic differentiation of neuroblastoma and neural/stem progenitor cells [178-182]. Strikingly, GDE2-overexpressing N1E-115 cells were unable to retract their developing neurites and round up in response to LPA, whereas the parental cells responded vigorously (Figure 3A,B; Figure S2; Movie S1 and S2). The apparent loss of LPA/GPCR responsiveness upon GDE2 overexpression is reminiscent of an activated Tiam1-Rac phenotype, where Rac hyperactivation is sufficient to inhibit LPA/RhoA-induced cytoskeletal contraction [183, 184]. GDE2-overexpressing N1E-115 or SH-SY5Y cells indeed showed a marked increase in basal Rac activity, which was insensitive to LPA stimulation (Figure 3C). Furthermore, we confirmed that expression of hyperactive Rac(L61A) induced prominent neuroblastoma cell spreading and conferred complete resistance to cytoskeletal contraction by LPA (results not shown).

Active Rac is known to oppose RhoA at multiple levels [175, 183-186]. We monitored LPA-induced RhoA activation in real-time using a RhoA-specific FRET-based biosensor, as described [187]. In parental N1E-115 cells, LPA evoked an immediate increase in RhoA activity that gradually levelled off to a sustained elevated level (Figure 3D). Upon GDE2 overexpression, however, the magnitude of LPA-induced RhoA activation was about 3-fold reduced (Figure 3D). Decreased RhoA activation was also observed in SH-SY5Y cells (Figure

⟶ **Figure 3. GDE2 Opposes RhoA-driven Neurite Retraction by LPA and Activates Rac** **(A)** Serum-starved N1E-115 cells expressing GDE2-mCh were stimulated with LPA (1 μM) for the indicated times. GDE2-mCh-expressing cells are indicated by black arrows, non-transfected cells by white arrows. Bar, 10 μm. **(B)** Quantification of LPA-induced cell rounding over time in control and GDE2- overexpressing cells (n= 200 cells; mean ± SEM). * p value < 0.05; *** p value < 0.001 of unpaired t-test. **(C)** Rac activity was measured in cells expressing empty vector (pcDNA3) or GDE2-GFP. Active GTP-bound Rac was assessed by pull-down assays and compared to total Rac levels in lysates of the same transfectants. (Left) Effect of LPA stimulation on Rac-GTP levels. (Middle) Densitometry analysis of Rac-GTP versus total Rac levels in the presence or absence of LPA (mean ± SEM of three independent experiments). * p value < 0.05 of unpaired t-test. (Right) Western blot showing Rac activity in SH-SY5Y cells as a function of GDE2 expression and LPA stimulation. **(D)** (Left) Activation of RhoA in N1E-115 cells expressing either GDE2-mCherry (red trace) or mCherry-CAAX (black trace) was monitored by a FRET-based biosensor. An increase in YFP/CFP ratio indicates increased RhoA activity (see Experimental Procedures). (Middle) Maximum RhoA activation by LPA (n= 9, mean ± SEM). ** p value < 0.01 of Wilcoxon test. (Right) Western blot of RhoA-GTP levels in Dox-induced SH-SY5Y cells. **(E)** Confocal images of N1E-115 cells transfected with Myc-RhoA(V14A) or co-transfected with GDE2-mCh and stained for Myc. GDE2 in red, RhoA(V14A) in green. Bar graph shows quantitation of morphology of RhoA(V14A)-expressing versus RhoA(V14A)/GDE2 co-expressing cells (n=300 cells, mean ± SEM); * p value < 0.05 of unpaired t-test. Bar 10 μm. See also Figure S2 and Movie S1 and S2.

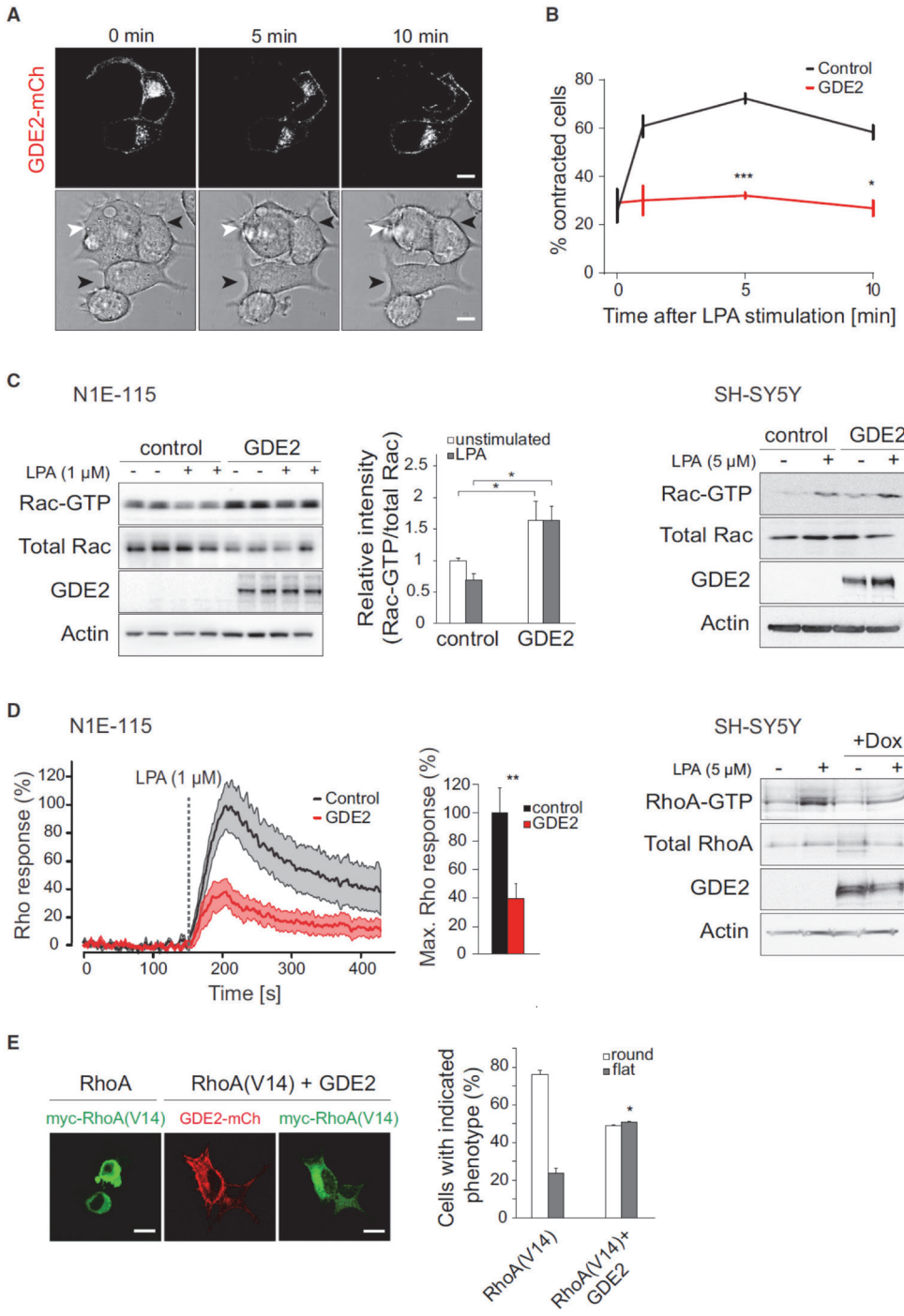
A
0 min
5 min
10 min
GDE2-mCh
B
% contracted cells
Control
GDE2
***
*
Time after LPA stimulation [min]
C
N1E-115
control
GDE2
LPA (1 µM)
Rac-GTP
Total Rac
GDE2
Actin
Relative intensity (Rac-GTP/total Rac)
unstimulated
LPA
control
GDE2
SH-SY5Y
LPA (5 µM)
D
N1E-115
LPA (1 µM)
Rho response (%)
Time [s]
Max. Rho response (%)
SH-SY5Y
+Dox
RhoA-GTP
Total RhoA
E
RhoA
RhoA(V14) + GDE2
myc-RhoA(V14)
GDE2-mCh
Cells with indicated phenotype (%)
round
flat
RhoA(V14)
RhoA(V14)+ GDE2

3D). Furthermore, overexpressed GDE2 opposed constitutively active RhoA(V14A) in promoting cell contraction, again consistent with an activated Rac phenotype (Figure 3E). From these results, along with previous findings on Rac-RhoA antagonism, we conclude that high GDE2 expression prevents neurite retraction by activating Rac and opposes RhoA action both at the level of RhoA-GTP accumulation and more downstream.

GDE2 Depletion Reverses the GDE2 Overexpression Phenotype and Uncovers GDE2-Regulated Gene Expression

Since low *GDPD5* expression correlates with poor clinical outcome, we examined how GDE2 depletion affects neuroblastoma phenotype through lentiviral shRNA transduction. To this end, we used Shep2 cells since these cells show relatively high *GDPD5* expression among 24 human neuroblastoma cell lines analyzed (Figure 4A; Figure S3). Using two (out of five) independent shRNAs, we achieved efficient GDE2 knockdown (Figure 4B). When compared to shControl cells, GDE2-depleted Shep2 cells were less well spread and

⟶ **Figure 4. GDE2 Depletion Reverses the GDE2 Overexpression Phenotype and Uncovers GDE2-Regulated Gene Expression**

(A) Immunoblot of GDE2 expression in the indicated cell lines, using anti-GDE2 antibody. See Figure S3 for *GDPD5* mRNA expression analysis. **(B)** (Left) *GDPD5* expression (relative to *GAPDH*) in control and GDE2-depleted Shep2 cells stably expressing shRNAs against GDE2. Maximal GDE2 knockdown was obtained with hairpins #4 and #5. Error bars, mean ± SEM; ** p value < 0.01; *** p value < 0.001 of unpaired t-test. (Right) Immunoblot analysis of GDE2 protein expression using five different hairpins, as indicated. Actin was used as loading control. **(C)** Rac-GTP levels in control and GDE2-depleted Shep2 cells (using hairpin #4). **(D)** Cell morphology and cytoskeletal organization (phalloidin and vinculin staining) in control and GDE2-depleted Shep2 cells Expression of RNAi-resistant GDE2 rescues the phenotype, as indicated. Black bar, 100 μm; white bar, 10 μm. **(E)** Immunoblot showing GDE2 expression in control, GDE2-depleted and "GDE2-rescued" Shep2 cells (transfected with RNAi-resistant GDE2). **(F)** Quantification of focal adhesion area in control, GDE2-depleted and GDE2-rescued Shep2 cells using Image J software (n=20 cells; mean ± SEM); **** p value < 0.0001 of one way ANOVA. **(G)** Cell-matrix adhesion of control, GDE2-depleted and rescued Shep2 cells. Cells were plated on fibronectin or collagen. At 30 min after plating, adherent cells were fixed and stained with Crystal Violet for quantification. Graph represents the mean ± SEM of two independent experiments; ** p value < 0.01; *** p value < 0.001 of unpaired t-test. **(H)** Analysis of random cell motility. (Left) Traces from individual cells are shown (control, GDE2 depleted and GDE2-rescued cells, as indicated). Tracks were generating from time-lapse movies. Images were captured every 10 min. for 12 hr. (Right) Quantification of mean migration distances (n≥ 60 cells, mean ± SEM); ** p value < 0.01; **** p value <0.0001 of unpaired t-test. **(I)** (Left) Heatmap showing differentially expressed genes upon GDE2 silencing in Shep2 cells as determined by whole-genome RNA-seq (cut-off: ^{2}log-fold change >1.5; p value < 0.001). Experiments were performed in duplicate, as indicated. For the complete list of genes with gene ontology (GO) annotations, see Table S1. (Right) Bar graph shows the GO terms that are significantly enriched among the differentially expressed genes. Transmembrane receptor signaling includes pathways mediated by G protein-coupled receptors, receptor protein tyrosine kinases, TGF-β, Wnt and Hedgehog. See also Table S1.

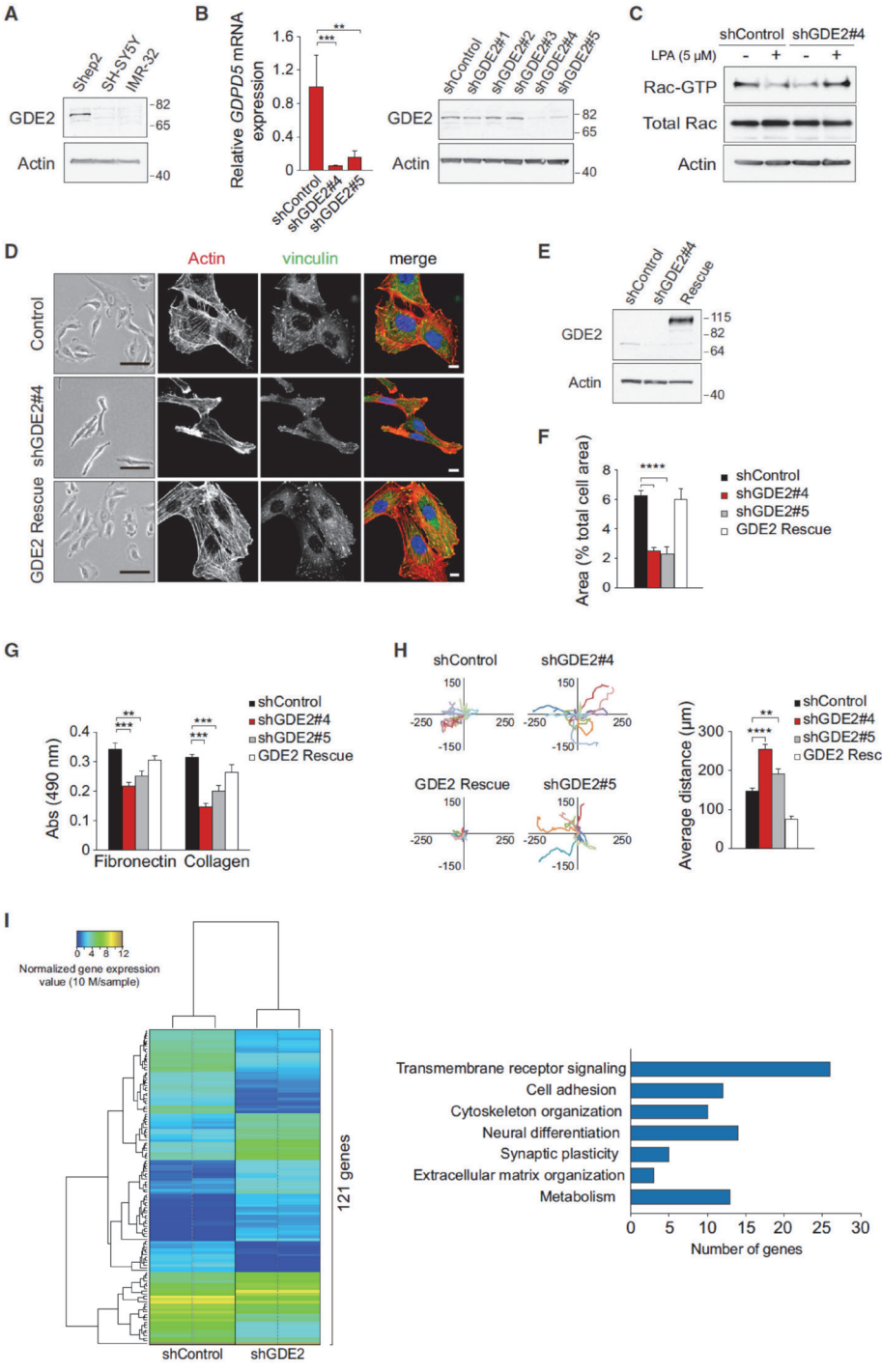
A
Shep2
SH-SY5Y
IMR-32
GDE2
Actin
82
65
40
B
Relative GDPD5 mRNA expression
1.6
1.2
0.8
0.4
0
**
***
shControl
shGDE2#4
shGDE2#5
shControl
shGDE2#1
shGDE2#2
shGDE2#3
shGDE2#4
shGDE2#5
GDE2
Actin
82
65
40
C
shControl
shGDE2#4
LPA (5 µM)
- + - +
Rac-GTP
Total Rac
Actin
D
Actin
vinculin
merge
Control
shGDE2#4
GDE2 Rescue
E
shControl
shGDE2#4
Rescue
GDE2
Actin
115
82
64
40
F
Area (% total cell area)
8
6
4
2
0
****
shControl
shGDE2#4
shGDE2#5
GDE2 Rescue
G
Abs (490 nm)
0.4
0.3
0.2
0.1
0
**
***
***
***
shControl
shGDE2#4
shGDE2#5
GDE2 Rescue
Fibronectin
Collagen
H
shControl
shGDE2#4
GDE2 Rescue
shGDE2#5
150
-250
250
-150
Average distance (µm)
300
200
100
0
**
****
shControl
shGDE2#4
shGDE2#5
GDE2 Rescue
I
0 4 8 12
Normalized gene expression value (10 M/sample)
121 genes
shControl
shGDE2
Transmembrane receptor signaling
Cell adhesion
Cytoskeleton organization
Neural differentiation
Synaptic plasticity
Extracellular matrix organization
Metabolism
0 5 10 15 20 25 30
Number of genes

smaller in size, and showed a reduction in basal Rac1 activity, which was now sensitive to LPA stimulation (Figure 4C). This was accompanied by marked cytoskeletal reorganization, less focal adhesions and reduced cell-matrix adhesion (Figure 4D-G). Moreover, GDE2 knockdown cells migrated faster and over longer distances than did shControl cells (Figure 4H). Shep2 cells were poorly responsive to LPA; upon GDE2 depletion, however, they showed more pronounced cytoskeletal contraction induced by LPA (results not shown). The knockdown phenotypes could be rescued by expression of RNAi-resistant GDE2, indicating that the observed effects are specific for GDE2 depletion (Figure 4D-H). Thus, GDE2 knockdown evokes phenotypic changes opposite to those induced by GDE2 overexpression.

Having shown that GDE2 activates Rac1 and opposes RhoA, we next examined how GDE2 may dictate neuroblastoma phenotype at the gene expression level. We analyzed differential gene expression in GDE2 knockdown versus shControl Shep2 cells using genome-wide RNA sequencing (RNA-seq). In duplicate experiments, RNA-seq-based analysis revealed 121 differentially expressed genes (^{2}log-fold change >1.5; p values <0.001) (Figure 4I; Table S1). The list of differentially expressed genes was markedly enriched (18%; 22/121) in those involved in neuronal differentiation, such a *RELN*, *NTM*, *ROBO4*, *RNF112, PLPPR4*, *KIRREL3*, and various genes (15%; 18/121) that regulate cell adhesion (*LAMA4, COL6A3, COL13A1, FN1, ITGA10, ITGA11*) and extracellular matrix organization (Table S1; Figure 4I). It is also noteworthy that some 20% (26/121) of the GDE2-regulated genes encodes proteins involved in transmembrane receptor activity, including signaling by receptor tyrosine kinases (*EPHB6, PDGFRA, TIE1, ERBB4*), GPCRs, Wnt, Hedgehog and TGF-β receptors, several of which play a role in neurodevelopment (Table S1). These data suggest a scenario where a unique set of differentiation regulatory genes, along with Rac hyperactivation, dictates the observed GDE2 phenotypes and may help explain the marked correlation between *GDPD5* expression and patient survival.

GDE2 Biochemical Activity: Release of GPI-Anchored Glypican-6

What is the relevant catalytic activity of GDE2 and how does it relate to the observed differentiated phenotype? Immunoprecipitated GDE2 hydrolyzes glycerophosphocholine into glycerol 3-phosphate [100], but this reaction has no signaling relevance. We examined GDE2 enzymatic activity using cell-based assays and mutational analysis. Prompted by the discovery that chicken GDE2 induces the release of GPI-anchored RECK from HEK293 cells [110], we measured GDE2 activity towards selected GPI-anchored proteins, including RECK and glypicans (GPCs). Glypicans are a family of six heparan sulfate proteoglycans that function as co-receptors or ligands to regulate diverse signaling pathways, either positively or negatively, particularly those involved in morphogenesis and neurodevelopment [188-190]. We co-expressed GDE2 and its candidate substrates, confirmed their proper expression at the plasma membrane (Figure S4A-C and data not shown), and assayed cell lysates

and the medium for substrate release by immunoblotting, essentially as described [110].

We confirmed that chicken GDE2 promotes the release of RECK, as did exogenous PI-PLC (Figure 5A). Unexpectedly, however, our efforts to detect RECK release by human GDE2 were unsuccessful (Figure 5A), suggesting that GDE2 substrate preferences may vary among vertebrates. We then examined the GPI-anchored glypicans as potential substrates. Human GDE2 induced the release of GPC3 and GPC6, but not that of GPC1, 2, 4 and 5 (Fig. S4D; Figure 5C). This indicates that GDE2 shows selectivity towards glypican family members, likely due to structural differences in the respective heparan sulfate chains and/or the GPI-anchor core.

GPC6 is widely expressed among neuroblastoma cell lines (Figure S4E), while GPC3 expression is more variable (Figure S4F). SH-SY5Y and N1E-115 cells express GPC6 but not GPC3 (Figure S4E,F,G and Figure 7A below). We therefore focused our subsequent experiments on GPC6. As one would predict, when co-expressed in N1E-115 cells, GDE2 and GPC6 co-localized in part to the same membrane microdomains (Figure S4B,C).

Mutating His233 Abolishes GDE2 Function

Uncertainty still exists as to the active site of GDE2. Residue His275 was reported to be critical for GDE2-induced neurogenesis [108]. Another potential catalytic residue is His233, located in a conserved GHRG motif [97] (Figure 5B). As shown in Figure 5C, mutants GDE2(H233A) and GDE2(H233A/275A) failed to induce the release of GPC6, whereas the H275A mutation reduced GDE2 activity only partially. This result defines His233 as key catalytic residue.

Previous in vivo studies suggested that GDE2 activity is enhanced after reduction of a putative disulfide bond (Cys25-Cys576) linking the N- and C-terminal tails [118] (Figure 5B), but the catalytic activity of relevant Cys mutants was not examined. In our glypican release assay, the supposedly hyperactive mutant GDE2(C25S), lacking the putative disulfide bond, showed the same catalytic activity as wild-type GDE2 (Figure 5D). This argues against a critical role for Cys25-Cys576 disulfide bonding/reduction in regulating GDE2 activity under the present assay conditions. Finally, to establish if GDE2 acts in *cis* (same cell) or/and in *trans* (adjacent cell), we mixed GDE2-expressing cells (lacking GPC6) with GPC6-expressing cells (lacking GDE2) and measured GPC6 release. GDE2-expressing cells were incapable of promoting GPC6 release from adjacent cells (Figure 5E). It thus appears that GDE2 acts in *cis*, consistent with GDE2 promoting differentiation in a cell-autonomous manner, not requiring intercellullar contacts.

When expressed in N1E-115 cells, catalytically dead GDE2(H233A) failed to promote cell spreading and neurite formation. GDE2(H275A) induced an intermediate phenotype, while the C25S mutation had no effect (Figure 6A-C), consistent with the above biochemical data. In addition, GDE2(H233A)-overexpressing cells showed a normal contractile response to LPA (results not shown). Thus, GDE2 catalytic activity is necessary and sufficient to induce neuroblastoma cell differentiation and to inhibit agonist-induced neurite retraction.

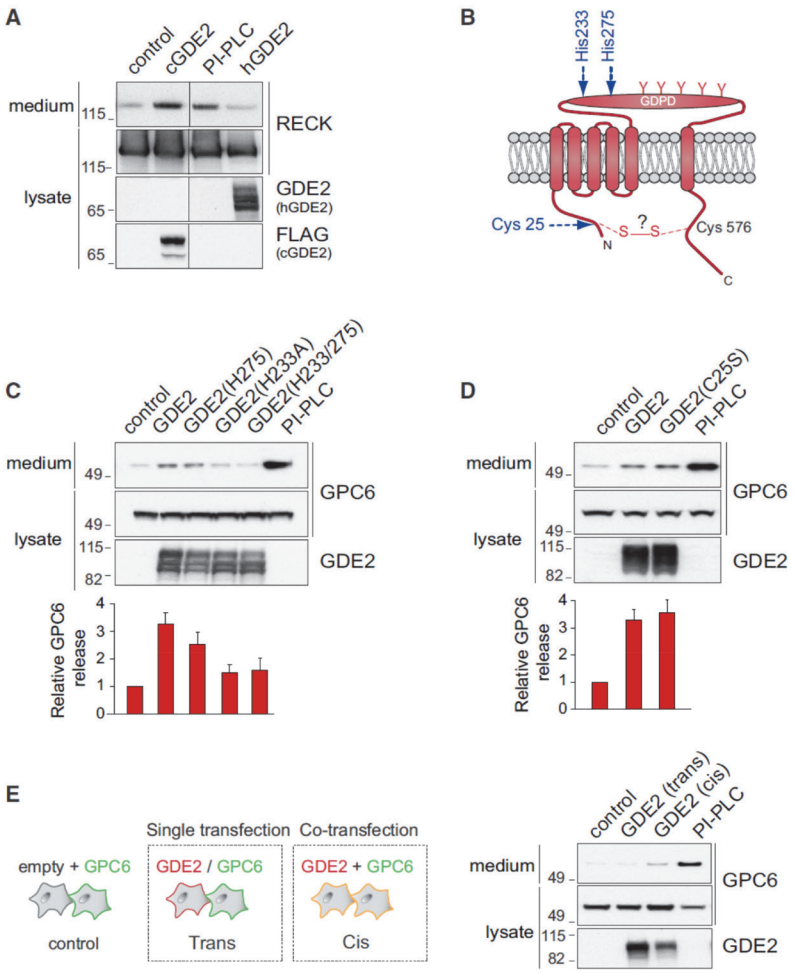

Figure 5. GDE2 Selectively Cleaves Glypican-6: Residue His233 is Essential for Activity

(A) HEK293 cells were co-transfected with RECK and either human GDE2-HA (hGDE2) or chicken GDE2-FLAG (cGDE2). Expression levels were assessed by immunoblotting in cell lysates and conditioned medium. PI-PLC was used as positive control in all experiments. **(B)** Schematic illustration of mutations made in GDE2. See text for details. **(C)** HEK293 cells were cotransfected with GPC6-HA and GDE2-mCh or the indicated mutants (GDE2(H27A), GDE2(H233A), GDE2(H233A/H275A)). The bar graph shows quantification of GPC6 released into the medium, as quantified using Image J software and expressed as GPC6 release relative to that in control cells. Error bars represent mean ± SEM of three independent experiments. **(D)** HEK293 cells transfected with GPC6-HA together with either GDE2-mCh or mutant GDE2(C25S)-mCh. Quantification of GPC6 release (bar graph) as in (C). **(E)** (Left) Scheme of the assay in HEK293 cells. GPC6-HA and GDE2-mCh co-transfected HEK293 cells or transfected with either GPC6-HA or GDE2-mCh were mixed and plated in PEI-coated plates. (Right) After 24 hr incubation in serum-free medium, GPC6 in the medium and cell lysates was analyzed by Western blotting. See also Figure S4.

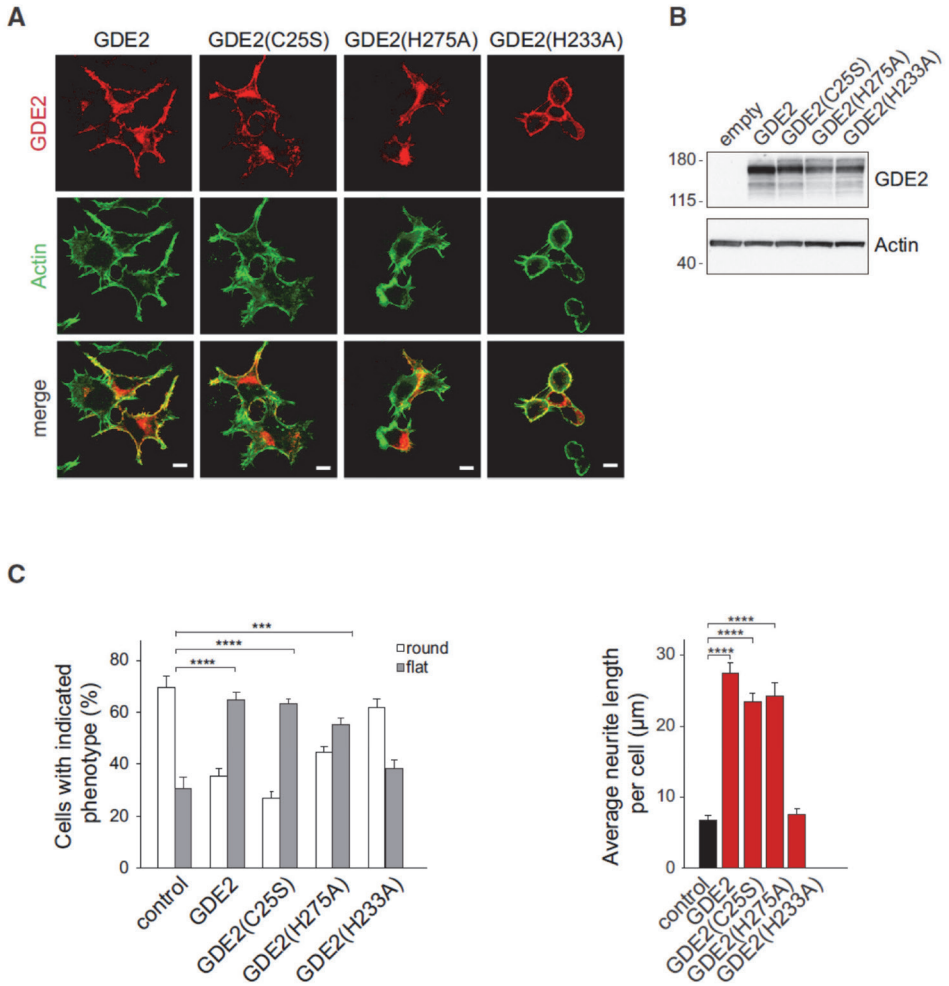

Figure 6. Mutating His233 Abolishes GDE2 Biological Activity

(A) N1E-115 cells were transfected with wild-type GDE2, GDE2(H233A), GDE2(H275A) or GDE2(C25S) (mCherry-tagged), as indicated. At 24 hr after transfection, cells were stained with phalloidin to visualize F-actin. GDE2 is shown in red, F-actin in green. Bar, 10 µm. **(B)** N1E-115 cells were transfected with wild-type GDE2 or the indicated mutants (mCherry-tagged). At 24 hr after transfection, GDE2 expression was analyzed by immunoblotting using GDE2 antibody. β-Actin was used as loading control. **(C)** Quantification of the morphological changes shown in (A). (Left) Percentage of N1E-115 cells with a round or flattened morphology. (Right) Neurite length quantification. Cells were transfected with pcDNA3 empty vector combined with mCherry as control (three independent experiments with >300 cells per experiment). Error bars, mean ± SEM. *** p value < 0.001; **** p value < 0.0001 of unpaired t-test.

GPC6 Underexpression Phenocopies GDE2 Overexpression and Correlates with Favorable Disease Outcome

We next asked to what extent GPC6 release may account for the biological activity of GDE2, Using SH-SY5Y cells, which express GPC6 as the only relevant glypican (Figure 7A), we established that dox-induced GDE2 expression promotes the release of endogenous GPC6 from the cell surface as measured by flow cytometry (Figure 7B).

GPC6 release from the cell surface predicts loss of GPC6 function. We stably knocked down GPC6 in SH-SY5Y cells by lentiviral transduction of different shRNAs (Figure 7C). GPC6 knockdown cells showed enhanced basal Rac1 activity, which was sensitive to LPA stimulation (Figure 7D), and increased neurite outgrowth (Figure 7E). To validate the knockdown result, we knocked out GPC6 using CRISPR/Cas9-based genome editing (Figure 7F and Figure S5A,B). CRISPR/Cas9-mediated GPC6 knockout led to even more prominent neurite outgrowth than observed with shRNA (Figure 7F). Neurites induced upon GPC6 silencing were fully resistant to LPA-induced contraction (results not shown). In addition, GPC6 depletion resulted in enhanced cell-matrix adhesion and reduced cell motility (Figure 7G,H). It thus appears that loss of GPC6 function is phenotypically equivalent to GDE2 overexpression. We also examined a possible contributing role of GPC3 in regulating neurite outgrowth using cells (IMR-32) that express both GPC3 and GPC6 (Figure S4E,F), but found no effect of GPC3 depletion on neurite formation (Figure S5C,D).

⟶ **Figure 7. GPC6 Silencing Phenocopies GDE2 Overexpression and Correlates with Favorable Outcome**

(A) Glypican mRNA expression (relative to *GAPDH*) in SH-SY5Y cells (qPCR analysis). Error bars, mean ± SEM (trlplicate measurements). **(B)** (Left) Cell-surface expression of GDE2-mCherry before (black) and after (red) doxycycline treatment of SH-SY5Y cells, as detected by Flow Cytometry. (Right) Cell-surface expression of GPC6 in GDE2-negative (black) and GDE2-positive (red) SH-SY5Y cells, as detected by Flow Cytometry. Control or Dox-induced GDE2 cells were labeled with second antibody alone (2^{nd} Ab) or anti-GPC6 antibody. Bar graph shows quantification (mean ± SEM) from three independent experiments. * p value < 0.05 according to paired t-test. **(C)** GPC6 knockdown in SH-SY5Y cells as determined by qPCR. GPC6 mRNA levels were normalized to *GAPDH*. ** p value < 0.01; *** p value < 0.001 of unpaired t-test. **(D)** Western blot showing that GPC6 depletion increases basal and LPA-stimulated Rac activity (SH-SY5Y cells). Bar graph shows quantification of relative Rac-GTP levels in the presence or absence of LPA (mean ± SEM of three independent experiments). * p value < 0.05 of unpaired t-test. **(E)** GPC6 depletion leads to longer neurites (arrows) in SH-SY5Y cells. Bar, 100 μm. Bar graph shows quantification of neurite length in control versus GPC6 knockdown cells (n= 250, mean ± SEM). **** p value < 0.001 of unpaired t-test. **(F)** CRISPR/Cas9-mediated GPC6 knockout promotes neurite outgrowth in SH-SY5Y cells. Bar, 100 μm. Bar graph shows percentage of neurite-bearing cells in CRISPR-GPC6 knockout cells (n ≥ 500 cells, n = 11 colonies, mean ± SEM). **** p value <0.0001. **(G)** shControl and shGPC6 were plated on fibronectin or laminin. At 1 hr after plating, adherent cells were fixed and stained with Crystal Violet for quantification. Bars represent the mean ± SEM of two independent experiments. **(H)** Quantification of average distances of cell migration of shControl and shGPC6 SY5Y cells. Bars represent averages ±SEM (>60 cells). For panels G and H: * p value < 0.05 of unpaired t-test. See also Figure S5.

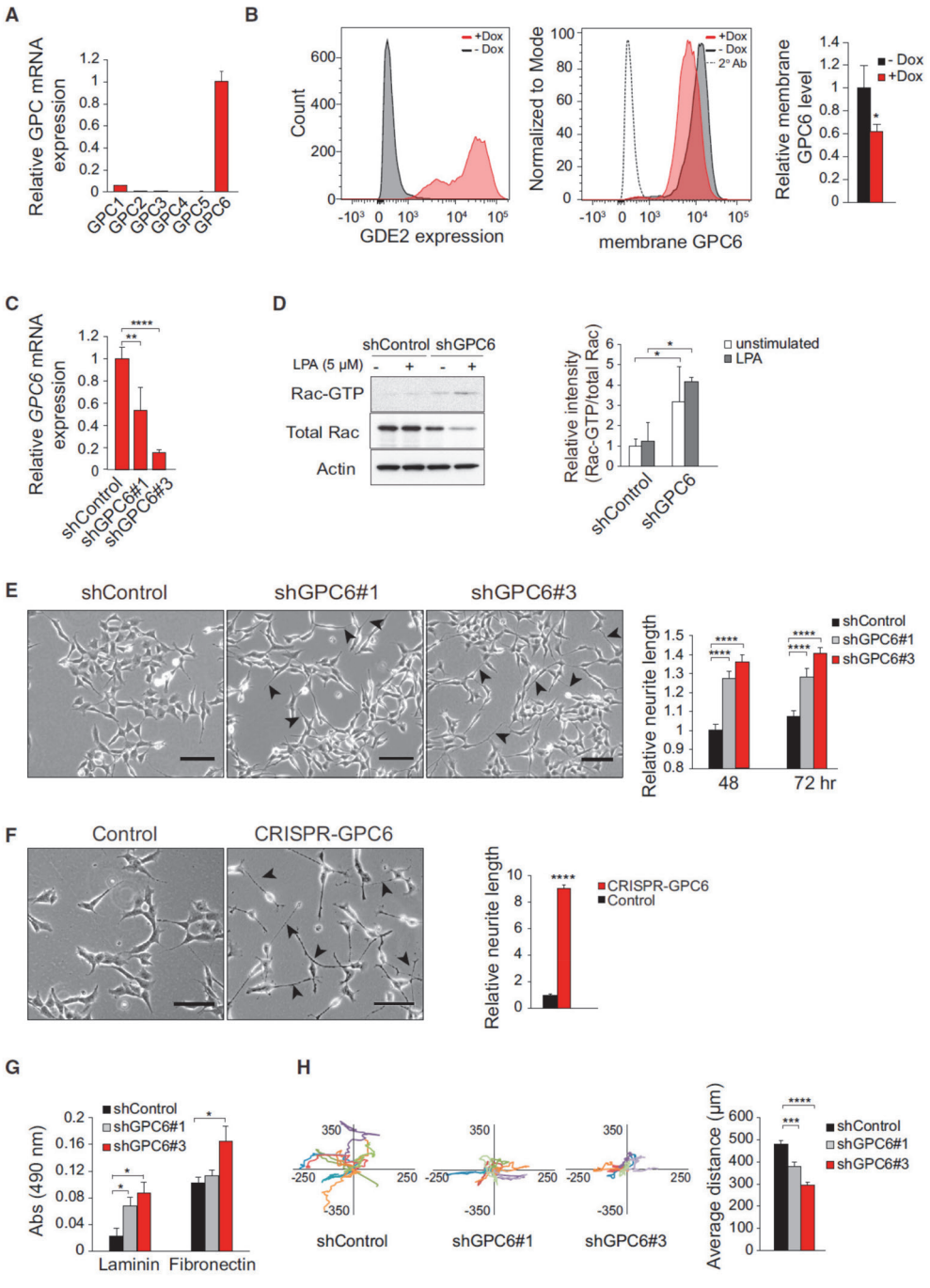
A
Relative GPC mRNA expression
GPC1
GPC2
GPC3
GPC4
GPC5
GPC6
B
+Dox
- Dox
Count
GDE2 expression
+Dox
- Dox
2° Ab
Normalized to Mode
membrane GPC6
Relative membrane GPC6 level
- Dox
+Dox
C
Relative GPC6 mRNA expression
shControl
shGPC6#1
shGPC6#3
D
shControl shGPC6
LPA (5 μM)
Rac-GTP
Total Rac
Actin
Relative intensity (Rac-GTP/total Rac)
unstimulated
LPA
shControl
shGPC6
E
shControl
shGPC6#1
shGPC6#3
Relative neurite length
48
72 hr
F
Control
CRISPR-GPC6
Relative neurite length
CRISPR-GPC6
Control
G
Abs (490 nm)
Laminin
Fibronectin
H
shControl
shGPC6#1
shGPC6#3
Average distance (μm)

Finally, low *GPC6* expression correlated significantly with favorable outcome in neuroblastoma patients (Figure 8A); no significant correlation was found for *GPC3* (Figure S6). When *GDPD5* and *GPC6* expressions were combined, patients classified as $GDPD5^{high}/GPC6^{low}$ showed the best disease outcome, whereas the $GDPD5^{low}/GPC6^{high}$ group had the poorest outcome (Figure 8B). This result is consistent with the functional interaction between GDE2 and GPC6 observed in neuroblastoma cell culture.

Discussion

In this study, we have identified and characterized transmembrane ecto-phosphodiesterase GDE2 as an inducer of neuroblastoma differentiation and as a powerful prognostic marker. We find that GDE2, previously shown to promote neurogenesis [108], acts through an enzymatic mechanism involving cleavage of the GPI-anchor of glypican-6 (GPC6). In the simplest model compatible with our findings, GDE2 releases GPC6 from the cell surface to modulate the activity of an as-yet-unknown transmembrane effector (Figure 8C), which leads to Rac activation, suppression of RhoA activity and altered gene expression. Together, these events direct neuroblastoma differentiation as evidenced by neurite outgrowth, increased cell-matrix adhesion, reduced cell motility and blockade of agonist-induced neurite retraction. The set of GDE2-regulated genes was markedly enriched in those involved in neuronal differentiation, cell-matrix adhesion and transmembrane receptor signaling. Future studies should assess whether a subset of these genes contributes to the GDE2-induced phenotypes and/or may represent a gene signature predictive of clinical outcome.

Although GDE2 can also release GPC3, and GPC3 has been implicated in the progression of various types of cancer [191-193], we find that (i) GPC3 is not expressed two of our model neuroblastoma cell lines (SH-SY5Yand N1E-115), (ii) GPC3 knockdown does not affect neurite outgrowth in IMR-32 cells, and (iii) GPC3 expression levels, unlike those of GPC6, do not correlate with clinical outcome. Nevertheless, it will be interesting to explore if and how GDE2-mediated release of GPC3 may regulate signaling pathways and cellular phenotype in other types of cancer or during development.

The cell-autonomous GDE2-GPC6 signaling axis underlying neuroblastoma differentiation contrasts with the non-cell-autonomous GDE2-RECK-Notch pathway that promotes neurogenesis in the spinal cord [109, 110]. Our efforts to detect RECK release [110] by human GDE2 were unsuccessful, suggestive of differential substrate preferences among vertebrates GDE2 enzymes. Moreover, GDE2 was unable to release GPC1, 2, 4 and 5, indicating that GDE2 is highly selective towards GPI-anchored substrates under our experimental conditions. Some caution is needed, however, since the GDE2 activity assays were conducted in HEK293 cells, and the availability of GPI-anchored substrates may depend on local membrane lipid organization and structure [194]. In addition, GDE2 substrate selectivity may be dictated by

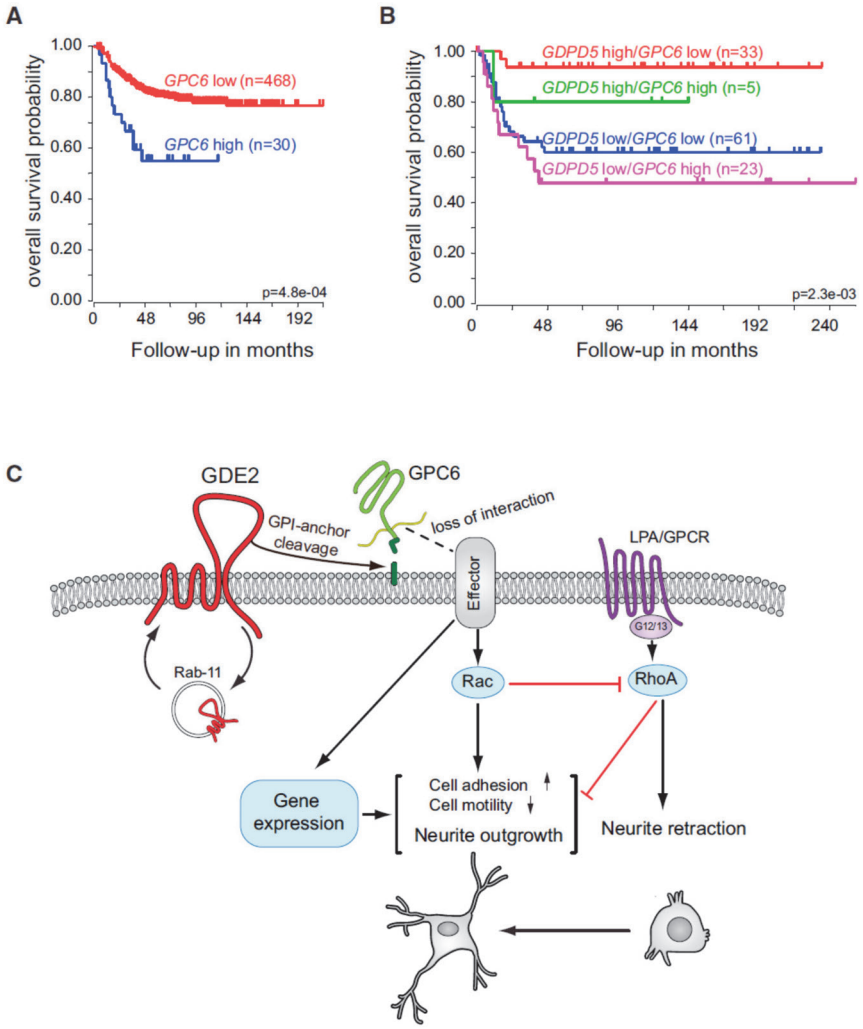

Figure 8. GPC6 Prognostic Significance and GDE2 Signaling Scheme

(A) Kaplan-Meier analysis of overall survival in a set of 498 neuroblastoma patients (RPM cohort). Patients were classified using the same *GPC6* cut-off value. See also Fig. S6. **(B)** Kaplan-Meier analysis based on the combined expression status of *GDPD5* and *GPC6* (AMC patient cohort). **(C)** Proposed GDE2 signaling scheme. In this model, GDE2 acts through GPI-anchor cleavage of GPC6 leading to GPC6 release from the cell surface with consequent loss of interaction with an as-yet-unknown transmembrane effector or receptor. This leads to Rac1 activation, increased cell adhesion and spreading, neurite outgrowth, reduced cell motility, and inhibition of LPA-$G_{12/13}$-RhoA-driven neurite retraction. Additionally, GDE2 regulates a unique set of genes involved in neuronal differentiation, cytoskeletal organization and cell-matrix adhesion (Figure 4I and Table S1). GDE2 cell-surface expression may be regulated by a Rab11-driven endocytic recycling pathway (Figure S1G,H), as illustrated. See text for further details.

structural modifications in the oligosaccharide core of the respective GPI-anchors and/or, in the case of glypicans, by the nature of the heparan sulfate chains which are located close to the cell surface [190] and hence may physically interact with the GDE2 ectodomain. We identified His233 as key catalytic residue of GDE2, but it remains as yet unclear whether GDE2 acts as a PLC- or PLD-type phosphodiesterase [110]. Regardless of how GDE2 selects and hydrolyzes its GPI-anchored substrates, the evidence from the present and previous studies [110] suggests that GDE2 may signal in both cell-autonomous and non-cell-autonomous modes to induce neuronal differentiation, depending on cell and tissue context.

Our findings raise a number of new questions. Foremost of all, how does GDE2-induced cleavage of GPC6 at the cell surface activate downstream signaling events? In other words, what is the GPC6-regulated transmembrane effector? Despite many advances in heparan sulfate proteoglycan research, our understanding of glypican outside-in signaling is still very limited, and that of GPC6 in particular. In fact, GPC6 is the least studied and arguably the most enigmatic glypican family member. Where studied, glypicans can function as co-receptors to regulate transmembrane signaling in various ways, both positively and negatively [188, 195]. As such, certain glypicans can bind specific ligands, including Wnt and Hedgehog proteins, and present them to cognate receptors. However, the emerging picture of glypican-regulated Wnt signaling is complex, involving both canonical and non-canonical signaling cascades, and to date has not led to a unifying model; moreover, findings are sometimes contradictory [196-198]. Whatever possible role of GPC6 in Wnt signaling, the finding that GDE2 acts cell-autonomously, not requiring nearby cells or extrinsic factors, seems hard to reconcile with a role for secreted Wnt ligands in GDE2-induced neuronal differentiation; however, we cannot formally rule out a possible cooperation with secreted ligands such as Wnt.

Interestingly, emerging evidence suggests that glypicans can also function as ligands themselves by binding to transmembrane receptors, namely type-II receptor protein tyrosine phosphatases (RPTPs) [199, 200]. Type-II RPTPs influence neuronal morphology and have multiple intracellular binding partners including regulators of Rac/Rho activity [199, 201]. Heparan sulfate proteoglycans can directly interact (in *cis*) with the ectodomain of RPTPσ to modulate RPTP oligomerization and transmembrane signaling [199, 200]. Loss of a glypican ligand might then lead to altered RPTP clustering at the plasma membrane with a consequent change in localized levels of tyrosine phosphorylated proteins involved in signaling pathways that stimulate neurite outgrowth. Precisely how glypicans in general, and GPC6 in particular, may affect RPTP clustering and activity and whether RPTPs can act as a signaling intermediate in GDE2 action awaits further studies.

Another outstanding question concerns the regulation of GDE2 activity. We could not confirm the proposed role of cytosolic disulfide bonding in regulating GDE2 activity [118, 202]. A relatively large proportion of GDE2 was detected in Rab11- and TrfR-positive recycling endosomes, supporting a model where GDE2 activity is regulated at the level of cell-surface expression by

membrane trafficking (Figure 8C). Interestingly, a recent study supports a scenario in which GDE2 is regulated by intracellular trafficking [119]. Regulation of GDE2 activity by C-terminal tail phosphorylation is another plausible scenario that warrants further investigation [203].

The identification of GDE2 as an inducer of neuroblastoma cell differentiation and as a favorable prognostic marker is consistent with the finding that patient survival is largely dependent on the degree of neuronal differentiation [160]. New therapeutic approaches are urgently needed in neuroblastoma, but their development has been hampered by the paucity of tractable oncogenic drivers [163, 164] and an incomplete understanding of neuroblastoma differentiation. In this respect, the present results open up possibilities for exploring new therapeutic approaches. In particular, pharmacological stimulation of GDE2 activity could be a promising strategy, not least because exo/ecto-phoshodiesterases are convenient drug targets. Therefore, the development of drug-like allosteric activators of GDE2 could be valuable for targeted differentiation therapy in neuroblastoma. Further structural and preclinical studies will be needed to confirm the feasibility and efficacy of this approach.

Experimental Procedures

Human Data Sets and Survival Analysis

All mRNA gene expression analyses were performed within R2: genomics analysis and visualization platform (http://r2.amc.nl). We have made use of the following publicly available data sets: Neuroblastoma Oberthuer (ArrayExpress: E-TABM-38), Neuroblastoma SEQC (GEO:GSE62564) and Neuroblastoma Versteeg (GEO:GSE16476 88/122). Kaplan scanning was performed within R2 (http://r2.amc.nl). In brief, for each gene or other numerical characteristic, R2 calculates the optimal cut-off expression level dividing the patients in a good and bad prognosis cohort. Samples within a data set are sorted according to the expression of the investigated gene and divided into two groups on the basis of a cut-off expression value. All cut-off expression levels and their resulting groups are analyzed for survival, with the provision that minimal group number is eight (or any other user-defined value) samples. For each cut-off level and grouping, the log-rank significance of the projected survival was calculated as described [204]. The best p value and corresponding cut-off value is selected. This cut-off level is reported and used to generate Kaplan-Meier graphs.

Materials, Cell Culture, Antibodies and Expression Vectors

Reagents, cell culture, expression vectors and transfection protocols are described in Supplemental Information. A GDE2 polyclonal antibody was raised against the very C-terminal tail of human GDE2 (sequence MVRHQPLQYYEPQ) and affinity purified, as described in Supplemental Experiment Procedures.

Cell Morphology and Neurite Induction
Phenotypic analyses were done as described in Supplemental Experiment Procedures.

Gene Silencing
shRNA-mediated knockdown and CRISPR/Cas9-mediated knockout experiments were performed as described in Supplemental Experiment Procedures.

Differential Gene Expression by RNA-seq
Differential gene expression in GDE2 knockdown versus control Shep2 cells was analyzed by whole-genome RNA sequencing (RNA-seq) as described in Supplemental Procedures.

qRT-PCR and Western Blotting
Real-time PCR and Western blotting assays were carried out as described in Supplemental Procedures.

Microscopy and Live Imaging
Confocal and super-resolution microscopy assays and live-imaging protocols are described in Supplemental Procedures**.**

Cell Adhesion and Motility Assays
Cell adhesion and random cell motility were measured as detailed in Supplemental Procedures.

GDE2 Enzymatic Activity Assays
GDE2 activity assays were carried out in HEK293 cells, essentially as described [110]. HEK293 cells were seeded on polyethyleneimine (PEI)-coated 6-well plates and co-transfected with expression vectors for chicken or human GDE2 together with substrates (RECK-Myc, GPC(1-6)-HA). GDE2 mutations were made using X-tremeGene 9 reagent (Roche). At 24 hr after transfection, cells were incubated for an additional 24 hr in serum-free DMEM. The conditioned medium was removed and cell lysates were prepared using NP40/NaDOC lysis buffer (50 mM TRIS ph7,4, 150 mM NaCl, 2mM EDTA, 1% NP40, 0,25% NaDOC and 5% Glycerol) supplemented with protease inhibitor cocktail. The amount of substrate proteins in the medium and cell lysates was analyzed by Western blotting.

Rac and RhoA Activity Assays
Activities of Rac and RhoA were measured by pull-down assays as described in Supplemental Experimental Procedures.

RhoA Activation Measurements

To monitor RhoA activity in real time, cells were transfected with a RhoA-specific FRET-based biosensor in which the HR1 region of protein kinase N was used as the effector domain for activated RhoA, essentially as described [187]. Further details and RhoA activity monitoring in single cells are described in Supplemental Experimental Procedures.

Acknowledgements

We thank Laurens van Meeteren, Paula Ruurs, Maikel Jongsma and Andrew J. Morris for performing pilot experiments, Bram van de Broek for image analysis and Elisabetta Argenzio

Supplemental Experimental Procedures

Cell Culture and Materials

SH-SY5Y, IMR-32, Shep2, N1E-115, Neuro2A and HEK293 cells were grown in Dulbecco's modified Eagle's medium (DMEM) supplemented with 10% fetal bovine serum (FBS) at 37°C under 5% CO2. Antibodies used: anti-HA, 3F10 from Roche Diagnostics; anti-Flag, M2 and β-Actin (AC-15) from Sigma; RECK (D8C7) from Cell Signaling Technology; anti-RhoA (26C4) (sc-418) from Santa Cruz; anti-Rac1 from BD Transduction Laboratories; anti-GPC6 from LSBio; anti-mCh and anti-GFP were home-made; 1-oleyl-LPA, puromycin, fibronectin, laminin-1, collagen and doxycycline were from Sigma. Bacterial PI-PLC was from Molecular Probes and Phalloidin red (actin-stain™ 555 phalloidin) from Cytoskeleton.

GDE2 Antibody Generation

GDE2 polyclonal antibody against the C-terminal 14 amino acids of human GDE2 (GGSHTKTLIERSGR) was raised in rabbits. The peptide was fused to mcKLH (Keyhole limpet hemocyanin; Pierce) in conjugation buffer (0.1 M Sodium phosphate, 0.15 M NaCl, pH 7.2; Pierce Kit) and then purified by a desalting column (Pierce Kit). For affinity purification, the antiserum was passed through a GDE2 peptide column, and the cross-absorbed serum was affinity purified using the Aminolink®Plus Immobilization Kit (Thermo Scientific).

Expression Vectors

Human cDNA GDE2 was subcloned into a pcDNA3 (-mCherry and –EGFP) plasmid by amplification with oligos and digestion was done with BamHI/EcoRV. GDE2 mutants (C25S, H233A, H275A and H233/275A were made by site-directed mutagenesis followed by Dpn1 digestion of the template. The viral plasmid pLIB-GDE2-GFP was constructed by subcloning the insert containing two mutations in residues 1731 and 1734 into pLIB vector. Constructs pCAGGS-HA-GPC1-6, pCAGGS-cGDE2-Flag, pCAGGSMyc-RECK were kindly provided by Dr. Sungjin Park (Johns Hopkins Medical School, Baltimore, USA).

Inducible GDE2 Expression

SH-SY5Y and IMR-32 cells with inducible GDE2 expression were generated using the Retro-X™ Tet-On® Advanced Inducible Expression System (ClonTech). After retroviral transduction, the cells were placed under selection with G418 (800 mg/ml) supplemented with puromycin (1 mg/ml) for 10 days. GDE2 induction (in the presence of 1 μg/ml doxycycline) was verified by Western blot and confocal microscopy.

Cell Morphology, Neurite Induction and Retraction

For quantification of cell morphology, cells were transiently transfected with GDE2, GDE2(H275A), GDE2(H233A), GDE2(H233/H275A) or GDE2 (C25S) (all mCherry-tagged). At 24h post-transfection, cells were fixed with 4% paraformaldehyde and F-actin was stained with phalloidin. Cells were visualized using an inverted Leica confocal microscope. Per experiment, ~300 cells were randomly scored as round or flat, or round or cells bearing neurites. For neurite length measurements, cells were seeded at 1x 10^5 cells/well in 6-well plates. GDE2 expression was induced by addition of 1 µg/ml doxycycline in DMEM containing 4% serum for 72 hr. Pictures were taken at 48 and 72 hr to monitor neurite outgrowth. Neurite length was measured using an Image J macro. Differentiated cells were defined as those with neurite lengths exceeding one cell-body diameter. Experiments were performed in triplicate. For quantification of neurite retraction, N1E-115 cells were serum starved for 24 hr and then treated with LPA. Next, cells were fixed and stained with phalloidin. Per time point, about 300 randomly selected cells were scored as round or flat.

Cell Adhesion and Motility

Cell adhesion and random cell motility were measured using standard procedures. For adhesion assays 96-well plates were coated at 37 °C with 10 µg/ml fibronectin, 5 µg/ml collagen or 10 µg/ml laminin-1 during 1hr. The plates were washed with PBS, blocked in 0.5% BSA for 1hr at 37 °C and washed twice with PBS. Cells were seeded at 1x10^5 per well and allowed to adhere at 37 °C for 1 hr. Non-adherent cells were washed away using PBS. Attached cells were fixed with 4% paraformaldehyde (PFA) for 10 min, washed twice and stained with crystal violet (5 mg/ml in 2% ethanol) for 10 min. Fixed cells were washed and lyse with 2% SDS for 30 min. Plates were read at 490 nm. To measure random cell motility, cells were seeded on fibronectin-coated 6-well plates in the presence of serum 24 hr earlier. Phase-contrast images were acquired using a Zeiss Axiovert 200M microscope equipped with a heated (37°C) chamber and CO2 controller. Images were taken every 10 min during 12 hr, and the distance covered by the cells and cell directionality were analyzed using ImageJ software.

Expression Profiling

The mRNA expression profile of 24 established neuroblastoma cell lines was established by microarray using the Affymetrix Human Genome U133 plus 2.0 platform. Expression data are deposited at GEO (accession number GSE28019).

Knockdown Studies

For knockdown studies, we used five independent shRNAs for each gene in the lentiviral vector pLKO, as listed below. To generate particles for stable infections, HEK293T cells were transfected with single shRNAs using the calcium phosphate protocol; the virus particles

were collected at 48 h after transfection. Stable GDE2 knockdown cells were selected and maintained in medium containing 2 μg/ml puromycin. For imaging studies, plasmids were transiently transfected using XtremeGene 9 agent (Roche) according to the manufacturer's instructions.

Gene	TRC ID	Full hairpin sequence
GDPD5	TRCN0000005173	CCGGCCTGGTAGAAGTGTTCTGGATCTCGAGATCCAGA ACACTTCTACCAGGTTTTT
	TRCN0000005174	CCGGGCTCTCCGTATGTTCAGACAACTCGAGTTGTCTGA ACATACGGAGAGCTTTTT
	TRCN0000005175	CCGGCCACAATGACTATGATGAATTCTCGAGAATTCATCA TAGTCATTGTGGTTTTT
	TRCN0000005176	CCGGGACAACAGTTATGACACATATCTCGAGATATGTGTC ATAACTGTTGTCTTTTT
	TRCN0000005177	CCGGGTCCTGGCACTATGTCACATTCTCGAGAATGTGAC ATAGTGCCAGGACTTTTT
GPC6	TRCN0000123094	CCGGGCTTCCTCTTTCCTTCAGCTACTCGAGTAGCTGAA GGAAAGAGGAAGCTTTTTG
	TRCN0000123095	CCGGGCCATTATGAACATGCAAGAACTCGAGTTCTTGCA TGTTCATAATGGCTTTTTG
	TRCN0000123096	CCGGGCCAACAAAGCAAACTCGAATCTCGAGATTCGAG TTTGCTTTGTTGGCTTTTTG
	TRCN0000123097	CCGGGCACAGCAAAGCCAGATACTTCTCGAGAAGTATC TGGCTTTGCTGTGCTTTTTG
	TRCN0000123098	CCGGACCCGATAGATGTCAAGATTTCTCGAGAAATCTT GACATCTATCGGGTTTTTTG
GPC3	TRCN0000078558	CCGGGCCAAATTATTCTCCTATGTTCTCGAGAACATAGGA GAATAATTTGGCTTTTTG
	TRCN0000078559	CCGGCCTGAAAGTATTTGGGAATTTCTCGAGAAATTCCC AAATACTTTCAGGTTTTTG
	TRCN0000078560	CCGGCCCATTCTCAACAACGCCAATCTCGAGATTGGCGT TGTTGAGAATGGGTTTTTG
	TRCN0000078561	CCGGGCTCTGGTGATGGAATGATAACTCGAGTTATCATTC CATCACCAGAGCTTTTTG
	TRCN0000078562	CCGGGCCTGTTTCCAGTCATCTATACTCGAGTATAGATGA CTGGAAACAGGCTTTTTG

CRISPR/Cas9-mediated GPC6 Knockout

SH-SY5Y *GPC6* knockout cell lines were generated using CRISPR/Cas9 genome editing. CRISPR sequences were designed to target *GPC6* (exon 2: 5'-AATGGCTTGTCTCTTCCACA-3'; exon 3: 5'-GCTGAAAAGGTACTACACTG-3') and cloned into pX330-eSpCas9(1.1) [205].

SH-SY5Y cells were transfected with the exon-specific pX330-eSpCas9(1.1) plasmids in addition to a plasmid containing a guide RNA to the zebrafish TIA gene (5'-ggtatgtcgggaacctctcc-3') plus a cassette of a cytomegalovirus promoter followed by a BlastR gene, flanked by two TIA target sites. Co-transfection results in infrequent integration of the BlastR gene at the targeted genomic locus by NHEJ, as previously described [155]. Successful integration of the cassette renders cells resistant to blasticidin. At seven days after transfection, the culture medium was supplemented with blasticidin (10 µg/ml). Surviving colonies were clonally expanded, screened for cassette integration and indels into the query gene by PCR (using primer sets 5'-GGGGAACACTTAAGAATCTGTCC-3' and 5'-CTTATGCCTGGACACAAAAGTG-3' and 5'- AGCTCCTGGAGAATGCAGAA-3' and 5'- GAAGTGATACTGAGGGTTTATCAGC-3' for exon 2 and 3, respectively). Plasmid SpCas9(1.1) was kindly provided by Feng Zhang (Addgene plasmid # 71814) and pTIA-CMV-BlastR by Thijn R. Brummelkamp.

qRT-PCR

Total RNA was extracted using the GeneJET purification kit (Fermentas). cDNA was synthesized by reverse transcription from 2 µg RNA using oligodT 15 primer and SSII RT enzyme (Invitrogen). RTqPCR was performed on a 7500 Fast System (Applied Biosystems) as follows: 95°C for 2 min, 95 °C for 0 min., 40 cycles at 95°C for 15 sec. followed by 60°C for 1 min. for annealing and extension. The final reaction mixtures (20 µl) consisted of diluted cDNA, 16SYBR Green Supermix (Applied Biosystems), 200 nM forward primer and

Gene	Forward primer 5'-3'	Reverse primer 5'-3'
GDPD5	GTACCTCTACAACCGCATGG	AATGTGACATAGTGCCAGGAC
GPC1	GATGACCACTTCCAGCACCT	CAGGTAGTCATCAGGCAGCA
GPC2	TGAGACAGAGCAGAGGCTGA	AGAGCTGGGTCAGAGAGTGC
GPC3	TGCTCTTACTGCCAGGGACT	GCTTTCCTGCATTCTTCTGG
GPC4	TTCGAGTGATGACCAGCAAG	AGCACTGTCGGCTTTCTCAT
GPC5	CAGTGGGGACTGTGATGATG	ACCAAATCCCGGGAAGTAAC
GPC6	CAACATTGAGTCGGTCATGG	ATTGTAGGGCCTGAAACGTG
GAPDH	GCCAAGGTCATCCATGACAAC	GAGGGGCCATCCACAGTCTT
MAP2	CCAATGGATTCCCATACAGG	TCCTTGCAGACACCTCCTCT
TUBB3	CCTGGAACCCGGAACCAT	AGGCCTGAAGAGATGTCCAAAG
ENO2	CTGATGCTGGAGTTGGATGG	CCATTGATCACGTTGAAGGC
SNAP25	AGTTGGCTGATGAGTCGCTG	TGAAAAGGCCACAGCATTTC
NEUROD1	CCGACAGAGCCCAGATGTAGTTCTT	GCCCCAGGGTTATGAGACTATCACT
GAP43	GAGGATGCTGCTGCCAAG	GGCACTTTCCTTAGGTTTGGT
NPY	TACCCCTCCAAGCCGGACAA	CATTTTCTGTGCTTTCTCTCAT
PPIA	CATCTGCACTGCCAAGACTGA	TTGCCAAACACCACATGCTT

200 nM reverse primer. Reactions were performed in 96-well plates in triplo. The primers used are listed below. As a negative control, the cDNA was replaced by milliQ. GAPDH and Cyclophilin , were used as reference genes. Each sample was analyzed in triplo. The normalized expression (NE) data were calculated by the equation NE= $2^{(Ct\ target\ -\ Ct\ reference)}$.

Western Blotting

For Western blotting, cells were washed in ice-cold PBS, lysed in RIPA buffer with protease inhibitors and spun down. Equal amounts of proteins were determined by BCA protein assay kit (Pierce), separated by SDS-PAGE using pre-cast gradient gels (4-12% Nu-Page Bis-Tris, Invitrogen) and transferred to nitrocellulose membranes. Nonspecific binding of proteins was blocked by incubation in 5% skimmed milk in TBST. Proteins were detected by 1 hr incubation of primary antibody at room temperature or overnight incubation at 4°C, followed by 1 hr incubation with horseradish peroxidase-conjugated secondary antibodies (DAKO, Glostrup, Denmark). Proteins were detected using ECL Western blot reagent (GE Healthcare, Chalfont St. Giles, UK).

Immunofluorescence

Cells were cultured on glass coverslips, fixed with 4% paraformaldehyde for 10 min, permeabilized by 0.1% Triton X-100 and subsequently blocked in 2% BSA for 30 min at room temperature. Incubation with primary antibody was done for 1hr and coverslips were then incubated with Alexa-conjugated secondary antibodies for 45 min at room temperature. Cells were washed with PBS before mounting with Immuno-Mount™ (Thermo Scientific). Slides were examined on a LEICA TCS-SP5 confocal microscope (63x objective).

Live-Cell Imaging

Live-cell imaging was done on a Leica TCS SP5 confocal microscope equipped with 63x oil immersion lens (numerical aperture 1.4; Leica, Mannheim, Germany). Coverslips were mounted in a metal ring system and exposed to buffer solution (140 mM, NaCl, 5 mM KCl, 2 mM MgCl2, 1 mM CaCl2, 23mM NaHCO3, 10 mM HEPES, 10 mM glucose). Cells were selected randomly. LPA was added while images were collected at appropriate time intervals (5-15 sec). GDE2-mCherry was visualized by exciting cells at 561 nm while emission was detected at 610 ± 10 nm.

Super-Resolution Microscopy

Cells were cultured on #1.5 uncoated coverslips and washed with PBS and fixed with 4% paraformaldehyde. Imaging was done on a SR-GSD [206] Leica microscope, using an oxygen scavenging system (GLOX: 10% glucose, 0.5 mg/ml glucose oxidase, 40 µg/ml catalase) with the reducing agent MEA (cysteamine hydrochloride, 100 mM). Images were taken in TIRF or EPI mode at 10 ms exposure time for 15000 frames. Post image analysis was performed

as follows: a temporal median filter was applied on the blinking movies to reduce structured background [207] using home-built software. The resulting movies were analyzed with the ImageJ plugin Thunderstorm (http://imagej.nih.gov/ij/) for blinking localizations, XY drift correction and construction of the final image, which were made with Normalized Gaussian visualization option (pixel size 20 nm). Chromatic aberration was corrected using 0.1 µm diameter Tetraspec microsphere (Invitrogen) images from which an affine transformation matrix was constructed. Correction of all images was performed with an ImageJ macro using the plugin Image Stabilizer.

Flow Cytometry

For GPC6 surface expression analysis, cells were grown in complete medium with 10% FCS with or without doxycycline. Cells were trypsinized into single-cell suspensions and then $8x10^5$ cells were incubated with 7 µl of anti-GPC6 antibody LS-C36518 (LifeSpan Bioscience). Bound antibodies were detected by incubating with a 1:200 dilution of goat anti-mouse Alexa-488 secondary antibody in 2% BSA for 45 min on ice. Fluorescence measurements were performed using BD LSRFORTESSA and using Flow Jo software.

Rho GTPase Activity Assays

Rac1 and RhoA GTPase activities were assayed as described previously (Sander *et al*., 1999). Briefly, cells were gradually cooled on ice, washed with cold PBS (containing 1mM CaCl2, and 0.5mM MgCl2+) and lysed with a lysis buffer containing 0.5% Nonidet P-40, 10mM Tris, 150 mM NaCl, 50 mM MgCl2, protease inhibitor and 2 µg/ml PAK-CRIB peptide [208] or GST-Rhotekin (Sander et al., 1999). Cell lysates were cleared by centrifugation, and cleared supernatants were added to washed streptavidin beads (Rac-PAK-CRIB) or with glutathione beads (Rho-GST-Rhotekin), solubilized in SDS sample buffer and rotated for 30 min. at 4oC. Beads were washed and bound proteins were taken up in sample buffer (NuPage, Invitrogen) and used for Western blot analysis.

RhoA Activation in Real-Time

RhoA activity was monitored in real-time using a RhoA-specific FRET-based biosensor, as previously described (Kedziora et al., 2016). A FRET pair consisting of Cerulean3 and circularly permutated Venus was used. The HR1 region of PKN was used as the effector domain for activated RhoA. Cells were transfected with the biosensor and assessed for RhoA activation by LPA. GDE2-mCherry or mCherry-CAAX was co-transfected. At 48 hr after transfection, coverslips were mounted in an imaging ring and transferred to an inverted wide-field microscope (Nikon) equipped with a heated 63x, oil immersion objective. Excitation was at 425 nm and acceptor (CFP) and donor (Venus or YFP) emission was detected at the same time at 470±20 nm and 530±25 nm, respectively. FRET was expressed as the ratio of acceptor to donor emission.

RNA Sequencing and Bioinformatics

RNA from Shep2 knockdown and shControl Shep2 cells was extracted and subjected to RNA sequencing (RNA-seq) at the NKI Genomics Core Facility. The reads (65bp single-end) were sequenced on a Illumina HiSeq-2500 platform and mapped to the human reference genome (hg38) using TopHat (version 2.0.12) [209], which allows to span exon-exon splice junctions. TopHat was supplied with a known set of gene models, the transcriptome-index parameter (Ensembl version 77). The samples were generated using a stranded protocol, meaning that TopHat was guided to use the first strand as the library type. Tophat was run with bowtie 1 version 1.1 and uses the prefilter-multihits and no coverage as additional arguments. To count the number of reads per gene, a custom script (Itreecount) was used, which is based on the HTSeq-count [210] and has comparable output. Itreecount generates a list of the total number of uniquely mapped sequencing reads for each gene that is present in the provided Gene Transfer Format (GTF) file. Differential expression was performed using the R package Limma. Limma contains the Voom method [211], which normalizes to log2 counts per million reads per sample and corrects for the library size of each sample. After data transformation, differential expression was analyzed. Samples were compared against each other using the standard Limma pipeline. This provided log2-fold changes and p-values corrected for multiple testing. A gene was considered differentially expressed if the p-value < 0.05. All raw sequence data are deposited at GEO (accession number GSE74345).

Supplementary figures

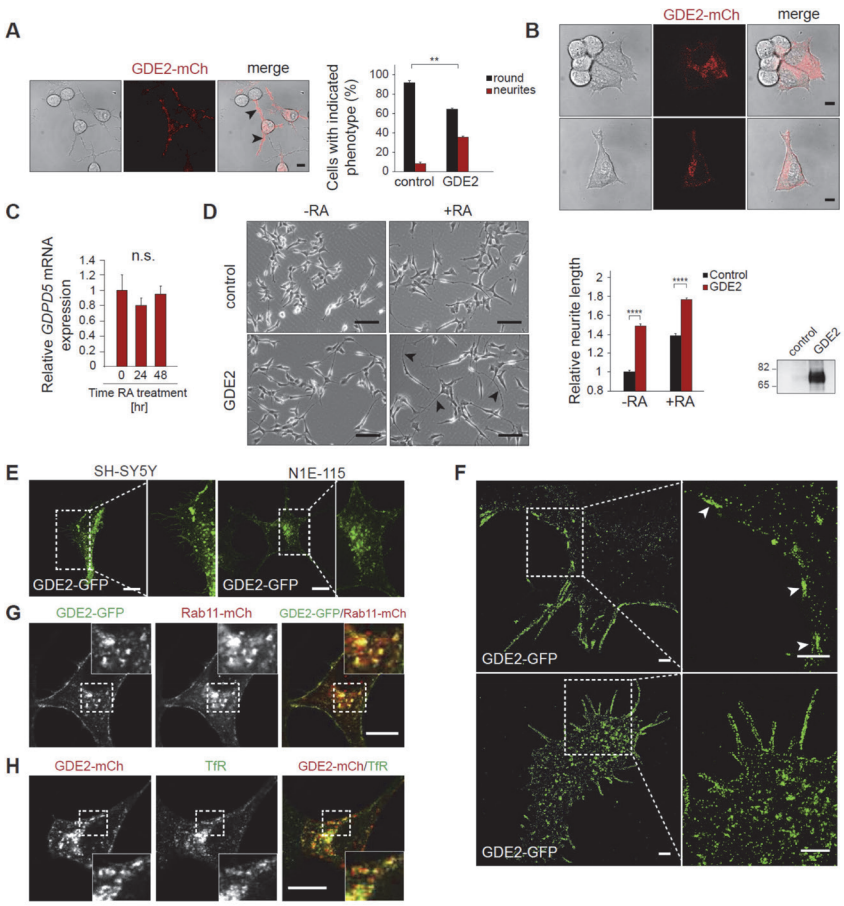

Figure S1. GDE2: morphological changes and subcellular localization. Related to Figure 2. **(A)** (Left) GDE2-induced neurite outgrowth (black arrows) in Neuro-2a cells expressing GDE2-mCh. Bar, 10 μm. (Right) Quantitative analysis of "round" or "neurite-bearing" morphologies of GDE2-overexpressing cells versus control cells (n= 300 cells, mean ± SEM). ** p value < 0.01 (Fisher's test). **(B)** Cell spreading in contacting and isolated N1E-115 cells expressing GDE2-mCh. Bar, 10 μm. **(C)** *GDPD5* expression (relative *to GAPDH*) in SH-SY5Y cells treated with retinoic acid (RA, 2 μM) for 0-48 hr (qPCR analysis). Error bars, mean ± SEM (triplicate measurements); n.s. not significant. **(D)** (Left) Neurite formation in control and GDE2-overexpressing SH-SY5Y cells in the absence or presence of RA (2 μM; 48 hr). (Right) Quantification of neurite outgrowth (n= 250 cells; mean ± SEM). **** p value < 0.0001 (unpaired t-test). GDE2 was detected using anti-GDE2 antibody. **(E)** Localization of GDE2-GFP in the indicated cell lines. Bar, 10 μm. **(F)** Localization of GDE2-GFP in N1E-115 cells as detected by super-resolution microscopy. White arrows point to distinct microdomains at the plasma membrane. Bar, 1 μm. **(G)** Localization of GDE2-GFP and Rab11-mCh in N1E-115 cells. Bar, 10 μm. **(H)** Localization of GDE2-mCh and endogenous transferrin receptor (TfR) in Dox-induced SH-SY5Y cells. Bar, 10 μm.

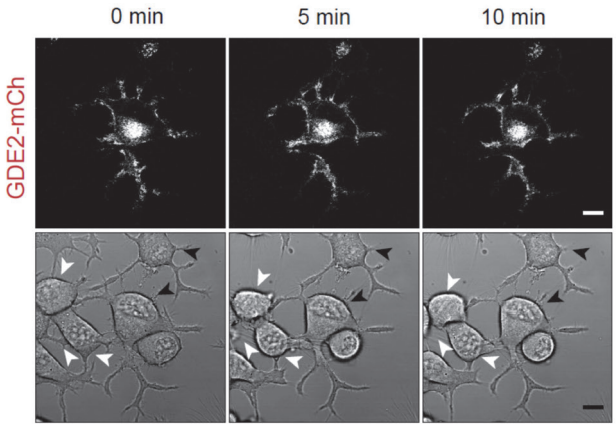

Figure S2. Inhibitory effect of GDE2 on neurite retraction by LPA. Related to Figure 3
N1E-115 cells were transfected with GDE2-mCh and stimulated by LPA (1 μM) for the indicated times. GDE2-mCh-expressing cells are indicated by black arrows, non-transfected cells by white arrows. See also Supplemental Movie S1 and S2.

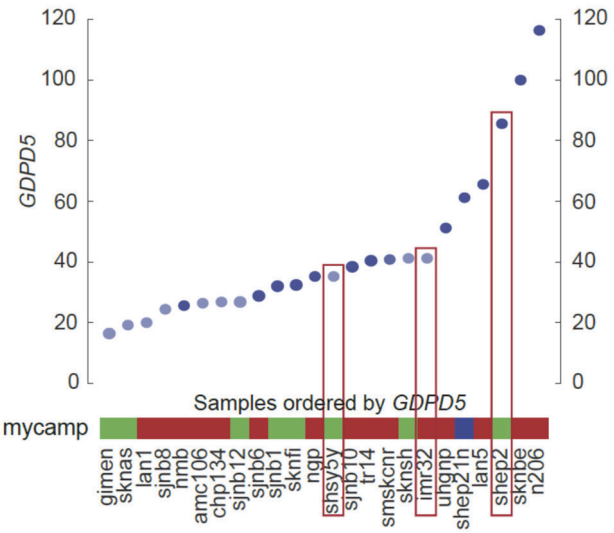

Figure S3. *GDPD5* expression in neuroblastoma cells. Related to Figure 4
GDPD5 expression in 24 different human neuroblastoma cell lines (microarray analysis); mycamp denotes *MYCN* amplification status. Shep2 cells were selected for knockdown studies.

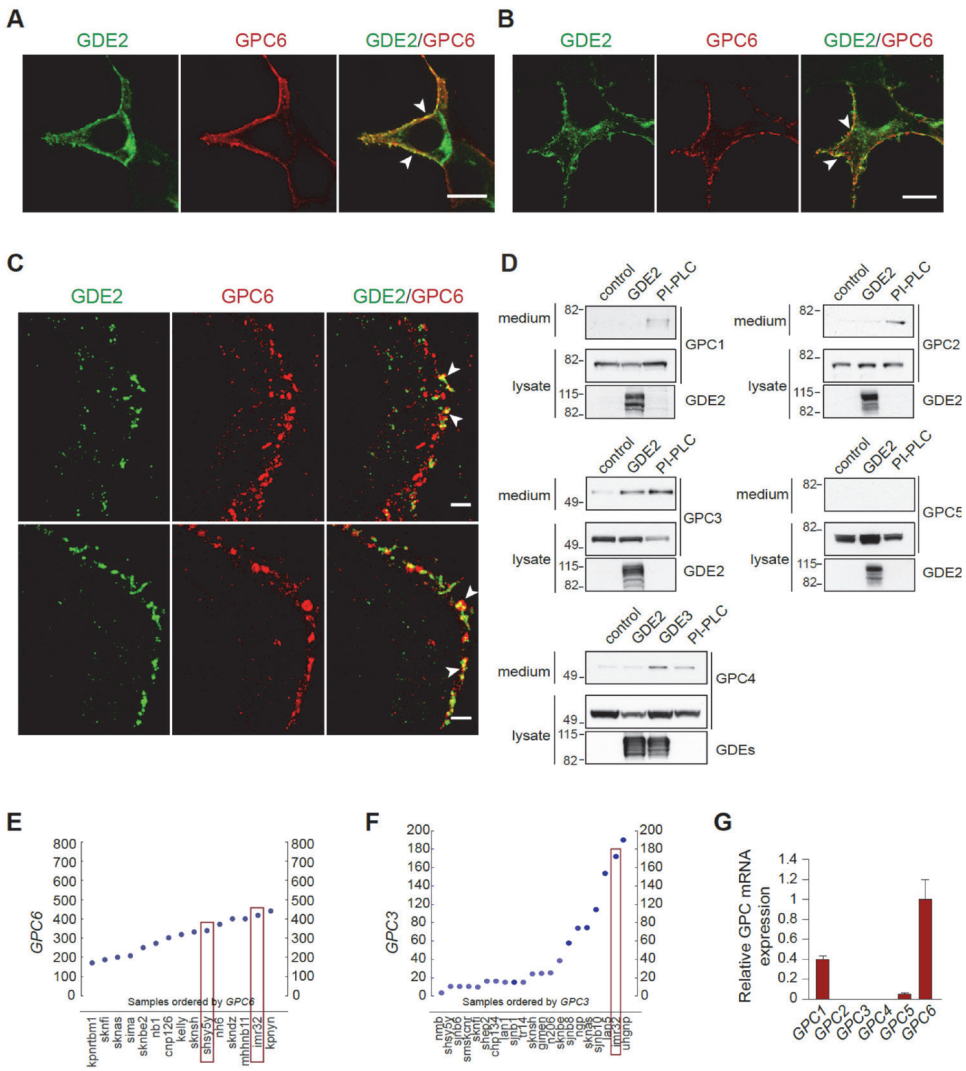

Figure S4. Glypican expression and GDE2-induced release. Related to Figure 5

(A,B) Confocal images of HEK293 cells (A) and N1E-115 cells (B) co-expressing GDE2-GFP and GPC6-HA. White arrows point to distinct microdomains (yellow) showing overlapping localization. Bar,10 μm. **(C)** Dual-color super-resolution images of N1E-115 cells co-expressing GDE2-GFP and GPC6-HA. White arrows point to distinct microdomains (yellow) showing overlapping localization. Bar, 1 μm. **(D)** HEK293 cells were co-transfected with GDE2-mCh and the indicated glypicans (HA-tagged). Glypican levels were assessed by immunoblotting of conditioned medium and cell lysates and. PI-PLC was used as positive control. **(E)** *GPC6* expression in the indicated neuroblastoma cell lines (microarray analysis). **(F)** *GPC3* expression in the indicated neuroblastoma cell lines (microarray analysis). **(G)** *GPC1-6* expression (relative to *GAPDH*) in N1E-115 cells (qPCR analysis). Error bars, mean ± SEM (triplicate measurements).

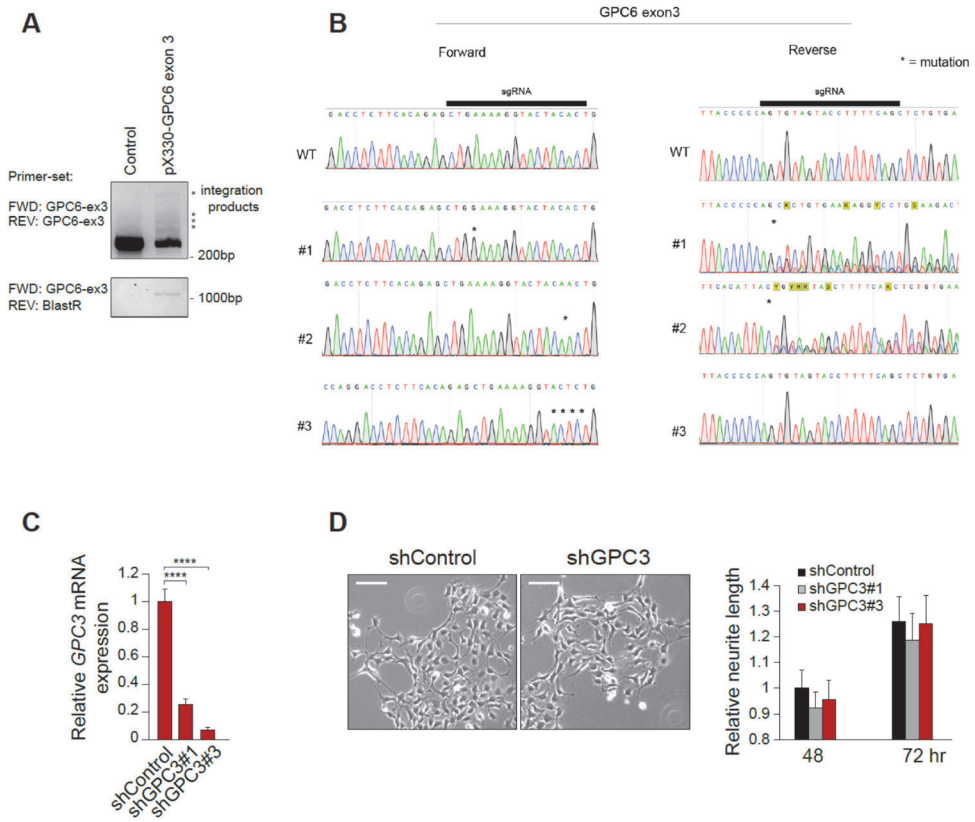

Figure S5. Validation of *GPC6* knockout in SH-SY5Y cells and assessment of GPC3 depletion in IMR-32 cells. Related to Figure 7

(A) *GPC6* knockout in SH-SH5Y cells was achieved using CRISPR/Cas9 genome editing. The panel shows incorporation of the BlastR gene as measured by PCR amplification of genomic DNA. **(B)** Sanger sequencing from clones targeted with CRISPR/Cas9 for GPC6 exon3. **(C)** *GPC3* mRNA expression (relative to *Cyclophilin A*) in control and GPC3-depleted IMR-32 cells, using two different shRNAs against GPC3. Errors bars, mean ± SEM; **** p value < 0.0001 (unpaired t-test). **(D)** (Left) IMR-32 cell morphology before and after GPC3 depletion. Bar, 100 µm. (Right) Quantification of neurite outgrowth in control and GPC3-depleted IMR-32 cells after 48 and 73 hr (n = 200 cells; mean ± SEM; differences

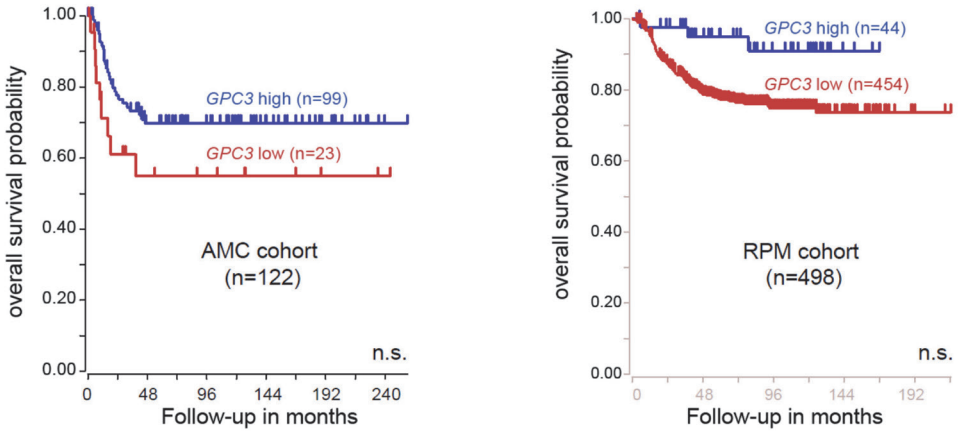

were not statistically significant).

Figure S6. *GPC3* expression and patient survival probability. Related to Figure 8
Kaplan-Meier analyses of *GPC3* expression versus overall survival in the indicated neuroblastoma patient cohorts.

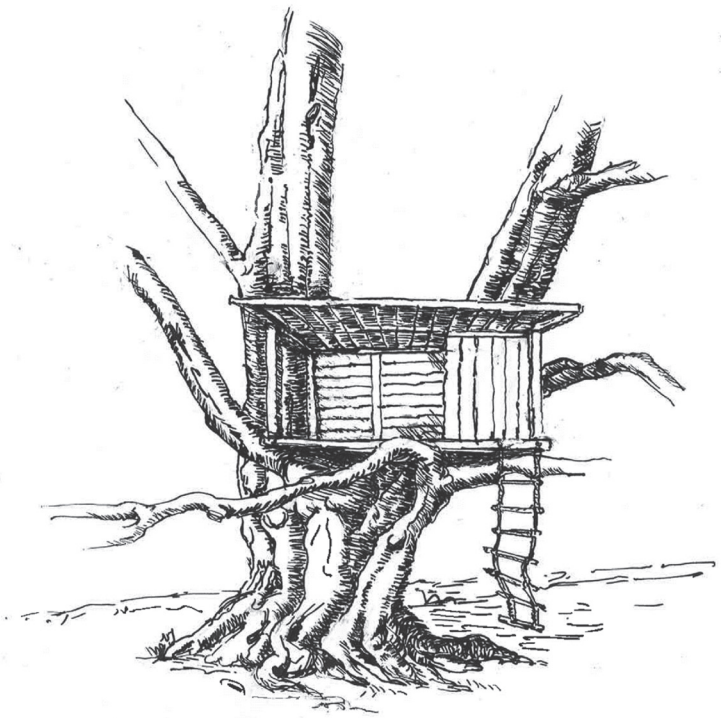

FAGUS SYLVATICA

Addendum Chapter 3

Neuronal differentiation through GPI-anchor cleavage

Adapted from: Oncotarget 2017;8:5672–5673 and Cell Cycle 2017;16:388-389

Elisa Matas-Rico, Michiel van Veen, Wouter H. Moolenaar
Division of Cell Biology, The Netherlands Cancer Institute, Amsterdam, Netherlands

Introduction

The cell surface of virtually all cell types harbors a great variety of Glycosylphosphatidylinositol (GPI)-anchored proteins with diverse biological functions. GPI-anchoring is a complex post-translational modification that anchors proteins in the outer leaflet of the plasma membrane [146]. GPI-anchoring may allow for lateral movement and some structural flexibility of membrane proteins, but otherwise the biological function of GPI anchors has long remained a mystery. Some GPI-anchored proteins are released from their anchor and detected in body fluids and cerebral fluid, implying involvement of putative GPI-specific phospholipases. But the mechanism and physiological significance, if any, of GPI-anchor cleavage has long remained unexplored. Recent studies have advanced the field by showing that selective cleavage of GPI-anchored proteins by an ecto-phosphodiesterase, termed GDE2, leads to neuronal differentiation [110, 137]. GDE2 (encoded by *GDPD5*) is a member of the glycerophosphodiesterase family [96] and characterized by six transmembrane domains and a large catalytic ectodomain. Since GDE2 hydrolyzes distinct substrates to promote neural differentiation, it will be important to explore the substrate selectivity of GDE2 in further detail and also that of its close relative GDE3 [96]. Here we focus on the nervous system since multiple GPI-anchored proteins are known to participate in the development and proper functioning. In fact, in humans, most germline mutations in the GPI-anchor synthesis pathway are presented with mental retardation phenotypes, underlining the importance of proper regulation of GPI-APs during neural development [212, 213]. Hence, comprehending the function and release of GPI anchored proteins in the nervous system could be indicative in finding new roles for GDE's.

GPI anchor release by GDEs

GDE2 was originally identified as a retinoic acid-inducible gene that promotes spinal motor neuron differentiation by inhibiting Notch signaling in adjacent neuronal progenitors [109]. Mechanistically, the Notch transmembrane receptor is activated by binding membrane-bound ligands on contacting cells. GDE2 was reported to cleave and release a GPI-anchored Notch regulator, termed RECK, that normally inhibits protease-dependent shedding of a Notch ligand [110]. By releasing RECK, GDE2 inactivates the ligand-Notch signaling axis and thereby promotes differentiation in contacting neuronal cells (**Fig.1**). Thus, in the developing spinal cord, GDE2 promotes neurogenesis in a non-cell-autonomous manner, requiring cell-cell contact [110]. Coherent with the previous findings we found that GDE induces neuroblastoma differentiation (Matas et al., 2017). Neuroblastoma is a highly heterogeneous disease, characterized by relatively few recurrent somatic mutations [214]. Some high-risk neuroblastomas are associated with mutations in Rho GTPase pathway genes that normally regulate the differentiated phenotype and are implicated in neuritogenesis and cell motility

[163]. Through overexpression and knockdown studies, GDE2 was found to change the Rac-RhoA activity balance leading to cell spreading, neurite outgrowth, inhibition of RhoA-driven neurite retraction and reduced cell motility in both mouse and human neuroblastoma cells. To our surprise we discovered that GDE2 does so through GPI-anchor cleavage of the heparan sulfate proteoglycan glypican-6 (GPC6) in a cell-autonomous manner, not requiring cell-cell contact [137] (**Fig.1**). It is of note that GDE2's closest family member GDE3, also cleaves GPC6 (and other GPI-anchored proteins) and is expressed in the nervous system, although its function there is unknown [17, 110]. Altogether these data suggest that GDE2 initiates a neuronal differentiation program and that understanding GPI-anchor release in the neuronal system may hint towards a possible role for other GDE's in general.

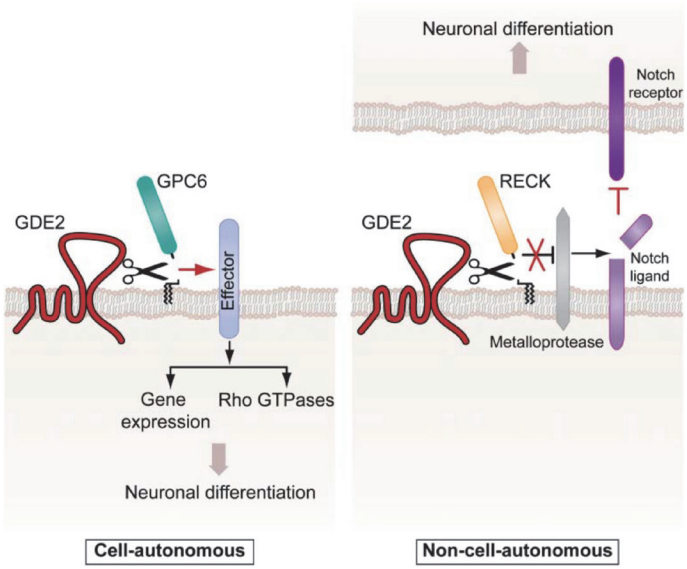

Figure 1. GDE2 cleaves GPI-anchored substrates to promote neuronal differentiation in distinct manners

Left panel, GDE2-induced cleavage of glypican-6 (GPC6) signals differentiation of neuroblastoma cells, involving both Rho GTPase-driven cytoskeletal remodeling and new gene transcription. Right panel, RECK cleavage is a trigger to downregulate Notch signaling in adjacent neural progenitors. It is unclear if GDE2 acts as a PLC or PLD.

GPI-anchored proteins in the nervous system

Glypicans

During neuronal development and normal homeostasis GPI-anchored proteins serve an important function as co-receptors and ligands of various signaling pathways. In fact, the

frequent occurrence of GPI-anchored proteins in the nervous system suggests a common underlying function, possibly being regulated release. One such protein family, glypicans, are indeed secreted in the nervous system. However, their soluble role remains largely unknown. Glypicans belong to the larger family of proteoglycans that are all composed of a core protein to which glycosaminoglycan side chains (GAGs) are attached. In vertebrates, GPCs play key roles during normal neuronal development [70, 215, 216], but are also associated with neurofibrillary tangles and amyloid plaques, formed during Alzheimer's disease [217, 218]. The six glypicans identified to date are known regulators of BMP/Wnt and Shh signaling pathways [219]. Mechanistically, they elicit their effect through direct binding of specific ligands, including Wnt and Hedgehog proteins, presenting them to cognate receptors. However, glypicans may also serve as (membrane-tethered) ligands in their own right by directly interacting with transmembrane receptors, such as the type-II receptor tyrosine phosphatases (RPTPs) and Leucine-rich repeat transmembrane receptors to modulate RPTP oligomerization and transmembrane signaling [199, 200, 220, 221]. Interestingly, type-II RPTPs influence neuronal morphology and have multiple intracellular binding partners including regulators of Rac/Rho activity [199, 201]. In a neuronal setting, loss of a glypicans (by GDE's) might thus lead to altered RPTP clustering at the plasma membrane with a consequent change in localized levels of tyrosine phosphorylated proteins involved in signaling pathways, like the Rac/Rho balance, that stimulates neurite outgrowth. Interestingly, releasing glypicans from the membrane not only depletes the membrane pool but also generates a soluble protein that may serve a distinctive role by itself. Notably soluble GPC4 and GPC6, secreted by astrocytes, activate synapse formation by recruiting and clustering dendritic AMPA receptors on neighboring membranes [189]. Mechanistically, soluble glypican 4 does so by signaling through presynaptic RPTPδ, leading to the release of presynaptic neuronal pentraxin 1 with consequent AMPA receptor accumulation on the postsynaptic terminal [222]. In line with the previous, mice lacking GPC4 or RPTPs both exhibit defects in synapse formation making them strong candidates for astrocyte-induced synapse homeostasis [189, 223]. Hence, by cleaving glypicans, GDE's could provoke a complex signaling cascade with loss of GPC-RPTP signaling *in cis* while simultaneously activating RPTP signaling *in trans*. Interestingly, GDE3 is highly expressed in GPC4 secreting astrocytes and *in vitro* studies have shown that GDE3 is capable of cleaving GPC4 (data unpublished and unpublished data from Shanthini Sockanathan). Moreover, mice lacking GDE3 exhibit similar synaptic defects as do GPC4-null mice (unpublished data from Shanthini Sockanathan). It is tempting to speculate that GDEs, through glypican cleavage and release, might alter the activation status of one or more transmembrane RPTPs to activate a biphasic neural program.

Candidate ligands

Multiple GPI-anchored ligands play essential roles in the nervous system and although the signaling axis they are involved in are generally well understood, the function of their GPI-anchor is not. The prion protein (PrP) is arguably the most enigmatic example. PrP can be secreted by metalloproteinases or unknown phospholipases [224]. When soluble, the PrP is thought to bind to a receptor for which multiple candidates exist. Interestingly, we have found in *in vitro* studies that PrP is a ligand for GDE2 (unpublished data), potentially being the long sought-after phospholipase for PrP. PrP exists in a normal PrP^{C} or a misfolded version, PrP^{Res}, which is associated with a variety of cognitive disorders like Creutzfeldt-Jakob disease. In contrast to wild type PrP^{C}, when mice express anchorless PrP^{C}, a secreted form is detected that accumulates in plaques, however, a clinical disease never develops [225]. On the contrary, when GPI-PrP and anchorless-PrP expression are combined, it accelerates the clinical symptoms. Based on these observations, the GPI anchor could play a role in the pathogenesis, although the physiological function of anchorless PrP is not well understood.

Ephrin A is another GPI-anchored ligand that is actively secreted from the membrane in glioblastoma cells [226]. Ephrin A belongs to a larger family of ephrins which are ligands for Eph receptor protein-tyrosine kinases. They play an important role during embryonic development and axon growth cone guidance by repelling migrating axons [227]. Ephrin signaling is complex and includes multiple distinct ligands and receptors. In general, when membrane bound, ephrin A ligands bind to their cognate receptor on opposing cells to mediate cell-cell communication that signals in both directions [228]. However, when cleaved, ephrin A is still able bind and activate its receptor, leading to, among others things, growth cone collapse [226]. Why ephrin A is secreted and whether phospholipases are involved is unknown.

Neurotrophic receptors

A GPI-anchored receptor specifically expressed in neurons is the ciliary neurotrophic factor receptor A (CNTFRa). CNTFRa is a member of the alpha-helical cytokine family and plays an important role during brain development [229]. CNTFRa enhances neuronal survival while deletion is embryonic lethal [230]. Upon ligand binding, by CNTF, CNTFRa forms a tripartite complex with LIFRβ and GP130 to activate the downstream signaling pathways JAK/STAT [231]. CNTFRa can be cleaved and soluble CNTFR is measured in cerebrospinal fluid [232]. Intriguingly, cleaved CNTFRa is still able to bind CNTF and LIFRβ to activate signaling pathways in distant cells, although the underlying mechanism is unclear [233, 234].

Another receptor, the Glial cell line-derived neurotrophic factor receptor (GDNFR or GFRα1) is a GPI-anchored receptor for GDNF and neurturin (NTN). GFRα1 is a coreceptor

that forms a complex with the Ret tyrosine kinase and plays key roles in neuron survival and differentiation. In fractionation studies GFRα1 was mostly recovered in the soluble fraction, indicating GFRα1 is actively secreted [235]. Moreover, the soluble form of the receptor is still able to promote neuronal survival in the presence of its ligand (GDNF), suggesting a distinctive role for the cleaved receptor in distant signaling [236].

Adhesion molecules

Contactin1 is an essential neuronal adhesion molecule and mutations in the gene cause a familial form of lethal congenital myopathy [237]. When membrane bound, contactin1 is involved in neurite extension and adhesion [238]. Interestingly though, when added in a soluble form, contactin1 continued to enhance neurite outgrowth without affecting adhesion [239]. When cerebrospinal fluid, a natural source of soluble contactin1, was used similar affects were observed that could be partially blocked by inhibitory antibodies. The underlying mechanism could be binding of contactin1 to PTPRζ which was shown to promote oligodendrocyte maturation [240]. How contactin1 is cleaved and if cleavage is essential for normal development is unknown.

Conclusion

While only a selection of GPI-anchored ligands, receptors and adhesion molecules present in the nervous system are discussed, they are all found in a soluble form. Until recently, little was known about the mechanisms and physiological relevance underlying their shedding. The finding that a cell-intrinsic phosphodiesterase, GDE2/GDPD5, hydrolyzes GPI anchors to modulate signaling pathways and alters cell behavior sheds new light on the mystery of these GPI-anchored proteins [110, 137, 138]. All GDE studies performed so far have focused on loss of function effects after cleavage of a GPI-anchored protein, but recent findings have shown that some soluble GPI-anchored proteins (e.g. GPC4) serve a distinct function by itself [189]. Therefore, the scenario that GDE's could be ligand forming instead of "cleave and release" type enzymes warrants further study. Future studies should also address whether (some of) these proteins are indeed GDE substrates, and how their cleavage and release may impact neuronal physiology. It will also be important to understand how neuronal GDE expression and activity are regulated by either cell-intrinsic or cell-extrinsic cues. Finally, from a clinical perspective, the new findings suggest that activation or inhibition of the GDE signaling pathway by pharmacological means might be of benefit to patients having low or high GDE expression levels. However, since GDE's are not classic phosphodiesterases, it will be quite challenging to develop drug-like allosteric activators or inhibitors.

AESCULUS HIPPOCASTANUM

Chapter 4

Glycerophosphodiesterase GDE2/GDPD5 affects pancreas differentiation in zebrafish

Int J Biochem Cell Biol. 2018; 94:71-78

Michiel van Veen[2&], Laurie A. Mans[1&], Elisa Matas-Rico[2], Jason van Pelt[1], Anastassis Perrakis[3], Wouter H. Moolenaar[2], and Anna-Pavlina G. Haramis[1]

[1] Institute of Biology, Leiden University, Leiden, The Netherlands
[2] Division of Cell Biology, Netherlands Cancer Institute, Amsterdam, The Netherlands
[3] Division of Biochemistry, Netherlands Cancer Institute, Amsterdam, The Netherlands
[&] These authors contributed equally

Abstract

Notch signaling plays an essential role in the proliferation, differentiation and cell fate determination of various tissues, including the developing pancreas. One regulator of the Notch pathway is GDE2 (or GDPD5), a transmembrane ecto-phosphodiesterase that cleaves GPI-anchored proteins at the plasma membrane, including a Notch ligand regulator. Here we report that Gdpd5-knockdown in zebrafish embryos leads to developmental defects, particularly, impaired motility and reduced pancreas differentiation, as shown by decreased expression of insulin and other pancreatic markers. Exogenous expression of human GDE2, but not catalytically-dead GDE2, similarly leads to developmental defects. Human GDE2 restores insulin expression in Gdpd5a-depleted zebrafish embryos. Importantly, zebrafish Gdpd5 orthologues localize to the plasma membrane and show catalytic activity against GPI-anchored GPC6. Thus, our data reveal functional conservation between zebrafish Gdpd5 and human GDE2, and suggest that strict regulation of GDE2 expression and catalytic activity is critical for correct embryonic patterning. In particular, our data uncover a role for GDE2 in regulating pancreas differentiation.

Introduction

A better understanding of pancreatic homeostasis is essential to identify new ways to increase insulin-producing beta cell number and to enhance their function, in order to tackle diabetes, a rising epidemic.

The Notch cell-to-cell signaling axis plays an important role in proliferation, differentiation and cell-fate decisions in the developing pancreas and other tissues [241, 242]. Notch receptor signaling is activated by transmembrane Notch ligands in adjacent cells [243]. Following ligand binding, Notch is cleaved by the metalloprotease TACE (factor-a-converting enzyme) [243]. Truncated Notch is in turn cleaved by the a secretase complex, leading to intracellular release of NICD (Notch intracellular domain) [243] and activation of Notch target genes [243].

Different levels of Notch can elicit distinct fates [241, 242]. Notch signaling maintains progenitor cells in an undifferentiated proliferative state and regulates timing of differentiation, not only in the embryonic pancreas but also in developing motor neurons [109, 244]. Loss of Notch signaling in mice [245] and zebrafish [244, 246] results in aberrant/excessive differentiation of pancreatic progenitors to endocrine cells, at the expense of the later-appearing exocrine cells [242]. Modulation of Notch signaling may thus affect the balance between proliferation and differentiation of pancreatic progenitor cells.

A recently identified modulator of Notch activity is GDE2 (aka GDPD5), a multipass membrane glycoprotein with an extracellular glycerophosphodiesterase (GDPD) domain. The GDE2 catalytic domain cleaves a subset of glycosylphosphatidylinositol (GPI)-anchored proteins, including a Notch ligand regulator (RECK) [110] and certain heparan sulfate proteoglycans, the glypicans (GPCs) [113, 137]. Through RECK cleavage, GDE2 sheds and inactivates the Notch ligand Delta-like 1 in the developing spinal cord, leading to Notch inactivation in adjacent progenitor cells [109, 110]. Thus, GDE2 promotes motor neuron differentiation by downregulating Notch signaling during spinal cord development. Mice lacking GDE2 exhibit selective losses of limb-innervating motor neuron pools leading to neurodegeneration [109, 113]. In addition, GDE2 can promote neuronal differentiation in a cell-autonomous manner, namely through GPI-anchor cleavage of glypican-6 (GPC6), which correlates with improved clinical outcome in neuroblastoma [247]. However, a possible role for GDE2 in regulating the fate of non-neuronal cell types has not been investigated to date.

Here, we examine the role of Gde2 during embryonic development, focusing on pancreas differentiation in zebrafish. Zebrafish is an excellent model to conduct developmental studies owing to the availability of large numbers of readily- accessible, transparent embryos. Importantly, mammalian and zebrafish pancreas share many morphological and physiological similarities [242], while important genes in mammalian islet development are functionally conserved in zebrafish [242]. The conservation of signaling pathways and mechanisms of

pancreas development suggests that results found in zebrafish will advance our understanding of pancreas development in humans.
We show that Gdpd5 knockdown affects the differentiation of specific endocrine and exocrine progenitors. Furthermore, exogenous expression of human GDE2 restores insulin expression in Gdpd5a-depleted zebrafish embryos. Expression of human GDE2 but not catalytically-dead GDE2 in zebrafish embryos leads to developmental defects, in a dose-dependent manner. Importantly, zebrafish Gdpd5 orthologues localize to the plasma membrane and show catalytic activity against GPC6. These results highlight the functional conservation of GDE2 and suggest that tight regulation of Gdpd5a levels and catalytic activity are important for correct embryonic patterning.

Results

Analysis of zebrafish Gde2/Gdpd5

GDE2, encoded by *GDPD5*, is a six-transmembrane-domain protein with an extracellular phosphodiesterase domain and intracellular N- and C-termini (Fig. 1A). GDE2 catalytic activity has long been elusive, but recent studies have shown that GDE2 cleaves GPI-anchored proteins at the plasma membrane to drive neuronal differentiation and survival, in either a cell-autonomous or non-cell-autonomous manner [110, 113, 137] (Fig. 1A). Human *GDPD5* has two orthologues in the zebrafish genome, *gdpd5a* and *gdpd5b. Gdpd5a* (glycerophosphodiester phosphodiesterase domain containing 5a) gives rise to three alternatively spliced isoforms; Isoforms *gdpd5a*-001 and *gdpd5a*-002 are included within the long isoform *gdpd5a*-201, which encodes for 595-aa protein. Phylogenetic analysis shows that the long isoform of zebrafish *gdpd5a* is closely related to human, rodent and chicken *GDPD5/Gdpd5* (Fig. 1B). The predicted catalytic domains of human GDE2 and zebrafish Gdpd5a share 53% identity and 81% similarity (Fig. 1C). *Gdpd5b* (ENSDARG00000076962) encodes a 566-aa protein that is characterized by a relatively short, truncated C-terminal tail (SFig. 1).

Gdpd5 depletion leads to developmental defects

To investigate the function of Gdpd5 during zebrafish embryonic development, we knocked down its function by using antisense morpholino oligonucleotides (MO) against *gdpd5a* and *gdpd5b* mRNAs. The MO against *gdpd5a* mRNA targets the 5'UTR of the long isoform, *gdpd5a*-201, and blocks translation of the message [248]. Since the other isoforms are included in *gdpd5a*-201, we reasoned that this MO would block translation of all isoforms.

Zebrafish embryos were injected with various amounts of *gdpd5a*MO at the 1-2 cell stage, and development of the injected embryos was followed up to 5 days post-fertilization (dpf). Injections with low amounts (< 8,4 ng/ul) MO did not result in morphological abnormalities. Following injection of 8,4 ng/ul (1 mM) *gdpd5a*MO, injected embryos

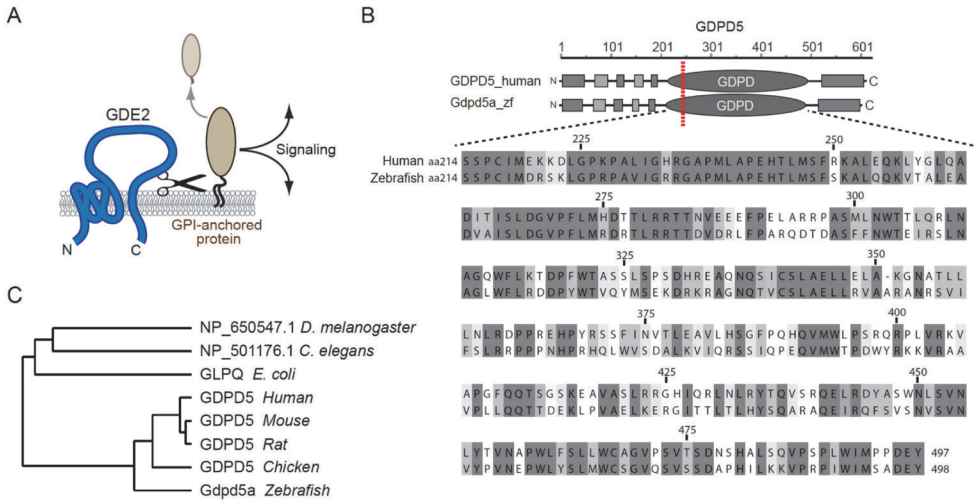

Figure 1. Sequence analysis of zebrafish Gdpd5a

(A) GDE2 cleaves GPI anchored proteins at the plasma membrane resulting in their shedding with consequent activation of signalling pathways, either in the same cell or in adjacent cells. **(B)** Amino acid sequence comparison between human GDPD5 and zebrafish Gdpd5a. The red line depicts key catalytic residue H^{233} in GDE2 [137]. Sequence comparison of the ecto-domain using Clustal Omega, shows identical residues in dark grey and similar residues in light grey. The catalytic domains share 52% sequence identity and 82% similarity. **(C)** Phylogenetic analysis showing that zGdpd5a is closely related to mammalian GDPD5. Protein sequences used: hGDPD5 (NP_110419.5), mGDPD5 (NP_958740.2), rGDPD5 (XP_006223480.1), cGDPD5 (NP_001032348.1), zGDPD5 (XP_005157799.1), *D. melanogaster* GDPD5 (NP_650547), *C. elegans* GDPD5 (NP_501176), *E. coli* GDPD5 (NP_416742.1).

exhibited developmental defects. Specifically, the majority of *gdpd5a*MO-injected embryos exhibited heart abnormalities accompanied by heart oedema, as well as a shorter and bent body axis (Fig. 2). Furthermore, while at 3 dpf almost all non-injected controls have hatched from their chorions, the majority of *gdpd5a*MO-injected embryos were still in their chorions, indicating inability to hatch (SFig. 2). At 5 dpf, very few of the *gdpd5a*MO-injected larvae had hatched. The Gdpd5a-depleted larvae that hatched (either on their own or following manual dechorionation) showed severe motility defects, either swimming inability or trembling (data not shown), consistent with *Gdpd5* knockout causing behavioral motor deficits in mice [113]. To investigate the function of Gdpd5b in zebrafish embryonic development, we injected a morpholino targeting the 5' UTR of the zebrafish *gdpd5b* mRNA. Embryos injected with *gdpd5b*MO at the one-cell stage, exhibited dose-dependent developmental defects at 3 dpf. Specifically, injection of 2ng/ul (0,25 mM) *gdpd5b*MO led to slight body curvature defects and heart oedemas (SFig. 3B). Following injection of 4 ng/ul (0,5 mM) *gdpd5b*MO, injected

embryos showed more severe axis defects, small eyes, and larger heart oedemas (SFig. 3C). Finally, embryos injected with 8 ng/ul (1mM) *gdpd5b*MO showed very severe antero-posterior axis truncations, cyclopia, and very large heart oedemas (SFig. 3D). In contrast to *gdpd5a* morphants however, the majority of *gdpd5b*MO-injected embryos hatched normally and did not show motor defects. These results indicate that the two zebrafish Gdpd5 homologs have both shared and distinct functions during zebrafish development.

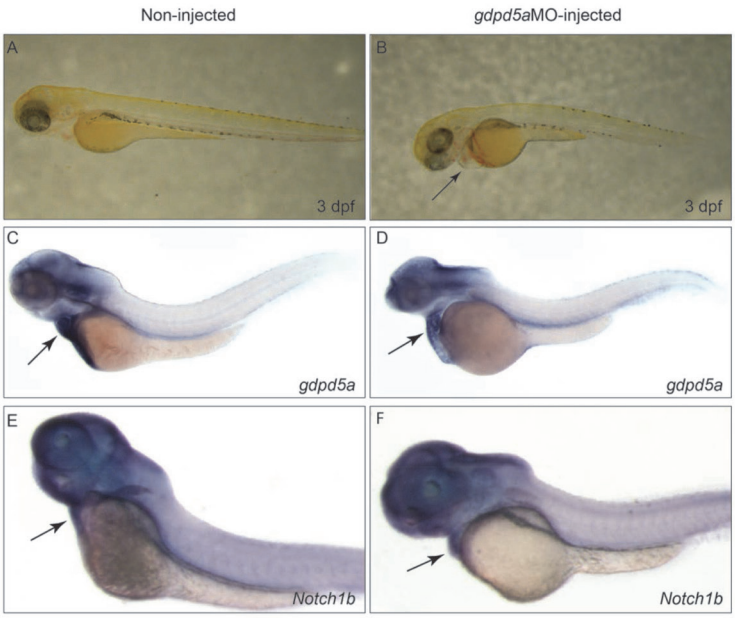

Figure 2. Gdpd5a depletion causes developmental defects
(**A)** Non-injected embryo at 3 dpf. Arrow indicates looped heart. (**B)** Representative example of a *gdpd5a*MO-injected embryo at 3 dpf. *Gdpd5a*MO-injected embryos show a bent and shorter body axis, heart oedemas (arrow) and unlooped heart. Whole-mount *in situ* hybridization (WISH) for expression of *gdpd5a* and *notch1b* in non-injected wt **(C, E**) and *gdpd5a*MO-injected embryos **(D, F)** at 3 dpf. Lateral views. (**C**) wt embryo at 3 dpf stained for *gdpd5a*. *Gdpd5a* expression is detected in the brain, strongly in the heart (arrow) as well as the intestine. (**D**) *Gdpd5*MO-injected embryo at 3 dpf stained for *gdpd5a*. *Gdpd5a* is expressed at comparable levels as in non-injected controls, except for reduced expression in the heart (arrow). **(E)** wt embryo at 3 dpf stained for *notch1b*. Strong expression in the head and heart (arrow) is detected **(F)** *Gdpd5*MO-injected embryo at 3 dpf stained for *notch1b*. The expression pattern of *notch1b* is similar to that of the non-injected controls.

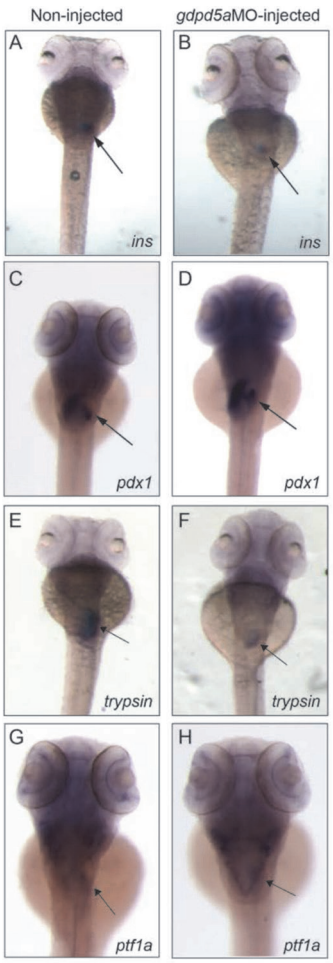

Figure 3. Expression of *insulin* and *trypsin*, but not *pdx1* or *ptf1a*, is reduced upon Gdpd5a knockdown

WISH for expression of the endocrine pancreas markers, *insulin (ins)* and *pancreatic and duodenal homeobox 1* (*pdx1)* and the exocrine pancreas markers, *trypsin* and *ptf1a* in non-injected wt (A, C, E, G) and *gdpd5a*MO-injected embryos at 3 dpf (B, D, F, H). Dorsal views. **(A)** wt embryo at 3 dpf stained for *insulin*. Strong expression is detected in the endocrine pancreas (arrow). **(B)** *Gdpd5*MO-injected embryo at 3 dpf. *ins* expression is dramatically reduced. **(C)** wt embryo at 3 dpf stained for *pdx1*. *Pdx1* is expressed in the intestine and endocrine pancreas (arrow). **(D)** *Pdx1* expression in the intestine and endocrine pancreas is very similar in *gdpd5*MO-injected embryos at 3 dpf. **(E)** wt embryo at 3 dpf stained for *trypsin*. Strong expression is detected in the exocrine pancreas (arrow). **(F)** *Gdpd5*MO-injected embryo at 3 dpf. *Trypsin* expression is dramatically reduced. **(G)** wt embryo at 3 dpf stained for *ptf1a. Ptf1a* expression is detected in the brain and the exocrine pancreas (arrow). **(H)** *Gdpd5*MO-injected embryo at 3 dpf. *Ptf1a* is expressed at comparable levels in the brain and exocrine pancreas (arrow) as in non-injected controls.

Expression studies

We next assayed *gdpd5a* and *notch1b* expression in *gdpd5a*MO-injected embryos at 3 dpf. We analysed expression of *gdpd5a* by *in situ* hybridization using an antisense riboprobe against *gdpd5a*-201. *Gdpd5a* mRNA was expressed in the brain and intestine, and at high levels in the heart and associated blood vessels in larvae at 3 dpf (Fig. 2C). This localization pattern suggests a role for *gdpd5a* during differentiation of these organs. The MO against *gdpd5a* is targeted to the 5' UTR including the ATG start codon blocking translation, and is not expected to influence mRNA levels. Nonetheless, we detected reduced expression of *gdpd5a* mRNA in *gdpd5a*MO-injected embryos, particularly in the heart (Fig. 2D), suggesting that the MO may affect the stability of the *gdpd5a* mRNA. We also assayed *notch1b* expression in *gdpd5a* morphants. *Notch1b* is expressed highly in brain and heart of 3 dpf un-injected embryos (Fig. 2E). *Notch1b* expression was comparable in *gdpd5a* morphants (Fig. 2F).

Pancreas differentiation is affected upon Gdpd5 depletion

Given the role of Notch1b signaling in pancreas differentiation and the purported role of Gdpd5 in modulating Notch activity, we examined how Gdpd5a depletion affects pancreas differentiation in zebrafish embryos. The pancreas in zebrafish develops from the posterior foregut endoderm; the dorsal bud which produces endocrine cells emerges after 24 hours post-fertilization (hpf), and the ventral bud emerges at 32 hpf and produces mostly exocrine and some endocrine cells [249]. At around 72 hpf the pancreas is fully developed [242]. At 14 hpf the pancreatic progenitor cells express different levels of *pdx1* (Pancreatic and duodenal homeobox 1) [242]. Cells expressing high levels of *pdx1* give rise to the endocrine cells, while cells with lower *pdx1* expression give rise to exocrine and intestinal cells. The first expression of *insulin* begins at 15 hpf when the insulin-producing cells begin to migrate towards the midline (Tehrani and Lin, 2011). In the mature pancreas, insulin is expressed exclusively in the beta cells.

To investigate the role of Gdpd5a in pancreas differentiation we studied the expression of markers of endocrine and exocrine pancreas components in wt and *gdpd5a* morphants at 3 dpf. In *gdpd5a*MO-injected embryos *insulin* (*ins*) expression was greatly reduced (Fig. 3A). *Pdx1* was expressed in the head, intestine and endocrine pancreas at 3 dpf (Fig. 3C and SFig. 4A), with no differences in *pdx1* expression between non-injected and *gdpd5a*MO-injected embryos (Fig. 3D and SFig. 4B). We therefore conclude that the defect in insulin expression is specific.

We next examined exocrine pancreas development in Gdpd5a-depleted embryos. *Trypsin* and *pancreas-specific transcription factor 1a* (*ptf1a*) mark the exocrine pancreas. As shown in Fig. 3E, *trypsin* expression was dramatically reduced in *gdpd5a*MO-injected embryos compared to un-injected controls. *Ptf1a* was strongly expressed in the head and the exocrine pancreas in un-injected controls at 3 dpf (Fig. 3G and SFig. 4C). The *ptf1a* expression pattern was not altered in *gdpd5a*MO-injected embryos (Fig 3H and SFig. 4D).

To investigate whether Gdpd5b depletion would also affect pancreas differentiation, we assayed *insulin* and *trypsin* expression in embryos at 3 dpf, following injection of 2 ng/ul *gdpd5b*MO at the one-cell stage. As mentioned, this concentration of *gdpd5b*MO leads to only mild developmental defects. We found that upon *gdpd5b*MO injection, expression of both *insulin* and *trypsin* was reduced in Gdpd5b morphants at 3 dpf (SFig. 5). Specifically, the *insulin* expression domain was smaller and appeared split in *gdpd5b*MO-injected embryos (SFig. 5B, D). Furthermore, the *trypsin* expression domain was smaller and irregularly shaped in *gdpd5b*MO-injected embryos (SFig. 5F, H). These results suggest that the two zebrafish Gdpd5 genes share common functions in pancreas differentiation.

Since Gdpd5a-depleted embryos exhibit mobility defects and impaired pancreas differentiation, and *Gdpd5* knockout in mice leads to motor neuron defects [109], we examined expression of *islet1* in Gdpd5a morphants. The transcription factor Islet1 is involved in both motor neuron differentiation and pancreas differentiation in mice and zebrafish [250] [251]. *Islet1* was expressed in the brain, spinal motor neurons and the pancreas in wt embryos at 3 dpf (Fig. 4A, C). In Gdpd5a morphants, *islet1* was expressed at high levels in the brain and pancreas (Fig. 4B, D). However, in the ventral spinal cord, *islet1* expression was reduced upon Gdpd5a knockdown (Fig. 4B).

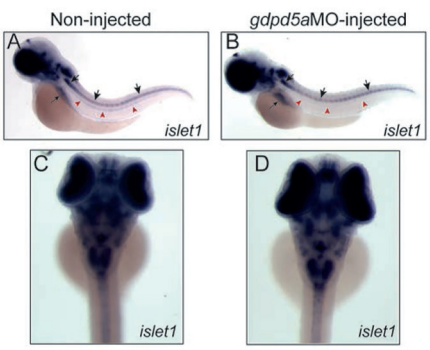

Figure 4. *Islet1* expression upon Gdpd5 knockdown
WISH hybridization for *islet1* expression on non-injected **(A, C)**, or *gdpd5*MO-injected embryos **(B, D)** at 3 dpf. **(A, B)** Lateral views, anterior to the left. **(A)** wt embryo at 3 dpf, *Islet1* is expressed in the brain, spinal cord (arrowheads) and the pancreas (arrow). **(B)** *Islet1* is expressed at similar levels in *gdpd5*MO-injected embryo. **(C, D)** Dorsal views of the head region. **(C)** wt embryo at 3 dpf. *Islet1* is expressed at distinct domains in the brain. **(D)** *Gdpd5*MO-injected embryos at 3 dpf show a staining pattern similar to that in non-injected controls.

Expression of human GDE2 in zebrafish leads to developmental defects

To investigate the functional conservation between human GDE2/GDPD5 and zebrafish Gdpd5, we injected mRNA encoding human GDE2 (hGDE2) tagged with HA in zebrafish embryos at the one-cell stage. Expression of hGDE2-HA mRNA led to developmental abnormalities in a dose-dependent manner (Fig. 5B, C). Specifically, hGDE2 mRNA-injected larvae showed malformations in the body axis and defects in the vasculature at 4 dpf (Fig. 5C). Higher doses resulted in more severe disruption of the axis, of the vasculature, blood accumulation and heart oedemas (Fig. 5C). Importantly, expression of catalytically-dead human GDE2 ($GDE2^{His233Ala}$ or $GDE2^{His233Ala/His275Ala}$) [137] did not induce morphological abnormalities (Fig. 5D). We verified that wt hGDE2, $hGDE2^{His233Ala}$ and $hGDE2^{His233Ala/His275Ala}$ are expressed in zebrafish at comparable levels (Fig. 5E). These data indicate that

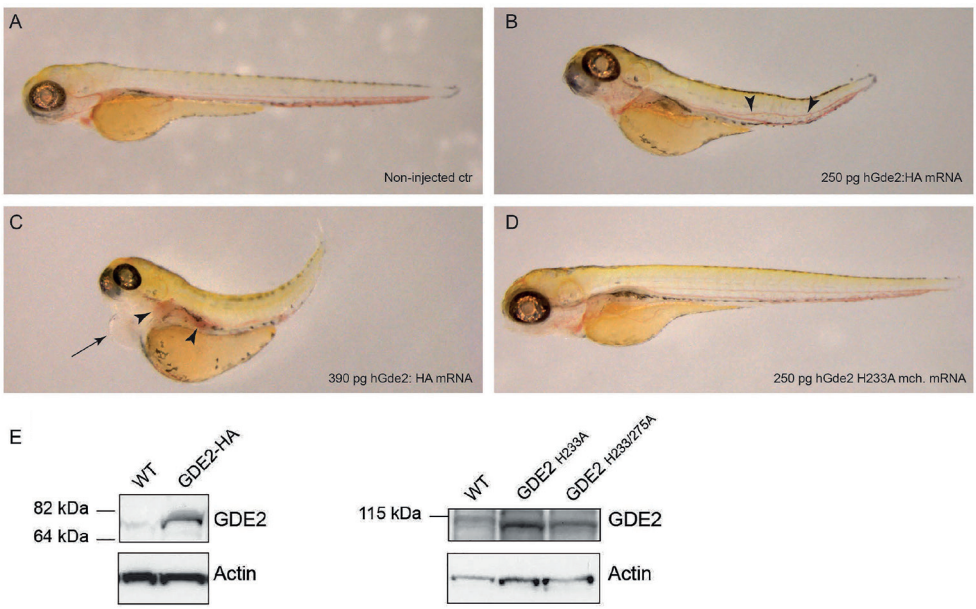

Figure 5. Expression of human GDE2 leads to developmental defects, depending on GDE2 catalytic activity

Representative pictures of zebrafish larvae at 4 dpf that have been injected at the one-cell stage with mRNAs encoding human GDE2:HA (B, C), or catalytically-dead $hGDE2^{H233A}$ mRNAs (D). Lateral views, anterior to the left. **(A)** Non-injected larva at 4 dpf. **(B)** Larva injected with 250 pg of wt hGDE2:HA mRNA. The body axis is shorter with an upward curvature, and defects in the organization of posterior vasculature can be observed (arrowheads). **(C)** Larva injected with 390 pg of hGDE2:HA. The defects are stronger, the body axis is severely shortened, there is blood accumulation and disruption of the posterior vasculature (arrowheads), as well as heart oedemas (arrow). **(D)** Larva injected with 250 pg of the catalytically-dead $hGDE2^{H233A}$; mcherry mRNA. No obvious morphological abnormalities are observed. **(E)** Western-blot analysis of zebrafish larvae at 4 dpf, expressing HA-tagged wt human GDE2, or mCherry tagged GDE2 catalytic dead mutant, $GDE2^{H233A}$. Actin is used as a loading control.

the malformations observed depend on the catalytic activity of GDE2, and they confirm functional conservation between human and zebrafish GDE2.

We next examined whether exogenously provided human GDE2 could rescue the defects in pancreas differentiation induced by Gdpd5a knock-down. We assayed for *insulin* expression in embryos that have been injected with either 1mM *gdpd5a*MO, 300pg hGDE2-HA mRNA, or co-injected with 1mM *gdpd5a*MO and 300pg hGDE2-HA mRNA. *Insulin* expression was dramatically reduced in Gdpd5a morphants at 3 dpf as we previously observed (Fig 6B). Expression of hGDE2-HA mRNA did not affect *insulin* expression (Fig. 6C). Notably, *insulin* expression was restored in embryos that have been co-injected with *gdpd5a*MO and hGDE2-HA mRNA (Fig. 6D). These results further validate functional conservation between zebrafish and human GDE2 in pancreas differentiation.

To further validate whether the conservation extends at the biochemical level, we examined zebrafish Gdpd5 enzymatic activity using cell-based assays. We co-expressed Glypican-6 (GPC6) and zebrafish constructs or human GDE2, confirmed that zebrafish Gdpd5 localized to the plasma membrane (Figure 7A), and examined the presence of GPC6 in the conditioned medium by immunoblotting, as described by [247]. We used intact cells treated with bacterial phospholipase C (PI-PLC) as positive control. As shown in Figure 7B, we found GPC6 released into the medium from cells transfected with zebrafish Gdpd5, although the amount of GPC6 detected into the medium appears to be smaller than that generated by hGDE2 cleavage.

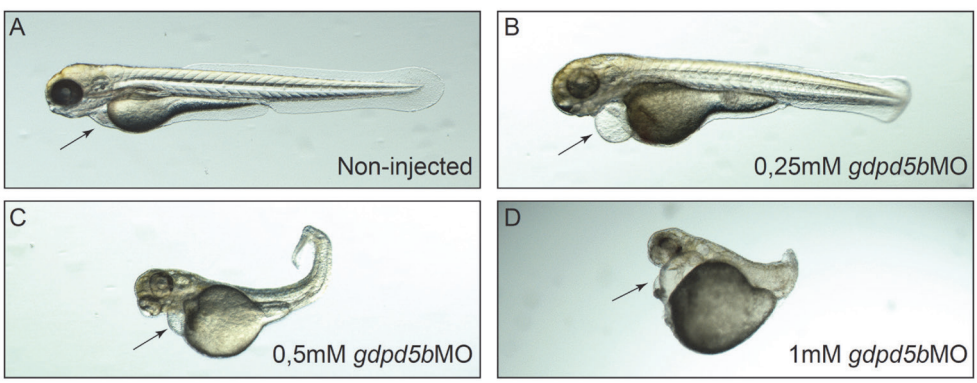

Figure 6. Human GDE2 mRNA restores *insulin* expression in Gdpd5a morphants.
Representative pictures of zebrafish embryos at 3 dpf stained for *insulin (ins)* expression that have been either non-injected (A), *gdpd5a*MO-injected (B), hGDE2 mRNA-injected (C) or co-injected with *gdpd5a*MO + hGDE2 mRNA (D), at the one-cell stage. Dorsal views, anterior to the right. **(A)** Non-injected control embryo at 3 dpf Strong *ins* expression is detected in the endocrine pancreas (arrow). **(B)** *Gdpd5*MO-injected 3 dpf embryo. *ins* expression is dramatically reduced (arrow). **(C)** 3 dpf embryo injected with 300 pg hGDE2 mRNA. Arrow indicates *ins* expression. **(D)** 3 dpf embryo that was co-injected with 1mM *gdpd5a*MO and 300 pg hGDE2 mRNA at the one-cell stage. *Ins* expression is restored (arrow).

Taken together, these results demonstrate that zebrafish Gdpd5 can cleave GPC6 and show that activity over GPC6 is conserved between hGDE2 and zebrafish GDPD5a.

Discussion

In this study we have identified a previously unknown role for glycerophosphodiesterase Gde2 (Gdpd5) in non-neuronal cell types, particularly the pancreas. Here, we focused on the possible role of Gdpd5 during pancreas development in zebrafish and show that Gdpd5 knockdown leads to defects in the differentiation of specific endocrine and exocrine progenitors.

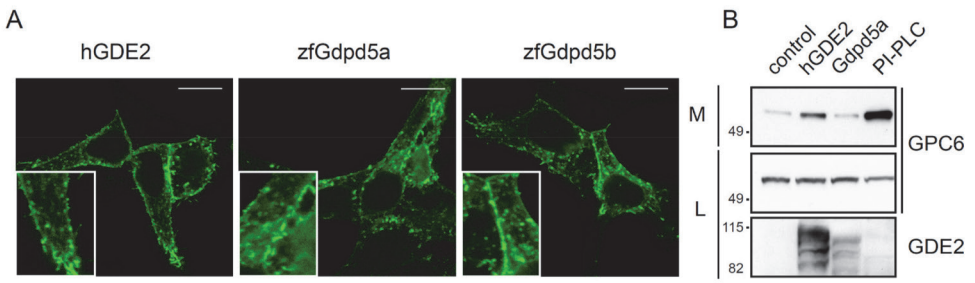

Figure 7. Zebrafish Gdpd5 orthologues localize to the plasma membrane and promote GPC6 release (**A**) Confocal images of HEK293 cells transiently transfected with human GDE2, zebrafish Gdpd5a or Gdpd5b (GFP-tagged), as indicated. Insets show high-power images of cells depicting that Gdpd5a and Gdpd5b localize to the plasma membrane, similarly to human GDE2-GFP. Scale bars, 10 µm. (**B**) HEK293 cells co-transfected with GPC6-HA and hGDE2-GFP or zebrafish Gdpd5-GFP, or transfected with GPC6 alone as control. The expression levels of the transfected proteins in cell lysates and conditioned media were assessed by Western-blot analysis. GPC6 expression is visualized by antibodies to HA, and both hGDE2 and Gdpd5 using anti-GFP antibody. Cells transfected with GPC6 and treated with PI-PLC were used as positive control.

Gdpd5-knockdown leads to dramatic reduction in expression of pancreatic markers *trypsin* (which marks exocrine cells) and *insulin*. Other markers of the endocrine pancreas, such as the transcription factor *pdx1* are not affected upon Gdpd5 depletion, indicating that Gdpd5 specifically affects *insulin* expression rather than the development of the entire endocrine pancreas. Our results therefore strongly suggest that Gdpd5 affects terminal differentiation of insulin-producing beta cells. With regard to the exocrine pancreas, expression of *ptf1a* is not affected by Gdpd5a knockdown. *Trypsin* expression, however, is strongly reduced. Gdpd5b knockdown also leads to defects in *insulin* and *trypsin* expression, indicating that both zebrafish GDPD5 homologs have important functions in pancreas development. Interestingly, GDPD5 is also expressed in the human pancreas [252] [253]. However, a role for

GDPD5 in pancreas differentiation has not previously been reported. It is of note that ectopic activation of Notch1 signaling inhibits acinar cell differentiation but not initial commitment to the exocrine lineage [246]. We therefore suggest that *gdpd5a* knockdown affects acinar cell differentiation likely through upregulation of Notch signaling. Consistent with this, *islet1*, a marker of early pancreas development, is not affected upon *gdpd5* knockdown, indicating that Gdpd5 affects differentiation of specific subtypes of pancreatic cells.

Given that GDPD5 promotes motor neuron differentiation in chicken embryos and mice [108] [109], while Gdpd5a morphants show severe mobility defects, it was unexpected to find *islet1* expression at relatively normal levels in the brain and spinal cord motor neurons in the morphants. A possible explanation could be that motor neurons are specified normally in the Gdpd5a-depleted zebrafish but undergo impaired terminal differentiation downstream of *islet1*. In addition, protein downregulation achieved by morpholino injections is not complete. Gdpd5 knockdown in zebrafish induces developmental defects including a short and curved body axis and heart defects. We observed reduced *gdpd5a* expression in the heart of Gdpd5a morphants, which may lead to increased Notch1 activity in the heart and account for the abnormalities. In chicken embryos and in mice, GDE2/GDPD5 downregulates Notch signaling in motor neuron progenitors. It was previously shown that GDE2 promotes neuroblastoma cell differentiation [137]. In adult mice, GDE2 prevents neurodegeneration by promoting motor neuron survival [113]. Mechanistically, GDE2 does so by specifically cleaving GPI-anchored Notch ligand regulator RECK as well as glypicans at the plasma membrane [137] [113]. In zebrafish, Glypicans are highly conserved and affect various signaling pathways including the Wnt and Bmp signaling axis [254, 255]. Interestingly, Gpc4 depletion in zebrafish results in strongly reduced cardiomyocyte proliferation [255]. Similarly, perturbations in Notch signaling affect cardiomyocyte proliferation during heart development [256] and regeneration [257]. We find that zebrafish Gde2 localizes to the cell surface, where it cleaves and releases GPC6, similarly to human. Thus, the biochemical properties of GDE2 are conserved between zebrafish and humans. Future studies should reveal if the observed heart malformations after perturbed Gde2 expression are associated with impaired Gpc4 or Notch signaling.

Exogenous expression of human GDE2 mRNA restores *insulin* expression in Gdpd5a-depleted zebrafish embryos indicating functional conservation between human and zebrafish Gde2. Notably, over-expression of human GDE2 leads to developmental abnormalities in zebrafish, namely body axis malformations and vasculature and heart defects, which strictly depend on GDE2 catalytic activity. Interestingly, zebrafish Gdpd5 orthologues localize to the plasma membrane of human cells and show activity against GPI-anchored GPC6. These results further highlight the functional conservation between human and zebrafish Gdpd5, and indicate that GDE2 expression levels must be tightly regulated for proper development.

Because of the functional conservation between human and zebrafish Gdpd5, the use of zebrafish is an effective model to elucidate the precise signaling axis of GDE2 in pancreas development with potential therapeutic value to diabetes.

Acknowledgements

We thank Dr. Rubén Marín-Juez, (MPI, Bad Neuheim, Germany) for probes, Yvette Stijf-Bultsma (NKI, Amsterdam) for technical assistance, and the animal caretakers at Leiden University for excellent care of the fish. The work was supported by grants from the Dutch Cancer Society (KWF UL 2012-5395) to APGH, and Netherlands Organization for Scientific Research (NWO; TOPGO 700.10.354) to WHM.

Experimental Procedures

Zebrafish strains and genotyping methods

Adult zebrafish were maintained at 28°C in compliance with the local animal welfare regulations. Their culture was approved by the local animal welfare committee (DEC) of the University of Leiden and all protocols adhered to the international guidelines specified by the EU Animal Protection Directive 2010/63/EU. Embryos were staged according to [258].

mRNA and Morpholino injections

For mRNA injections, GDE2 constructs previously described in [137] were used. Briefly, a GDE2 image clone was used as template for PCR amplification and BamH1 and EcoRV were used to clone human full-length GDE2 into pcDNA3 vector containing a C-terminal mCherry or HA tag. The vectors were linearized with XbaI. Capped mRNA was synthesised using the SP6 mMessage mMachine kit (Ambion). mRNA (200-500 pg) encoding either wt hGDE2:HA or hGDE2^{H233A} was injected into one-cell stage zebrafish embryos. Translation-blocking morpholinos (MOs) directed against *gdpd5a* (5' GTTTCACCATAGTCAGGCCACAGC 3'), or *gdpd5b* (5'-TGCTTCACCATGCTCCTTCAATCCA-3') were obtained from Gene-Tools (Oregon, USA). Embryos were injected at the 1-2-cell stage with 0,25 to 1mM of MOs.

Whole-mount *in situ* hybridization

Whole-mount *in situ* hybridizations were carried out according to standard protocols [259]. Riboprobes against *notch1b, ins, trypsin* have been previously described. Plasmids encoding *pdx1* and *ptfa1* were a kind gift from Dr. Rubén Marín Juez. The probe against *islet1* was generated from cDNA clone MGC: 73031, IMAGE: 4144017 (Source Bioscience Lifesciences, Germany), which was linearized with NotI and transcribed using SP6 RNA Polymerase. To generate a riboprobe against *gdpd5a*, an 870 bp fragment was amplified from zebrafish cDNA using the following primers: Forward: 5' CAGGTTGTAACTCTGGCGGT 3', Reverse: 5' TGGGACGAGGCACTTTCTTC 3'. The fragment was cloned into the PGEMT vector, was linearized with XhoI and was transcribed using SP6 RNA polymerase.

Western blot analyses

Approximately 20 larvae/sample were lysed (3 µl per larva) in ice-cold standard RIPA buffer supplemented with proteinase inhibitors. Lysates were dounced for 5 min and homogenized using an insulin syringe, followed by centrifugation at 13.000 rpm for 15 min at 4 °C to pellet nuclei and cell debris. The protein concentration was measured using a standard BCA protein assay kit (Pierce). Lysates containing 4x Bolt LDS sample buffer, supplemented with DTT were boiled for 5 min. 12 – 30 ug was loaded onto 12% Bis-Tris SDS-PAGE precast gel (Nu-Page Invitrogen) and transferred to nitrocellulose membranes. Nonspecific protein binding was blocked using 5% skimmed milk in TBST. Primary antibodies were incubated overnight at 4C followed by 1hr incubation with HRP-conjugated secondary antibodies (DAKO, Glostrup, Denmark) and detection using ECL Westernblot reagent (GE Healthcare). Antibodies used were: home-made rabbit anti-GDE2 [137], mouse anti-beta-actin (1:10.000, Sigma, #A5441).

GDE activity assays

GDE activity assays were carried out in HEK293 cells, as previously described [137]. In brief, HEK293 cells were seeded on polyethyleneimine-coated 6-well plates and co-transfected with expression vectors for human GDE2, or zebrafish Gdpd5a/5b (GFP-tagged) together with GPC6-HA. Bacterial PI-PLC was used as positive control. The amount of GPC6 in the medium and cell lysates was analyzed by western blotting. GPC6 expression was assessed using anti-HA antibody (3F10, Roche), zebrafish Gdpd5 and hGDE2 with home-made anti-GFP antibody.

Microscopy

HEK293 cells were cultured on 24 mm glass coverslips and transiently transfected with human GDE2- or zebrafish Gdpd5a-GFP, Gdpd5b-GFP using Fugene 6 reagent (Invitrogen). After 24 hr, the cells were washed with PBS, fixed with 4% PFA, mounted with Immnuno-MountTM (Thermo Scientific) and visualized on a LEICA TCS-SP5 confocal microscope.

Expression vectors

Human GDE2 cDNA was subcloned as described (Matas-Rico et al., 2016). Zebrafish Gdpd5a and Gdpd5b were PCR amplified from synthetic g-Blocks gene fragments (Integrated DNA Technologies Inc., USA) and cloned into pcDNA3-GFP digested with BamHI/EcoRV using SLiCE (*S*eamless *Li*gation *C*loning *E*xtract)[260] cloning. Primers used: *gdpd5a*, Forward:5' AAACTTAAGCTTGGTACCGAGCTCGGATCCATGGTGAAACACCAGCCG 3', Reverse: 5' GCTCCTCGCCCTTGCTCACCATGATATCTAGTTTGGCGGTATGTCGC 3'; *gdpd5b,* Forward: 5' AAACTTAAGCTTGGTACCGAGCTCGGATCCATGGTGAAGC 3', and Reverse: CTCCTCGCCCTTGCTCACCATGATATCATTGGTGTAGTAGTTAAA TCCATTTTCTG 3'.

Supplementary figures

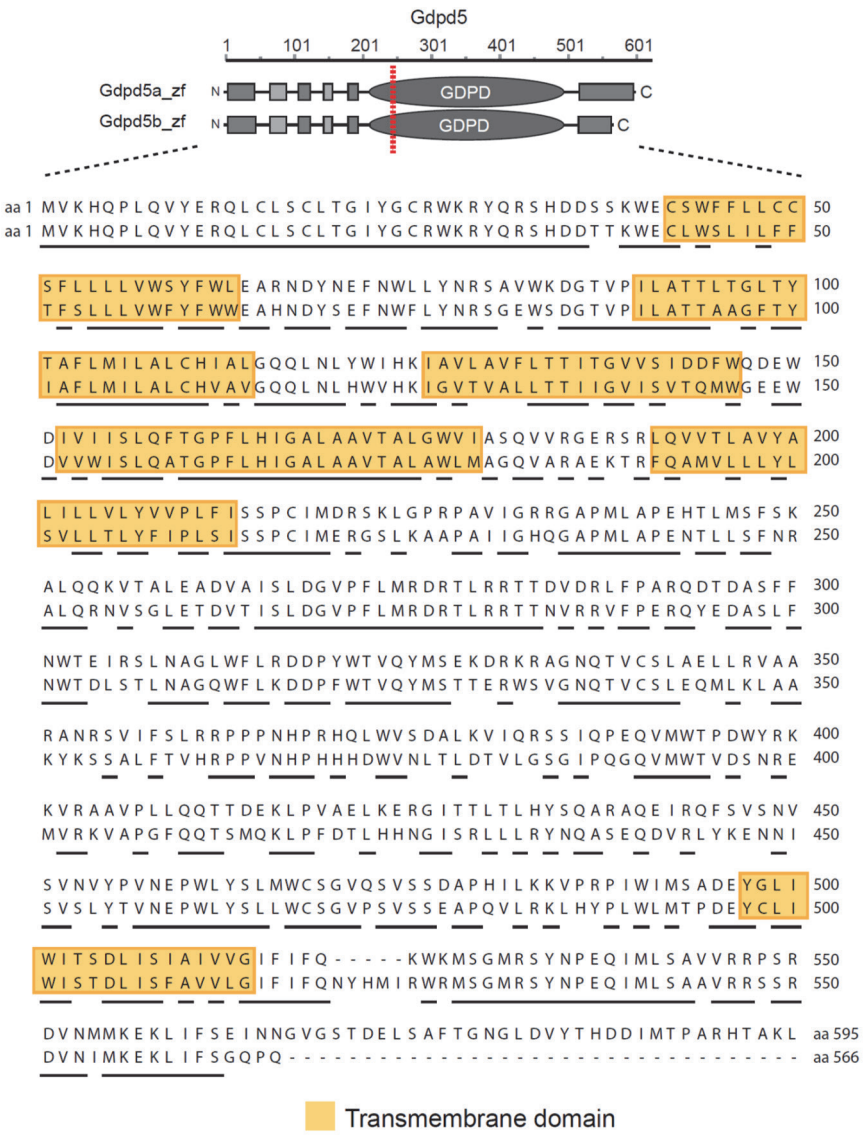

Supplementary Figure 1. Comparison of zebrafish Gdpd5a and Gdpd5b
Protein sequence comparison between zebrafish Gdpd5a and Gdpd5b, using Clustal Omega. Identical aminoacids are shaded in grey. Gdpd5b is characterized by a truncation at the C-terminal cytoplasmic tail. The key catalytic residue (H233 in human GDE2) is indicated by the red line.

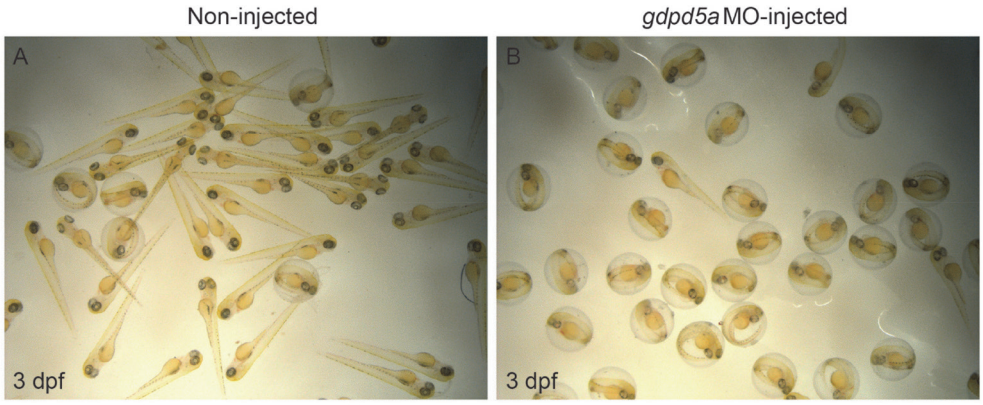

Supplementary Figure 2. The majority of gdpd5aMO-injected larvae do not hatch
(A) Population of non-injected zebrafish larvae at 3dpf. Almost all the embryos have hatched from their chrorions. (B) Population of *gdpd5a*MO-injected embryos at 3dpf. The majority of the morphants are still in their chrorions and very few have hatched. In addition, Gdpd5a-depleted ambryos do not swim away upon poking.

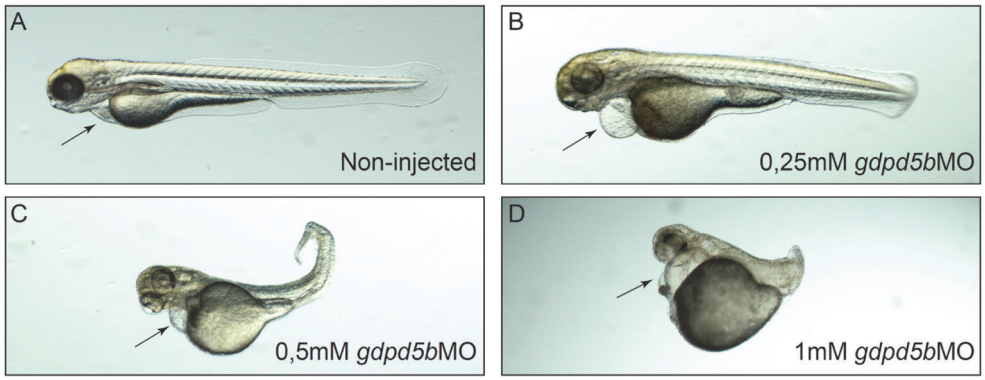

Supplementary Figure 3. Gdpd5b depletion causes developmental defects
Representative pictures of zebrafish embryos at 3 dpf micro-injected with different amounts of *gdpd5b*MO at the one-cell stage. **(A)** Un-injected embryo at 3 dpf. Arrow indicates looped heart. **(B)** Embryo injected with 2 ng/ul (0,25mM) *gdpd5b*MO. Arrow indicates heart oedema and unlooped heart. Note the slightly shorter antero-posterior body axis. **(C)** Embryo injected with 4 ng/ul (0,5mM) *gdpd5b*MO. Arrow indicates heart oedema and unlooped heart.Note the shorter and kinked body axis. **(D)** 3 dpf embryo injected with 8 ng/ul (1mM) *gdpd5b*MO. Note the severe body truncations, defective eye development, large heart oedema and unlooped heart (arrow).

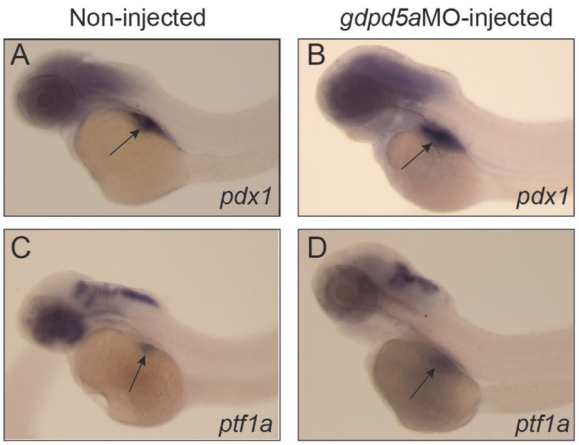

Supplementary Figure 4. The expression of *pdx1* and *ptf1a* is not affected in Gdpd5a morphants
WISH for expression of the endocrine pancreas marker *pdx1* and exocrine pancreas marker *ptf1a* and in non-injected wt (A,C) and *gdpd5a*MO-injected embryos at 3dfp (B,D). Lateral views, anterior to the left. **(A)** wt embryo at 3dpf stained for *pdx1*. *Pdx1* is expressed in the brain and the endocrine pancreas (arrow). **(B)** *Gdpd5a*MO-injected embryo at 3dpf. Strong *pdx1* expression is detected in the endocrine pancreas (arrow). **(C)** wt embryo at 3dfp stained for *ptf1a*. *Ptf1a* expression is detected in the brain and the exocrine pancreas (arrow). **(D)** *Gdpd5a*MO-injected embryo at 3dfp. *Ptf1a* is expressed at comparable levels in the brain and the exocrine pancreas (arrow) as in non-injected controls.

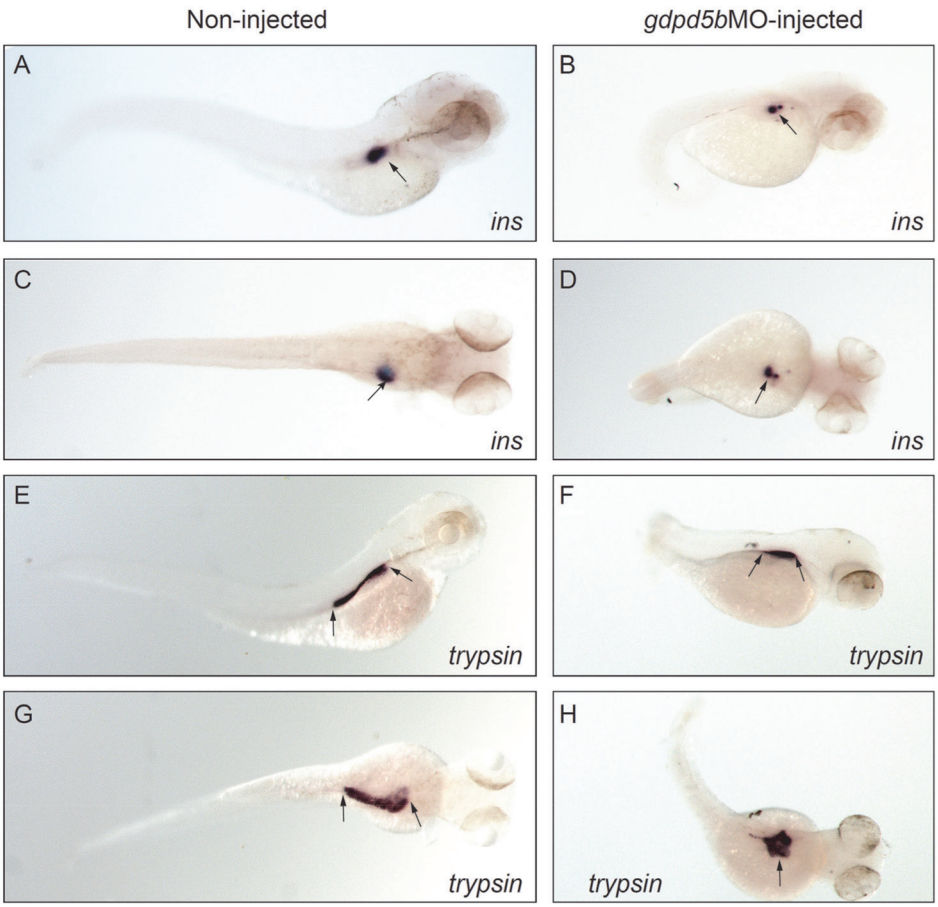

Supplementary Figure 5. Expression of *insulin* and *trypsin* is reduced upon Gdpd5b knockdown
WISH for expression of *insulin* (*ins*) (A-D) and *trypsin* (E-G) in non-injected wt (A, C, E, G) and 2ng/ul *gdpd5b*MO-injected embryos (B, D, F, H) at 3 dpf. (A, B, E, F) lateral views, and (C, D, G, H) dorsal views, anterior to the right. **(A)** Lateral view of a 3 dpf non-injected embryo stained for *insulin*. Strong expression is detected in the endocrine pancreas (arrow). **(B)** *Gdpd5b*MO-injected embryo at 3 dpf. *ins* expression is reduced and the expression domain appears split (arrow). **(C)** Dorsal view of a 3 dpf wt embryo, arrow depicts *insulin* expression. **(D)** Dorsal view of a *gdpd5b*MO-injected embryo, the *insulin* expression domain is smaller and split (arrow). **(E)** Lateral view of non-injected 3 dpf embryo stained for *trypsin*. The arrows demarcate the *trypsin* expression domain. **(F)** Lateral view of a *gdpd5b*MO-injected embryo at 3 dpf. The *trypsin* expression domain is smaller and irregularly shaped (arrows). **(G)** Dorsal view of non-injected 3 dpf embryo, arrows demarcate *trypsin* expression. **(H)** Dorsal view of a Gdpd5b morphant, the *trypsin* expression domain is reduced (arrow).

BETULA

Chapter 5

GDE2 and GDE3: differences in regulation and substrate recognition

Michiel van Veen[1], Nassos Adamopoulos[2], Daniela Leyton-Puig[1], Bram van den Broek[1], Kees Jalink[1], Anastassis Perrakis[2], Wouter H. Moolenaar[1], Elisa Matas-Rico[1]

[1] Division of Cell Biology,
[2] Division of Biochemistry, The Netherlands Cancer Institute, Amsterdam, Netherlands

Abstract

The glycosylphosphatidylinositol (GPI) anchor is a C-terminal protein modification that tethers proteins to the plasma membrane. Because of their very nature, GPI-anchored proteins are unlikely to be internalized like classical transmembrane receptors to shut off their activities. Instead, they can be cleaved by GPI-specific phospholipases. Recent studies have identified a family of enzymes, the so called GDEs, that selectively cleave and release GPI-anchored proteins; yet it remains unknown how they are regulated and recognize their specific substrates. Here we report that GDE2 and GDE3, when co-expressed, co-localize at the plasma membrane but are differentially regulated, with GDE2, but not GDE3, being detected at Rab11-positive vesicles. We find that the GDE2 N- and C-terminus are both involved in vesicle localization, while the extracellular catalytic domain determines substrate recognition. Swapping the respective GPI-attachment signals had no effect on substrate specificity. Although preliminary, our findings suggest that GDE2 and GDE3 are differentially regulated and that substrate specificity is largely determined by the protein rather than the attached PI lipid moiety.

Introduction

In eukaryotic cells, proteins can span the membrane or be tethered to the outer membrane leaflet via a glycosylphosphatidylinositol (GPI) anchor. This unique and complex modification is attached to the protein in the endoplasmic reticulum (ER) before being transported to the plasma membrane [29]. The class of GPI-anchored proteins is very diverse, ranging from enzymes to receptors, ligands, complement factors and adhesion molecules [146]. Consequently, impairments in the GPI-anchor due to acquired mutations can cause diseases like paroxysmal nocturnal hemoglobinuria [261, 262]. Because GPI-anchored proteins do not share a common function, the anchor itself appears to attribute a general feature to the proteins; one of which is the cleavage by phospholipases [263]. A bacterial phospholipase C (PI-PLC) cleaves GPI-anchored proteins from the membrane, corroborating the function of GPI anchors as substrates for phospholipases [64]. However, mammalian GPI-specific phospholipases have long been elusive [4, 69, 76, 264]. Recent studies have identified two members of a family of glycerophosphodiester phosphodiesterases (GDEs), that cleave GPI-anchored proteins from the membrane; notably GDE2 and GDE3 [17, 110, 116]. GDE2, the best characterized family member, cleaves the GPI-anchored protein RECK [110]. By cleaving RECK in the developing spinal cord, GDE2 indirectly inactivates a Notch ligand (Delta-like1). As a consequence, Notch signaling is inactivated in adjacent progenitor cells to initiate differentiation. GDE2 also promotes differentiation of neuroblastoma cells in a cell-autonomous way, through cleavage and release of glypican-6 [17]. GDE2 activity is specific for glypican-6 and glypican-3, leaving other glypicans unaffected [17]. GDE2's closest family member, GDE3, was recently shown to cleave uPAR [116]. GDE3 cleaves uPAR in a phospholipase-C like manner. Homology modeling of GDE2 and GDE3 revealed striking differences in electrostatic surface properties [116]. Together, these results suggest that GDE2 and GDE3 have evolved to selectively cleave and release GPI-anchors proteins.

A possible clue as to how GDEs recognize different substrates is the structural heterogeneity of the GPI-anchor that may hinder and modulate substrate cleavage [29, 146, 147]. For example, palmitoylation of the inositol group confers resistance to a PI-PLC attack [265]. Moreover, GPI-anchoring may also affect protein localization to the apical or basolateral membrane, as well as modulating protein clustering [48, 266-268].

Here we examine the substrate specificity of GDE2 and GDE3 by analyzing their localization and how the GPI anchor may dictate substrate recognition. We show that GDE2 and GDE3 co-localize on the plasma membrane but are differentially regulated. Replacing the N-terminus of GDE2 with GDE3 affected endosome localization but not substrate recognition. By contrast, swapping the GDE2 and GDE3 ecto-domains did affect substrate specificity. Furthermore, replacing the GPI anchors of GDE substrates had no effect on their specific release. Together our results support the notion that GDE's cleave GPI-anchored proteins through specific protein-protein interactions.

Results

GDE2 and GDE3 co-localize at the plasma membrane but are differentially regulated

GDE2 and GDE3 have a different tissue distribution and have specific substrates [101, 116]. We have previously shown that GDE2 localizes to intracellular vesicles in N1E-115 cells but GDE3 localization remains to be determined [17]. When expressed at relatively low levels in N1E-115 cells – a well characterized neuroblastoma cell line that we have used in previous GDE2 studies – GDE2 and GDE3 co-localize to distinct microdomains at the plasma membrane (Figure 1A). The localization of substrates glypican 6 and uPAR was analyzed to assess if localization would affect substrate specificity. When expressed in N1E-115 cells, glypican 6 and uPAR co-localize to the same membrane domains (Figure S1), arguing against localization-dependent substrate specificity. We next assessed if GDE2 and GDE3 may also co-localize intracellularly. We co-transfected GDE2 (GFP- or HA-tagged) with GDE3 (mCh- or GFP-tagged) in HEK293 and N1E-115 cells. A relatively large pool of GDE2 was detected in intracellular vesicles. Remarkably, however, GDE3 was not detected in these vesicles, as shown by confocal microscopy (Figure 1B, C) and super-resolution microscopy (Figure S2A). Quantification of their relative localization, using an imageJ macro, is shown in Figure S2B. Consistent with this, intracellular GDE2 co-localized with Rab11 but GDE3 did not (Figure 1D), suggesting that surface expression of both enzymes is differentially regulated.

Differences in GDE localization do not determine enzymatic activity or substrate specificity

GDE2 and GDE3 contain intracellular N- and C-termini that might be involved in regulatory processes. To test whether these cytosolic tails determine localization, enzyme activity or/and substrate specificity; we made use of chimeric constructs. We swapped the N- and C-terminal tails of GDE2 with those of GDE3 and analyzed the localization of the chimeric proteins in N1E-115 cells. Wild-type GDE2 and GDE2 with an GDE3-C-terminal tail (GDE2(C-GDE3)) partially localized to intracellular vesicles (Figure 2A). Surprisingly, GDE2 containing the GDE3-N-terminal tail (GDE2(N-GDE3)) or GDE3-N and -C-terminal tail, was detected only at the plasma membrane. Because altered localization could be caused by the deletion of an GDE2-specific tail, we generated additional N- and C-terminal deletion mutants; these were found to co-localize with wild-type GDE2 (Figure S3A). It thus seems that the N-terminus of GDE3 prohibits endosome localization. To assess how this might affect enzymatic activity, glypican 6 or uPAR were co-transfected with the chimeric constructs, followed by immunoblotting of the conditioned medium (Figure 2B). No differences were observed, suggesting that GDE2 recycling is not a determinant of GDE2 activity.

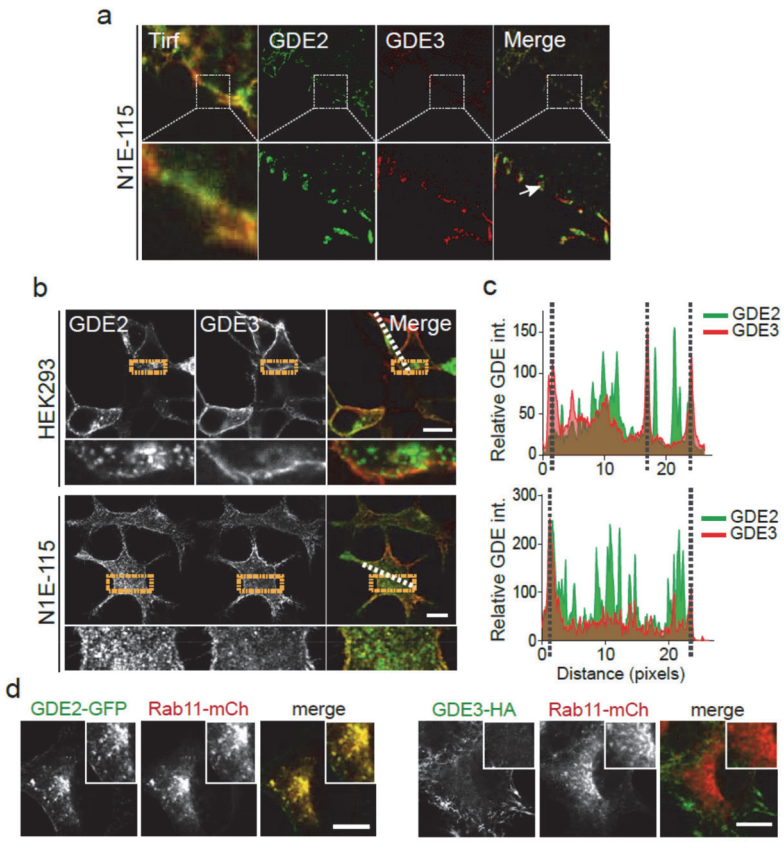

Figure 1. GDE2 and GDE3 colocalize at the plasma membrane but not in intracellular vesicles
(A) GDE2 and GDE3 co-localize to specific microdomains on the plasma membrane. Dual-color super-resolution images of N1E-115 cells, co-expressing GDE2-HA and GDE3-GFP. White arrow depicts distinct microdomain. **(B)** Confocal images of HEK293 and N1E-115 cells co-expressing GDE2-GFP and GDE3-mCh. Only GDE2 localizes to intracellular vesicles as shown by a line intensity profile **(C)**; quantification of the dashed white line. Bar,30 μm. **(D)** GDE and Rab11-mCh localization in N1E-115 cells. Bar, 10 μm.

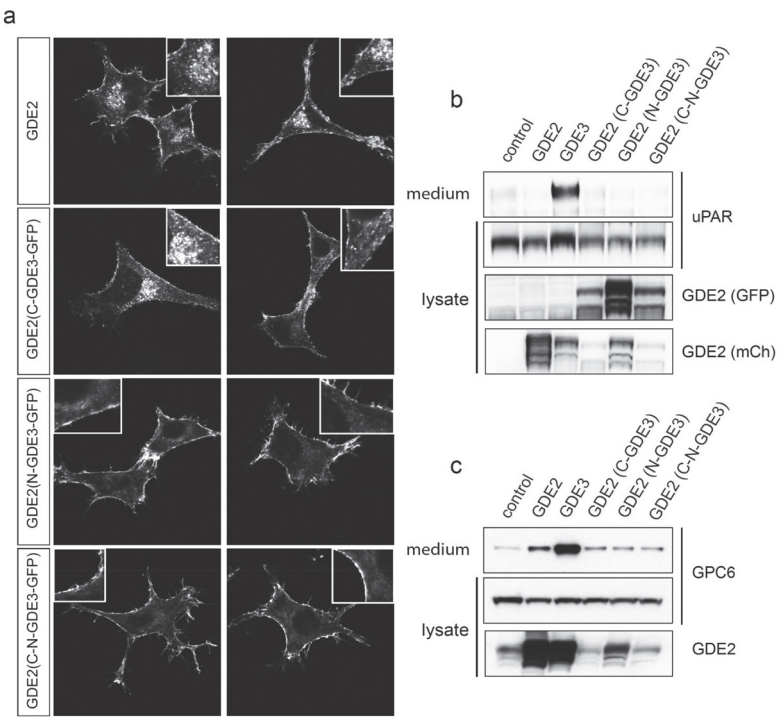

Figure 2. Swapping the N-termini of GDE2 with GDE3 prevents vesicle localization without affecting enzymatic activity

(A) Confocal images of N1E-115 cells transfected with wild-type GDE2-GFP, GDE2(C-GDE3-GFP), GDE2(N-GDE3-GFP) and GDE2(C-N-GDE3-GFP), as indicated. **(B,C)** HEK293 cells were co-transfected with either glypican 6-HA or uPAR-GFP together with wild-type GDE2, GDE3 or the indicated mutants. uPAR or glypican 6 release was analyzed by immunoblotting of the conditioned medium and corresponding lysates.

The GDPD ectodomain determines GDE substrate specificity

Swapping the GDPD domains of GDE2 and GDE3 did not affect subcellular localization (Figure 3A). However, it altered its substrate specificity into that of GDE3. Of note, GDE2 containing the GDE3 GDPD domain was less efficient in cleaving uPAR compared to wild-type GDE3 (Figure 3B). Thus, other regulatory domains must contribute to catalytic activity. Unfortunately, swapping the ecto-domain of GDE3 with that of GDE2 was unsuccessful since the chimeric construct was not expressed at the plasma membrane (Figure 3B). A possible explanation could be misfolding or protein instability.

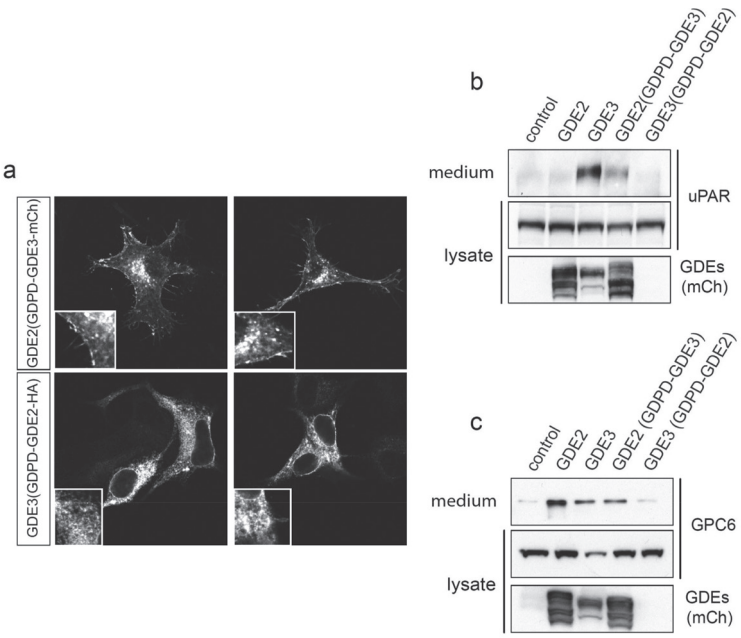

Figure 3. GDE2 substrate selectivity is dictated by the extracellular GDPD domain
(A) Confocal images of N1E-115 cells were transfected with GDE2(GDPD-GDE3-mCh), or GDE3(GDPD-GDE2-HA), as indicated. **(B,C)** HEK293 cells were co-transfected with either glypican 6-HA or uPAR-GFP together with wild-type GDE2, GDE3 or the indicated mutants. uPAR or glypican 6 release was analyzed by immunoblotting of the conditioned medium and corresponding lysates.

GDE substrate selectivity does not depend on the GPI-attachment signal

We next asked what determines substrate specificity. To address this, we focused on glypican-6 and uPAR as substrates. Previous studies have shown that the GPI anchor is a requisite for cleavage by GDE's [110, 116]. Because modifications in the GPI anchor core structure can affect protein clustering or cleavage by phospholipases, we swapped the GPI-anchor attachment signal of uPAR with that of glypican 6 and tested substrate release by GDE's (Figure 4) [48, 266-268]. The uPAR protein consists of three domains (I-III) with a small disordered region at the C-terminus. At the N-terminus, a signal peptide targets the premature protein to the endoplasmic reticulum were a C-terminal signal is responsible for GPI-anchor attachment at the ω-site (Figure 4A, B). Two chimeric constructs were generated: uPAR with the propeptide of glypican 6 and uPAR with the propeptide plus the disordered region replaced by glypican 6 (Figure 4C); which did not affect localization (data not shown). To test release by GDE2 and GDE3, HEK293 cells were co-transfected with uPAR or the chimeric constructs. GDE2 was unable to release any of the chimeric constructs (Figure 4D). It thus appears that GDE substrate recognition does not simply depend on the respective GPI anchors.

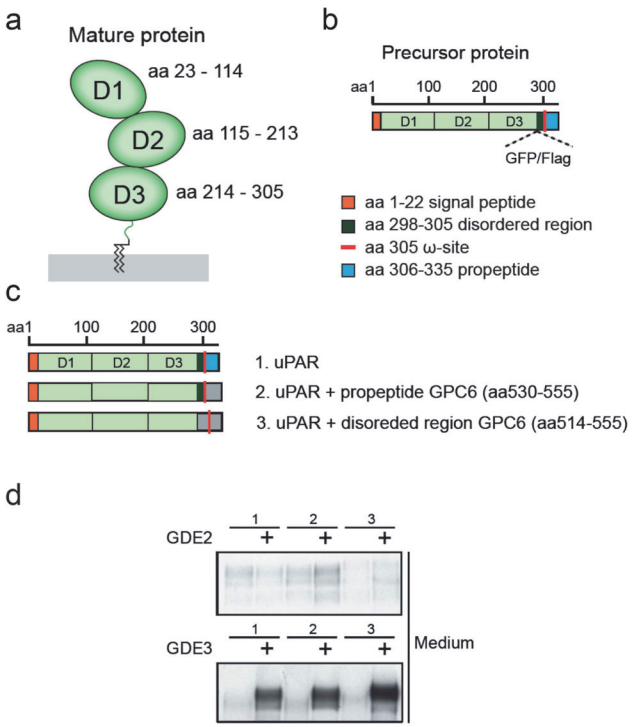

Figure 4. GDE substrate selectivity does not simply depend on GPI-anchor heterogeneity **(A)** Schematic representation of the mature uPAR protein as expressed on the plasma membrane. **(B)** Schematic representation of the immature uPAR protein with the N-terminal signal peptide and the C-terminal GPI-attachment signal. **(C)** Illustration of wild-type and glypican 6 chimeric uPAR constructs, as indicated. The GPI-attachment signal was replaced with that of glypican 6. **(D)** HEK293 cells were co-transfected with either uPAR-GFP or a chimeric construct (1,2 or 3) together with wild-type GDE3 (+) or an empty vector control. uPAR release was analyzed by immunoblotting of the conditioned medium.

Discussion

In this preliminary report, we show that GDE2 and GDE3 co-localize to specific domains at the plasma membrane but are differentially regulated. Remarkably, GDE2 cleaves only a subset of the GPI-anchored proteins released by GDE3. While exchange of the GDPD domain of GDE2 with that of GDE3 resulted in the cleavage of uPAR (a substrate for GDE3 but not GDE2), it was not equally efficient as GDE3, suggesting that other domains are involved in regulating GDE2 activity. Since vesicular localization is exclusive to GDE2, its activity might be regulated through recycling and membrane expression. Moreover, transmembrane receptors and adhesion molecules are known to be internalized to regulate their activity,

where the C-terminal tail is often used as a docking site for adapter proteins [269, 270]. Interestingly, while GDE2 and GDE3 share a high-level sequence similarity, their C-termini are not conserved [116]. To test whether the C-terminus is involved in GDE2 internalization or recycling, we made use of deletion mutants. Unfortunately deleting the N or C-terminus had no effect on GDE2 activity (data not shown) or vesicular localization. Interestingly, a previous study suggested that GDE2 activity is regulated through the cleavage of an intracellular disulfide bond between the N and C-terminus [118]. By contrast, the present deletion mutants together with an earlier study - where we mutated the respective cysteine residues - suggest that GDE2 activity is not regulated in this way [17]; but it should be noted that deletion of the complete GDE2 C-terminal tail resulted in a misfolded protein. Therefore, the remaining amino acids could still be essential for its recycling or internalization. However, this is unlikely since swapping the full-length C-terminal tail with GDE3 – which does not localize to intracellular vesicles - had no effect. Our data suggest that the N-terminus of GDE3 prevents GDE2 internalization (or recycling). If so, replacing the N-terminus of GDE3 with GDE2 should mimic GDE2 localization. Further studies should address if membrane expression levels alone, or other factors like disulfide bridges in the ectodomain [119], affect GDE2 enzymatic activity.

Selective cleavage by GDE2, in contrast to bacterial PI-PLC, suggests a higher order substrate recognition beyond the core GPI-anchor itself [17, 110, 116]. Specific GPI-anchor modifications could serve this function by dictating the sensitivity of GPI-anchored proteins to a GDE2 attack [146, 147]. This is an attractive hypothesis since it would allocate multiple regulatory steps to the specific cleavage by GDE's. To test this, we swapped the GPI-anchor attachment signal, and the 5'prime unstructured region of uPAR with glypican 6. We next assessed cleavage by GDE2, but without success. We therefore conclude that GDE2 cleaves GPI-anchored proteins through specific protein-protein interactions. A notion that is supported by homology modeling of GDE2 and GDE3, revealing striking differences in electrostatic surface properties [116]. Future structural studies should address the question how protein-protein interaction contribute to GDE2 substrate specificity.

Experimental Procedures

Cell Culture and Materials

HEK293 and N1E-115 cells were grown in Dulbecco's modified Eagle's medium (DMEM) supplemented with 10% fetal bovine serum (FBS) at 37°C under 5% CO2. Antibodies used: anti-HA from Sigma; anti-mCh and anti-GFP (home-made). Bacterial PI-PLC from Molecular Probes. Transient transfections were done using a calcium phosphate protocol or XtremeGene 9 agent (Roche).

Expression Vectors

Human cDNA GDE2 and GDE3 were subcloned into a pcDNA3 (-mCherry and –EGFP) plasmid as previously described [17, 116]. The pCAGGS-HA-glypican 6 was kindly provided by Dr. Sungjin Park (Johns Hopkins Medical School, Baltimore, USA) and uPAR-GFP is previously described [153]. GDE2 N and C-terminal truncation mutants were generated by pcr amplification. Swapping the GDE2 and GDE3 GDPD domain or C and N-terminus (as annotated by uniprot; Q8WTR4 and Q9HCC8) was done by pcr amplification. Thereafter, the GDPD ecto-domain was cloned into the GDE backbone using Gibson assembly (Gibson Assembly Cloning kit, New England Biolabs). For the uPAR-GFP chimeric constructs, uPAR; aa1-aa305 and aa1-aa298 was fused to glypican 6 aa530-aa555 and aa514-aa555 respectively.

Western Blotting

For Western blotting, cells were washed with cold PBS, lysed in RIPA buffer supplemented with protease inhibitors followed by a centrifugation step. A BCA protein assay kit (Pierce) was used tom measure protein concentration and LDS sample buffer (NuPAGE, Invitrogen) was added to the lysate or medium. Samples were loaded on SDS-PAGE pre-cast gradient gels (4-12% Nu-Page Bis-Tris, Invitrogen) followed by transfer to nitrocellulose membrane. Membranes were blocked by 5% skimmed milk in TBST followed by overnight incubation with the primary antibodies at 4° C in TBST supplemented with 2% skimmed milk. Horseradish-peroxidase conjugated secondary antibodies (DAKO, Glostrup, Denmark) were incubated for 1 hr at room temperature; ECL Western blot reagent was used to detect proteins.

Microscopy

Cells were cultured on 24 mm, #1,5 coverslips, washed and fixed with 4% PFA, permeabilized with 0.1% Triton X-100 and blocked with 2% BSA for 1 hr. Incubation with primary antibodies was done for 1 hr followed by incubation with Alexa-conjugated antibodies. For confocal microscopy, cells were washed with PBS, mounted with Immnuno-MountTM (Thermo Scientific) and visualized on a LEICA TCS-SP5 confocal microscopy (63 x objective). The total vesicle area of GDE2 and GDE3 was measured using confocal pictures of co-transfected N1E-115 cells. An imageJ macro analyzed bright spots in a predefined region representing the intra-cellular area. Background intensity and vesicle intensity were measured as control. Super-resolution imaging was done using a SR-GSD Leica microscope equipped with an oxygen scavenging system, as previously described [137]. In short, 15000 frames were taken in TIRF mode, at 10 ms exposure time. After post image analysis, movies were analyzed and corrected using the ImageJ plugin Thunderstorm (http://imagej.nih.gov/ij/) followed by correction with an ImageJ macro using the plugin Image Stabilizer.

Supplementary figures

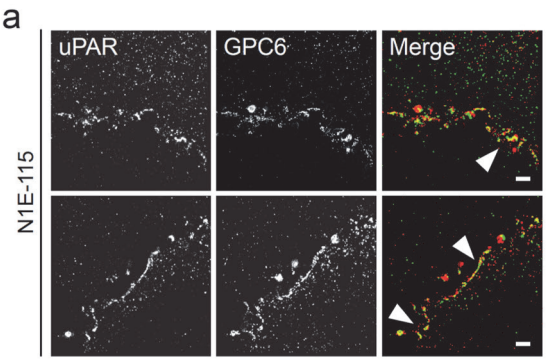

Supplementary Figure 1. Membrane localization of glypican 6 and uPAR
(A) Membrane localization of glypican 6-HA and uPAR-GFP in N1E-115 as detected by super-resolution microscopy. White arrows depict distinct microdomains at the plasma membrane. Bar, 1 µm.

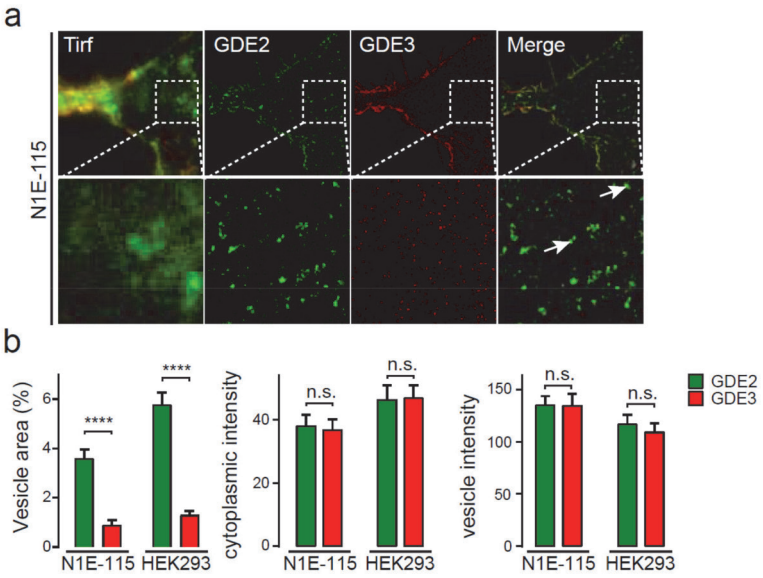

Supplementary Figure 2. GDE2 and GDE3 subcellular localization
(A) Localization of GDE2-HA and GDE3-GFP in N1E-115 cells as detected by dual color super-resolution microscopy. White arrows point to intracellular vesicles **(B)** Quantification of the total vesicle area of GDE2 and GDE3 in HEK293 and N1E-115 cells. Vesicle area was measured using an ImageJ macro that detects bright vesicles in confocal microscopy images. Cytoplasmic intensity and vesicle intensity were measured as background control (mean ± SEM). **** p value < 0.0001 (unpaired t-test).

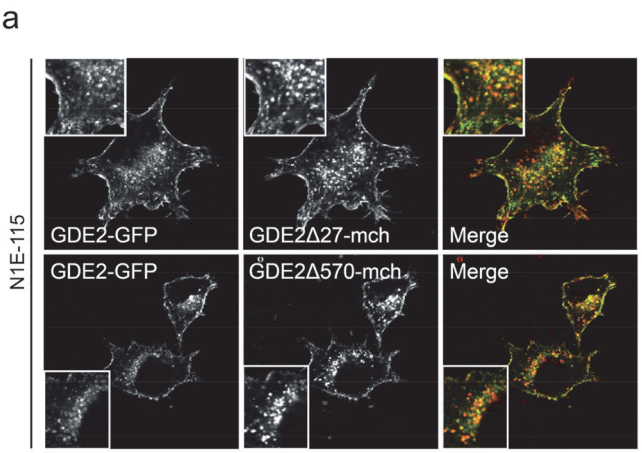

Supplementary Figure 3. Localization of N- and C-terminal truncated GDE2 constructs
(A) Confocal images of N1E-115 cells co-transfected with wild-type GDE2-GFP together with GDE2Δ27-mCh or GDE2Δ570-mCh, as indicated.

PICEA

Chapter 6

Summary and Discussion

Discussion

The GPI anchor, an enzyme substrate or a membrane attachment signal?

In general, the membrane has a fluid-like nature in which different proteins and lipids interact to influence its organization, dynamics and function. In this fluid-like environment, rafts were postulated to serve as stable sorting platform for specific lipids, GPI-anchored proteins and other proteins, that "float" on top of the membrane [271, 272]. Although demonstrated in artificial membranes, evidence for native raft domains was never convincingly shown, which raises the question why proteins are GPI-anchored [268, 273-276]. A vast amount of studies, using a wide variety of techniques (i.e. fluorescence recovery after bleaching (FRAP), Fluorescence energy transfer (FRET), super resolution imaging or single particle analysis), have focused on the contribution of the GPI-anchor to specific localization in transient micro-domains. To date a picture has emerged in which GPI-anchored proteins have diffusion coefficients comparable to membrane lipids, yet, only a part of the total fraction is mobile and diffuses freely, albeit in constricted domains [46, 268, 277-281]. In addition, recent studies suggest that (indirect) interaction of GPI anchors with the cortical actin contributes to the formation of domains [194, 282-285]. Although still under debate, these results indicate that some order or microdomains, where GPI-anchored proteins reside, may be present.

Remarkably, localization to microdomains alone does not comply with the complexity of the GPI-anchor, as the contribution of the inositol and mannose groups in the GPI anchor remain unanswered or even ignored. Hence, bacterial phospholipases and bacterial toxins, that specifically recognize this part of the GPI anchor, are of special interest and raise the question whether the primary function of the structure is to be a substrate for mammalian enzymes [286, 287]. **Chapter 2 and 3** endorse the latter and identify GDE2 and GDE3 (unlike other GDE family members) as trans-membrane GPI-hydrolyzing phosphodiesterase's. An additional observation that favors the hypothesis that GPI anchors serve as a ligand, is the finding of various circulating, but still active GPI-anchored proteins (partially described in **Addendum Chapter 3**) [189, 222, 288]. In line with the previous, GPI-anchored proteins that are resistant to a PLC attack but still harbor a lipid tail, can have a deleterious effect during fertilization [9, 33].

Various enzymes can release GPI-anchored proteins including: GDE2 and GDE3 [17, 110, 116], a recently identified phospholipase A2 [77], the more enigmatic GPI-PLD , Notum and ACE [16, 18, 65] and various metalloproteinases [289, 290]. To distinguish their relative role, in releasing GPI-anchored proteins, more research is needed. For example; to sperate GPI-anchored proteins released by metalloproteinases or phospholipases (-C and -D), the presence

or absence of the glycan core should be carefully evaluated (e.g. by HPLC or alpha-toxins). Previous studies on circulating GPI-anchored proteins have often used metalloproteinase inhibiters to proof the underlying molecular mechanism but these inhibiters rely on metal chelation which is a critical component in GPI anchor synthesis as well as the cleavage by phospholipases [65, 291, 292]. Therefore, the contribution of phospholipases in releasing GPI-anchored proteins could be underestimated and caution should be taken when evaluating these results. In addition, GPI-anchored proteins released by phospholipases can still undergo cleavage by metalloproteinases, potentially masking GDE activity.

GPI-specific phospholipases C or D?

Ever since the discovery of bacterial GPI-PLC, mammalian GPI specific phospholipases (PLC or PLD) have been proposed to serve an important function in the regulation of GPI-AP's; reducing cell-surface expression while at the same time generating a soluble protein. A notion supported by the discovery of various soluble GPI-APs in body fluids [293], tissues [294, 295], urine [296], and cerebrospinal fluid [263, 297]. Evidence for the existence of GPI-APs released by GPI-PLCs has been obtained using an anti-CRD antibody that selectively recognizes the epitope of a GPI-PLC cleaved protein [295]. Using this antibody, multiple soluble GPI-APs were detected which proofs the existence of an unidentified mammalian GPI-PLC [295, 296, 298, 299]. In **Chapter 2** we performed a mass-spec analysis on the released product of GDE3 and found that GDE3 cleaves in a phospholipase C dependent manner, thus identifying GDE3 as the first mammalian GPI-PLC. Interestingly however, immunoblot analysis of GPI-anchored RECK released by GDE2, with an anti-CRD antibody proofed that GDE2 is not a classical type C-phospholipase [110]. In line with the previous, GDE3 attacks glycerophosphoinositol as a phospholipase C while cleavage of glycerophosphocholine by GDE2 occurs in a phospholipase D like manner [99, 100]. Together these observations hint to divergent kinetics between the evolutionary conserved GDE2 and GDE3. The latter is of special interest since it could account for GDE2 and GDE3 substrate specificity; PLC's, unlike PLD's, are sterically hindered by structural heterogeneity of the GPI moiety and therefore cleave only a selective pool of GPI-anchors [265, 300]. One such GPI modification, palmitoylation of the inositol group, occurs during biosynthesis in the ER and is later removed in the Golgi by PGAP1 [32, 33]. Interestingly, mice lacking PGAP1 have severe defects including infertility due to an accumulation of GPI anchors on the membrane. This suggests a role for an, as yet unidentified, GPI-PLC in releasing GPI-anchors [9, 33]. Further studies using PGAP1 mutant cell lines could answer the question whether GDE2 is indeed a GPI-PLD (i.e. Is GPI-anchored cleavage by GDE2 attenuated in PGAP1 mutant cell lines?). It is of note that in our hands, GDE2 cleaves only a selection of GPI anchors compared to GDE3. Hence, factors other than enzyme kinetics are likely to affect cleavage.

Until now GDE studies have focused on the release of GPI-anchors and not on the remaining lipid in the plasma membrane. PLC's or PLD's generate a specific lipid when cleaving a GPI-anchored protein; diacylglycerol (DAG) or phosphatidic acid (PA) respectively. DAG is of special interest because it is a second messenger signaling lipid that activates protein kinase C (PKC), which consequently leads to phosphorylation of downstream substrates. Interestingly, recent research has shown that a pool of DAG is present in the plasma membrane outer leaflet and fast trans bilayer movement could occur [301]. GDE-mediated protein release could therefore directly affect intracellular DAG signaling. More research is needed to assess if DAG generated by GDE3 in the outer leaflet has a signaling function on its own.

The role of the GDE signaling axis in cancer

Selective GPI-anchored proteins as well as total circulating GPI-anchored protein levels have been described as plasma biomarkers for specific cancers (e.g. mesothelin and carcinoembryonic antigen) [287, 302]. Also, expression of multiple enzymes involved in GPI-anchor synthesis (*GPAA1, PIGT* and *PIGU* described in the introduction*)* is increased in different cancer types and is associated with increased cell division [303-305]. Interestingly, in breast carcinomas, increased expression of these enzymes was found to increase overall GPI-anchored protein expression, thereby connecting GPI synthesis and expression in cancer cells [306]. Based on these results, elevated circulating GPI-anchored proteins can reflect an increase in cleavage or simply increased synthesis of the GPI anchor itself. Research on ovarian cancer derived, circulating mesothelin, demonstrated that mannose residues are present; excluding a role for metalloproteinases but not phospholipases [307].

We found that GDE3, unlike GDE2, hydrolyses the GPI anchor of the urokinase receptor (uPAR) in triple-negative breast cancer (TNBC). uPAR mediates degradation of the extracellular matrix through protease recruitment and enhances cell adhesion, migration and signaling through vitronectin binding and interaction with integrins. Expression is elevated in many human cancers and contributes to the aggressiveness of triple-negative breast cancer [120-122, 308]. As such, soluble uPAR derived from the tumor, stroma or infiltrating immune cells is often used as a marker for disease severity although the molecular mechanism behind uPAR shedding is unknown [120, 121, 128, 130-132, 309]. If GDE3 activity is fully responsible for the increase in total circulating GPI-anchor levels, observed in several cancer types, is questionable since we have found that GDE3 cleaves only a small uPAR fraction from the membrane. In addition, GDE3 expression was found to correlate with an increased survival probability in triple-negative breast cancer patients which contradicts soluble uPAR being a marker for disease severity. To assess the contribution of GDE3 in the total circulating uPAR levels, more research, focusing on the tissue origin (cancer cells or stroma) and type of circulating uPAR (cleaved or secreted), is needed.

Our results suggest that GDE3 cleaves uPAR at specific sites to elicit its effect. In accordance with this hypothesis, we find that GDE3 co-localizes with a known interactor of uPAR, integrin β3 (unpublished data) [123]. Although direct integrin activation by uPAR is proposed, Ferraris and colleagues showed that uPAR binding to Vitronectin activates integrin signaling in a non-canonical ligand-independent fashion [124]. The proposed model whereby uPAR, upon binding to vitronectin, creates membrane tension and in turn activates Integrin signaling, fits with the previously described model of GPI-anchored proteins affecting cortical actin and membrane dynamics. Importantly, in both models, integrin activation is essential for uPAR induced morphological changes. Hence, cleaving uPAR in the proximity of integrins will disrupt the signaling axis and inhibit the uPAR induced morphology. If GDE3 releases uPAR from these specific sites remains to be explored.

The GDE-glypican signaling axis and their role in neuronal differentiation

GDE2 and GDE3 expression in the developing embryo is mutually exclusive, where GDE3 expression is restricted to glial precursors, GDE2 is mainly expressed in neurons. Previously, the retinoic acid-inducible gene, GDE2/GDPD5, was shown to be necessary and sufficient for motor-neuron differentiation during the embryonic development of the spinal cord [107, 108]. In contrast, the role of GDE3 during neuronal development remains largely unknown.

We found that GDE2 strongly correlates with a favorable clinical outcome for neuroblastoma, a childhood disease characterized by impaired neuronal differentiation [159-161]. Mechanistically GDE2 cleaves a small fraction of Glypican 6 in a cell-autonomous manner to suppress cell motility, oppose Rho-induced neurite retraction and alter gene transcription. We show that forced GDE2 overexpression pushes cells into differentiation and concomitant knockdown reversed the phenotype. Besides glypican 6 (GPC6), GDE2 also releases its family member glypican 3 (GPC3). However, unlike GPC6, does GPC3 knockdown not result in increased differentiation nor do expression levels correlate with a clinical outcome. Therefore, these findings raise the question of what determines GDE2 substrate recognition and how GPC6 specific cleavage leads to increased differentiation?

To date, six glypican family members have been identified which have a conserved overall structure but share only 25% sequence similarity [188]. Based on the primary structure, glypican 3 and 5 form one subgroup while glypican 1,2 and 6 constitute the other. From this, it remains unclear why GDE2 specifically cleaves GPC3 and 6 [188]. If heparin sulfates or the tertiary structures are involved in GDE2 substrate recognition warrants further investigation.

Although indirect, glypicans play an essential role in cellular signaling which is demonstrated by multiple genetic studies. As for GPC3, in mice, knockdown leads to overgrowth and limb defects reminiscent of phenotypes observed in Wnt or Bmp signaling defects [310-312]. Consistent with this, in humans, GPC3 and GPC4 function is conserved and mutations are associated with the Simpson-Golabi-Behmel syndrome (SGBS), characterized by postnatal overgrowth and morphological abnormalities [313-315]. Intriguingly, coherent to our observation that GPC6 inhibits differentiation in neuroblastoma, is GPC3 widely used as a marker for hepatocellular differentiation, in which high GPC3 staining reflects poorly differentiated hepatocellular carcinomas [316]. Whether GPC3 expression by itself is sufficient to keep cells in an undifferentiated state remains an open question.

Glypicans elicit their effect by modulating the kinetics of receptor activation in various ways. For example, they can stabilize ligand-receptor interactions to activate receptor signaling. Alternatively, through direct ligand binding, glypicans can concentrate the ligand at the target site to prolong receptor activation or create a gradient which is essential for cell polarity during drosophila development [317-320]. Interestingly more recent evidence suggests a possible role for glypicans as direct ligands for type II receptor protein tyrosine phosphatases (RPTPs) [199, 200]. Through their heparin sulfate proteoglycans, glypicans directly bind in *cis* to the ectodomains of RPTPs resulting in receptor clustering and consequent altered transmembrane signaling. Loss of GPC attenuates these clusters which leads to a change in localized phosphorylated tyrosine levels to stimulate neurite outgrowth. In accordance, we show that GDE2 localizes to the neurite tips where localized depletion of GPC6 could lead to decreased phosphor-tyrosine signaling and increased neurite formation.

Glypican 6 is arguably the least studied glypican and very little is known about the function. Though it was recently published that mutations in this gene lead to Autosomal-recessive omodysplasia (OMOD1) caused by defective hedgehog signaling [321]. Since GDE2 dependent cleavage of GPC6 drives neuroblastoma differentiation in *cis*, a role for Wnt signaling seems unlikely. If neuroblastoma differentiation, through GDE2 dependent release of GPC6, is indeed dependent on hedgehog or RPTP signaling is a subject for future studies. In conclusion, our findings uncover a role for GDEs in general and GDE2 specific in regulating GPI-APs at the membrane during neuronal differentiation. Further evidence for a role of GPI-specific phospholipases during neuronal differentiation is described in **Addendum Chapter 3**.

A non-neuronal role for GDE2

In **Chapter 4** we identified the zebrafish orthologues (Gdpd5a and Gdpd5b) of human GDE2. Phylogenetic analysis revealed that Gdpd5a is closely related to human GDE2 while Gdpd5b is characterized by a relatively short, truncated C-terminal tail. Phenotypic analysis of zebrafish depleted of Gdpd5a by specific morpholino's (MOs) revealed anomalies similar to that observed in knockout mice and chicken, including defects in motility [110]. Overexpression of human GDE2, but not the catalytically dead GDE2, also gave rise to a curved body axis and motility defects, hinting to a tight balance and functional conservation for GDE2 transcription during development. Besides motility defects we also observed malformations in the heart and a dramatic reduction in pancreatic markers trypsin and insulin in the pancreas. Strikingly, other endocrine markers, such as pdx1, were not affected, which suggests a specific role for GDE2 in terminal differentiation of insulin-producing beta-cells. Also, in the exocrine pancreas, trypsin was strongly reduced while *ptf1a* was unaffected. In humans, GDE2 is also expressed in the pancreas which suggests that the function of GDE2 is conserved between the two species [252].

Upon retinoic acid induced transcription, GDE2 induces motor neuron differentiation through the release of GPI-anchored RECK from pre-motor neurons and concomitant inhibition of Notch signaling in neighboring cells [110]. It is of note that perturbations in the GDE2 effector, Notch, in zebrafish leads to inhibition of acinar cell differentiation but not initial commitment to the exocrine lineage [246]. In agreement with this, the GDE2 transcriptional activator retinoic acid, promotes endocrine at the expense of exocrine differentiation in the dorsal pancreas and correlates with specific inhibition of Notch signaling. Also, RA enhances exocrine marker gene expression in the ventral pancreas [322, 323]. Together these data suggest a possible role for the RA-GDE2-Notch signaling axis in the developing pancreas. Another possible mechanism, described in **Chapter 3** includes the release of GPC6 by GDE2. Unfortunately, little is known about the function of GPC6 in zebrafish. However, depletion of its closest family member GPC4 in zebrafish, results in strongly reduced cardiomyocyte proliferation [255]. Also, consistent with our observations, in rat, glypicans are expressed during pancreas development and inhibition of proteoglycan sulphation using chlorate, results in a dramatic increase in beta cells and consequent insulin staining [324]. If the observed malformations upon *Gdpd5a* knockdown or human GDE2 overexpression are glypican- or RECK-specific is a subject for future studies.

Regulation and GDE substrate specificity

Throughout our studies we were interested in the substrate specificity of GDE2 versus GDE3. While both proteins are able to cleave GPI-anchored proteins, only GDE2 cleaves a specific subset of GPI anchors, revealing a second order substrate recognition beyond the GPI-anchor structure itself. Localization studies, described in **Chapter 5**, revealed that GDE2 is present in vesicles as well as on the membrane while GDE3 is mainly located on the membrane. This raises the question of whether GDE2 activity and membrane localization could be regulated through vesicular trafficking and recycling. In fact, previous studies proposed that activation of GDE2 is regulated in a redox dependent manner that involves vesicular trafficking. To this end, intracellular Peroxiredoxin 1 interacts with GDE2 to reduce an intramolecular disulfide bond that bridges the N- and C-terminus, leading to GDE2 activation and concomitant neuronal differentiation [118]. However, when we mutated the respective cysteine residues we did not observe any increase in activity nor did we observe a change in localization which raises the question if this is a critical step in the regulation of GDE2 (Chapter 3).

We hypothesized that although GDE2 is differentially regulated, its substrate recognition does not depend on the localization to specific plasma membrane domains. To verify this, we swapped the enzymatic domain of GDE2 with that of GDE3, leaving the GDE localization intact and analyzed GPI-AP release. Indeed, swapping the domain changes GDE2 specificity but not activity.

Because GDE2 is a GPI-specific phospholipase, its substrate is the GPI anchor and specificity must be determined by modifications within the GPI anchor itself (the potential modifications are discussed in Chapter 1) or by intrinsic properties of the attached protein. To test this, we fused the GPI anchor of GPC6 to uPAR and analyzed GDE2 and GDE3 activity. While GDE3 was able to cleave all constructs, GDE2 was unable to cleave uPAR. Together, these results suggest that besides GPI recognition, protein-protein interactions may determine substrate recognition by GDE family members.

Concluding remarks and perspectives

Although cleaved GPI-anchored proteins are readily detected in biological fluids, their origin and involved phospholipases have long been elusive. The studies presented in this thesis describe a novel role for the GDE family in selectively cleaving GPI-anchored proteins. Additionally, we show that GPI-anchor cleavage plays an important role in multiple (patho) physiological settings which opens up a new field of research. Thus far we have only focused on individual GDE family members and their role in shedding one specific GPI-AP, however,

the total subset of GPI-APs cleaved by GDE2 and GDE3 is unknown. We have shown that GDE's only cleave a small fraction from the membrane but with profound effects. Because GDE's cleave only a small fraction of the GPI-AP, efforts to identify substrates through mass spec analysis of the total membrane-bound GPI-anchored protein pool were until now unsuccessful. A new approach that detects the released protein, using a bacterial toxin (alpha toxin from *clostridium septicum*) that specifically recognizes the sugar moieties of the GPI anchor, has proven to be more promising (data not shown). This, together with structural studies should give a better insight into how GDE's recognize and cleave their substrates. Another caveat in our current understanding of GDE's is how they are regulated. It seems unlikely that GDE's are continuously active to "shave" the membrane. In accordance to this, our localizations studies reveal specific intra-cellular localization, of GDE2 and GDE3, suggesting differential localized activation. A possible clue was observed in differentiating (polarized) neuronal cells where GDE2 preferentially localizes to the neurite tips, where GPI-anchored proteins may also reside [325]. While many questions remain to be addressed in the emerging GDE field of research, the new findings emphasize GPI-anchor hydrolysis by GDE's as a cell-intrinsic signaling mechanism to affect cell behavior and, in a broader context, help to clarify the biological significance of the once mysterious GPI anchors [326].

IUNIPERUS
"Battere
la
coccola"

Addendum

References
Nederlandse samenvatting voor leken
Curriculum Vitae
List of Publications
Acknowledgements

References

1. Hooke, R., *Micrographia: or Some Physiological Description of Minute Bodies, Made by Magnifying Glasses with Observations and Inquiries Thereupon* J. Martyn and J. Allestry, London, 1665.
2. Schwann, T., *Mikroskopische Untersuchungen uber die Uebereinstimmung in der Struktur und dem Wachsthum de Thiere und Pflanzen* G. E. Reimer 1839.
3. Ferguson, M.A., et al., *Glycosyl-phosphatidylinositol moiety that anchors Trypanosoma brucei variant surface glycoprotein to the membrane.* Science, 1988. **239**(4841 Pt 1): p. 753-9.
4. Low, M.G., *The glycosyl-phosphatidylinositol anchor of membrane proteins.* Biochim Biophys Acta, 1989. **988**(3): p. 427-54.
5. Orlean, P. and A.K. Menon, *Thematic review series: lipid posttranslational modifications. GPI anchoring of protein in yeast and mammalian cells, or: how we learned to stop worrying and love glycophospholipids.* J Lipid Res, 2007. **48**(5): p. 993-1011.
6. Hazenbos, W.L., et al., *Impaired FcepsilonRI stability, signaling, and effector functions in murine mast cells lacking glycosylphosphatidylinositol-anchored proteins.* Blood, 2011. **118**(16): p. 4377-83.
7. Hazenbos, W.L., et al., *Enhanced responses of glycosylphosphatidylinositol anchor-deficient T lymphocytes.* J Immunol, 2004. **173**(6): p. 3810-5.
8. Hazenbos, W.L., et al., *GPI-anchor deficiency in myeloid cells causes impaired FcgammaR effector functions.* Blood, 2004. **104**(9): p. 2825-31.
9. Ueda, Y., et al., *PGAP1 knock-out mice show otocephaly and male infertility.* J Biol Chem, 2007. **282**(42): p. 30373-80.
10. Nozaki, M., et al., *Developmental abnormalities of glycosylphosphatidylinositol-anchor-deficient embryos revealed by Cre/loxP system.* Lab Invest, 1999. **79**(3): p. 293-9.
11. Kawagoe, K., et al., *Glycosylphosphatidylinositol-anchor-deficient mice: implications for clonal dominance of mutant cells in paroxysmal nocturnal hemoglobinuria.* Blood, 1996. **87**(9): p. 3600-6.
12. Edvardson, S., et al., *Mutations in the phosphatidylinositol glycan C (PIGC) gene are associated with epilepsy and intellectual disability.* J Med Genet, 2017. **54**(3): p. 196-201.
13. Almeida, A.M., et al., *Hypomorphic promoter mutation in PIGM causes inherited glycosylphosphatidylinositol deficiency.* Nat Med, 2006. **12**(7): p. 846-51.
14. Inoue, N., Y. Murakami, and T. Kinoshita, *Molecular genetics of paroxysmal nocturnal hemoglobinuria.* Int J Hematol, 2003. **77**(2): p. 107-12.
15. Zhang, X., et al., *Notum is required for neural and head induction via Wnt deacylation, oxidation, and inactivation.* Dev Cell, 2015. **32**(6): p. 719-30.
16. Traister, A., W. Shi, and J. Filmus, *Mammalian Notum induces the release of glypicans and other GPI-anchored proteins from the cell surface.* Biochem J, 2008. **410**(3): p. 503-11.
17. Matas-Rico, E., et al., *Glycerophosphodiesterase GDE2 Promotes Neuroblastoma Differentiation through Glypican Release and Is a Marker of Clinical Outcome.* Cancer Cell, 2016. **30**(6): p. 986.
18. Kondoh, G., et al., *Angiotensin-converting enzyme is a GPI-anchored protein releasing factor crucial for fertilization.* Nat Med, 2005. **11**(2): p. 160-6.
19. Field, M.C., A.K. Menon, and G.A. Cross, *A glycosylphosphatidylinositol protein anchor from procyclic stage Trypanosoma brucei: lipid structure and biosynthesis.* EMBO J, 1991. **10**(10): p. 2731-9.
20. Rudd, P.M., et al., *The glycosylation of the complement regulatory protein, human erythrocyte CD59.* J Biol Chem, 1997. **272**(11): p. 7229-44.
21. Kinoshita, T., M. Fujita, and Y. Maeda, *Biosynthesis, remodelling and functions of mammalian GPI-anchored proteins: recent progress.* J Biochem, 2008. **144**(3): p. 287-94.

22. Ferguson, M.A.J., T. Kinoshita, and G.W. Hart, *Glycosylphosphatidylinositol Anchors*, in *Essentials of Glycobiology*, A. Varki, et al., Editors. 2009, Cold Spring Harbor Laboratory Press The Consortium of Glycobiology Editors, La Jolla, California.: Cold Spring Harbor (NY).
23. Butikofer, P., et al., *GPI-anchored proteins: now you see 'em, now you don't.* Faseb j, 2001. **15**(2): p. 545-8.
24. McConville, M.J. and M.A. Ferguson, *The structure, biosynthesis and function of glycosylated phosphatidylinositols in the parasitic protozoa and higher eukaryotes.* Biochem J, 1993. **294 (Pt 2)**: p. 305-24.
25. Deeg, M.A., et al., *Glycan components in the glycoinositol phospholipid anchor of human erythrocyte acetylcholinesterase. Novel fragments produced by trifluoroacetic acid.* J Biol Chem, 1992. **267**(26): p. 18573-80.
26. Redman, C.A., et al., *Structure of the glycosylphosphatidylinositol membrane anchor of human placental alkaline phosphatase.* Biochem J, 1994. **302 (Pt 3)**: p. 861-5.
27. Roberts, W.L., et al., *Lipid analysis of the glycoinositol phospholipid membrane anchor of human erythrocyte acetylcholinesterase. Palmitoylation of inositol results in resistance to phosphatidylinositol-specific phospholipase C.* J Biol Chem, 1988. **263**(35): p. 18766-75.
28. Roberts, W.L., et al., *Structural characterization of the glycoinositol phospholipid membrane anchor of human erythrocyte acetylcholinesterase by fast atom bombardment mass spectrometry.* J Biol Chem, 1988. **263**(35): p. 18776-84.
29. Fujita, M. and T. Kinoshita, *GPI-anchor remodeling: potential functions of GPI-anchors in intracellular trafficking and membrane dynamics.* Biochim Biophys Acta, 2012. **1821**(8): p. 1050-8.
30. Mayor, S. and H. Riezman, *Sorting GPI-anchored proteins.* Nat Rev Mol Cell Biol, 2004. **5**(2): p. 110-20.
31. Galian, C., et al., *Efficient glycosylphosphatidylinositol (GPI) modification of membrane proteins requires a C-terminal anchoring signal of marginal hydrophobicity.* J Biol Chem, 2012. **287**(20): p. 16399-409.
32. Fujita, M. and T. Kinoshita, *Structural remodeling of GPI anchors during biosynthesis and after attachment to proteins.* FEBS Lett, 2010. **584**(9): p. 1670-7.
33. Tanaka, S., et al., *Inositol deacylation of glycosylphosphatidylinositol-anchored proteins is mediated by mammalian PGAP1 and yeast Bst1p.* J Biol Chem, 2004. **279**(14): p. 14256-63.
34. Fujita, M., et al., *GPI glycan remodeling by PGAP5 regulates transport of GPI-anchored proteins from the ER to the Golgi.* Cell, 2009. **139**(2): p. 352-65.
35. Watanabe, H. and G. Kondoh, *Mouse sperm undergo GPI-anchored protein release associated with lipid raft reorganization and acrosome reaction to acquire fertility.* J Cell Sci, 2011. **124**(Pt 15): p. 2573-81.
36. Fujita, M., et al., *Sorting of GPI-anchored proteins into ER exit sites by p24 proteins is dependent on remodeled GPI.* J Cell Biol, 2011. **194**(1): p. 61-75.
37. Doering, T.L., P.T. Englund, and G.W. Hart, *Detection of glycophospholipid anchors on proteins.* Curr Protoc Protein Sci, 2001. **Chapter 12**: p. Unit 12.5.
38. Strating, J.R. and G.J. Martens, *The p24 family and selective transport processes at the ER-Golgi interface.* Biol Cell, 2009. **101**(9): p. 495-509.
39. Strating, J.R., T.G. Hafmans, and G.J. Martens, *Functional diversity among p24 subfamily members.* Biol Cell, 2009. **101**(4): p. 207-19.
40. Strating, J.R., T.G. Hafmans, and G.J. Martens, *COP-binding sites in p24delta2 are necessary for proper secretory cargo biosynthesis.* Int J Biochem Cell Biol, 2009. **41**(7): p. 1619-27.
41. Castillon, G.A., et al., *The yeast p24 complex regulates GPI-anchored protein transport and quality control by monitoring anchor remodeling.* Mol Biol Cell, 2011. **22**(16): p. 2924-36.
42. Paladino, S., et al., *Protein oligomerization modulates raft partitioning and apical sorting of GPI-anchored proteins.* J Cell Biol, 2004. **167**(4): p. 699-709.
43. Paladino, S., et al., *Golgi sorting regulates organization and activity of GPI proteins at apical membranes.* Nat Chem Biol, 2014. **10**(5): p. 350-7.

44. Suzuki, K.G., et al., *Transient GPI-anchored protein homodimers are units for raft organization and function.* Nat Chem Biol, 2012. **8**(9): p. 774-83.
45. Gowrishankar, K., et al., *Active remodeling of cortical actin regulates spatiotemporal organization of cell surface molecules.* Cell, 2012. **149**(6): p. 1353-67.
46. Goswami, D., et al., *Nanoclusters of GPI-anchored proteins are formed by cortical actin-driven activity.* Cell, 2008. **135**(6): p. 1085-97.
47. Paladino, S., et al., *GPI-anchored proteins are directly targeted to the apical surface in fully polarized MDCK cells.* J Cell Biol, 2006. **172**(7): p. 1023-34.
48. Paladino, S., et al., *Different GPI-attachment signals affect the oligomerisation of GPI-anchored proteins and their apical sorting.* J Cell Sci, 2008. **121**(Pt 24): p. 4001-7.
49. de Hoop, M.J. and C.G. Dotti, *Membrane traffic in polarized neurons in culture.* J Cell Sci Suppl, 1993. **17**: p. 85-92.
50. Brown, D.A. and J.K. Rose, *Sorting of GPI-anchored proteins to glycolipid-enriched membrane subdomains during transport to the apical cell surface.* Cell, 1992. **68**(3): p. 533-44.
51. Lipardi, C., L. Nitsch, and C. Zurzolo, *Detergent-insoluble GPI-anchored proteins are apically sorted in fischer rat thyroid cells, but interference with cholesterol or sphingolipids differentially affects detergent insolubility and apical sorting.* Mol Biol Cell, 2000. **11**(2): p. 531-42.
52. Imjeti, N.S., et al., *N-Glycosylation instead of cholesterol mediates oligomerization and apical sorting of GPI-APs in FRT cells.* Mol Biol Cell, 2011. **22**(23): p. 4621-34.
53. Delacour, D., et al., *Apical sorting by galectin-3-dependent glycoprotein clustering.* Traffic, 2007. **8**(4): p. 379-88.
54. Benting, J.H., A.G. Rietveld, and K. Simons, *N-Glycans mediate the apical sorting of a GPI-anchored, raft-associated protein in Madin-Darby canine kidney cells.* J Cell Biol, 1999. **146**(2): p. 313-20.
55. Mayor, S., K.G. Rothberg, and F.R. Maxfield, *Sequestration of GPI-anchored proteins in caveolae triggered by cross-linking.* Science, 1994. **264**(5167): p. 1948-51.
56. Sabharanjak, S., et al., *GPI-anchored proteins are delivered to recycling endosomes via a distinct cdc42-regulated, clathrin-independent pinocytic pathway.* Dev Cell, 2002. **2**(4): p. 411-23.
57. Nichols, B., *Endocytosis of lipid-anchored proteins: excluding GEECs from the crowd.* J Cell Biol, 2009. **186**(4): p. 457-9.
58. Howes, M.T., S. Mayor, and R.G. Parton, *Molecules, mechanisms, and cellular roles of clathrin-independent endocytosis.* Curr Opin Cell Biol, 2010. **22**(4): p. 519-27.
59. Doherty, G.J. and H.T. McMahon, *Mechanisms of endocytosis.* Annu Rev Biochem, 2009. **78**: p. 857-902.
60. Nieznanski, K., et al., *Soluble prion protein inhibits amyloid-beta (Abeta) fibrillization and toxicity.* J Biol Chem, 2012. **287**(40): p. 33104-8.
61. Skorecki, K.L. and B.I. Freedman, *A suPAR Biomarker for Chronic Kidney Disease.* N Engl J Med, 2015. **373**(20): p. 1971-2.
62. Watanabe, K., et al., *Requirement of glycosylphosphatidylinositol anchor of Cripto-1 for trans activity as a Nodal co-receptor.* J Biol Chem, 2007. **282**(49): p. 35772-86.
63. Barboni, E., et al., *The glycophosphatidylinositol anchor affects the conformation of Thy-1 protein.* J Cell Sci, 1995. **108 (Pt 2)**: p. 487-97.
64. Titball, R.W., *Bacterial phospholipases C.* Microbiol Rev, 1993. **57**(2): p. 347-66.
65. Metz, C.N., et al., *Release of GPI-anchored membrane proteins by a cell-associated GPI-specific phospholipase D.* EMBO J, 1994. **13**(7): p. 1741-51.
66. Verghese, G.M., M.F. Gutknecht, and G.H. Caughey, *Prostasin regulates epithelial monolayer function: cell-specific Gpld1-mediated secretion and functional role for GPI anchor.* Am J Physiol Cell Physiol, 2006. **291**(6): p. C1258-70.
67. Wilhelm, O.G., et al., *Cellular glycosylphosphatidylinositol-specific phospholipase D regulates urokinase receptor shedding and cell surface expression.* J Cell Physiol, 1999. **180**(2): p. 225-35.
68. Ikezawa, H., *Glycosylphosphatidylinositol (GPI)-anchored proteins.* Biol Pharm Bull, 2002. **25**(4): p. 409-17.

69. Low, M.G. and K.S. Huang, *Factors affecting the ability of glycosylphosphatidylinositol-specific phospholipase D to degrade the membrane anchors of cell surface proteins.* Biochem J, 1991. **279 (Pt 2)**: p. 483-93.
70. Kreuger, J., et al., *Opposing activities of Dally-like glypican at high and low levels of Wingless morphogen activity.* Dev Cell, 2004. **7**(4): p. 503-12.
71. Kakugawa, S., et al., *Notum deacylates Wnt proteins to suppress signalling activity.* Nature, 2015. **519**(7542): p. 187-92.
72. Kirchhoff, C. and G. Hale, *Cell-to-cell transfer of glycosylphosphatidylinositol-anchored membrane proteins during sperm maturation.* Mol Hum Reprod, 1996. **2**(3): p. 177-84.
73. Takayama, T., et al., *Sexually dimorphic expression of the novel germ cell antigen TEX101 during mouse gonad development.* Biol Reprod, 2005. **72**(6): p. 1315-23.
74. Fujihara, Y., et al., *Expression of TEX101, regulated by ACE, is essential for the production of fertile mouse spermatozoa.* Proc Natl Acad Sci U S A, 2013. **110**(20): p. 8111-6.
75. Yamaguchi, R., et al., *Aberrant distribution of ADAM3 in sperm from both angiotensin-converting enzyme (Ace)- and calmegin (Clgn)-deficient mice.* Biol Reprod, 2006. **75**(5): p. 760-6.
76. Leisle, L., et al., *Angiotensin-converting enzyme as a GPIase: a critical reevaluation.* Nat Med, 2005. **11**(11): p. 1139-40.
77. Lee, G.H., et al., *A GPI processing phospholipase A2, PGAP6, modulates Nodal signaling in embryos by shedding CRIPTO.* J Cell Biol, 2016. **215**(5): p. 705-718.
78. Larson, T.J., M. Ehrmann, and W. Boos, *Periplasmic glycerophosphodiester phosphodiesterase of Escherichia coli, a new enzyme of the glp regulon.* J Biol Chem, 1983. **258**(9): p. 5428-32.
79. Larson, T.J. and A.T. van Loo-Bhattacharya, *Purification and characterization of glpQ-encoded glycerophosphodiester phosphodiesterase from Escherichia coli K-12.* Arch Biochem Biophys, 1988. **260**(2): p. 577-84.
80. Tommassen, J., et al., *Characterization of two genes, glpQ and ugpQ, encoding glycerophosphoryl diester phosphodiesterases of Escherichia coli.* Mol Gen Genet, 1991. **226**(1-2): p. 321-7.
81. Munson, R.S., Jr. and K. Sasaki, *Protein D, a putative immunoglobulin D-binding protein produced by Haemophilus influenzae, is glycerophosphodiester phosphodiesterase.* J Bacteriol, 1993. **175**(14): p. 4569-71.
82. Janson, H., et al., *Effects on the ciliated epithelium of protein D-producing and -nonproducing nontypeable Haemophilus influenzae in nasopharyngeal tissue cultures.* J Infect Dis, 1999. **180**(3): p. 737-46.
83. Corda, D. and M.A. De Matteis, *Lipid signalling in health and disease.* FEBS J, 2013. **280**(24): p. 6280.
84. Forsgren, A., K. Riesbeck, and H. Janson, *Protein D of Haemophilus influenzae: a protective nontypeable H. influenzae antigen and a carrier for pneumococcal conjugate vaccines.* Clin Infect Dis, 2008. **46**(5): p. 726-31.
85. Huu, T.N., et al., *Safety and reactogenicity of primary vaccination with the 10-valent pneumococcal non-typeable Haemophilus influenzae protein D conjugate vaccine in Vietnamese infants: a randomised, controlled trial.* BMC Infect Dis, 2013. **13**: p. 95.
86. Johnson, R.W., et al., *Abrogation of nontypeable Haemophilus influenzae protein D function reduces phosphorylcholine decoration, adherence to airway epithelial cells, and fitness in a chinchilla model of otitis media.* Vaccine, 2011. **29**(6): p. 1211-21.
87. Kusser, W. and F. Fiedler, *A novel glycerophosphodiesterase from Bacillus pumilus.* FEBS Lett, 1984. **166**(2): p. 301-6.
88. Hadler, K.S., et al., *Structural flexibility enhances the reactivity of the bioremediator glycerophosphodiesterase by fine-tuning its mechanism of hydrolysis.* J Am Chem Soc, 2009. **131**(33): p. 11900-8.
89. Yip, S.H., et al., *Directed evolution combined with rational design increases activity of GpdQ toward a non-physiological substrate and alters the oligomeric structure of the enzyme.* Protein Eng Des Sel, 2011. **24**(12): p. 861-72.
90. Santelli, E., et al., *Crystal structure of a glycerophosphodiester phosphodiesterase (GDPD) from Thermotoga maritima (TM1621) at 1.60 A resolution.* Proteins, 2004. **56**(1): p. 167-70.

91. Zheng, B., et al., *GDE1/MIR16 is a glycerophosphoinositol phosphodiesterase regulated by stimulation of G protein-coupled receptors.* Proc Natl Acad Sci U S A, 2003. **100**(4): p. 1745-50.
92. Zheng, B., D. Chen, and M.G. Farquhar, *MIR16, a putative membrane glycerophosphodiester phosphodiesterase, interacts with RGS16.* Proc Natl Acad Sci U S A, 2000. **97**(8): p. 3999-4004.
93. Bachmann, A.S., F.F. Duennebier, and G. Mocz, *Genomic organization, characterization, and molecular 3D model of GDE1, a novel mammalian glycerophosphoinositol phosphodiesterase.* Gene, 2006. **371**(1): p. 144-53.
94. Kopp, F., et al., *The glycerophospho metabolome and its influence on amino acid homeostasis revealed by brain metabolomics of GDE1(-/-) mice.* Chem Biol, 2010. **17**(8): p. 831-40.
95. Simon, G.M. and B.F. Cravatt, *Anandamide biosynthesis catalyzed by the phosphodiesterase GDE1 and detection of glycerophospho-N-acyl ethanolamine precursors in mouse brain.* J Biol Chem, 2008. **283**(14): p. 9341-9.
96. Corda, D., et al., *The emerging physiological roles of the glycerophosphodiesterase family.* FEBS J, 2014. **281**(4): p. 998-1016.
97. Yanaka, N., *Mammalian glycerophosphodiester phosphodiesterases.* Biosci Biotechnol Biochem, 2007. **71**(8): p. 1811-8.
98. Okazaki, Y., et al., *A novel glycerophosphodiester phosphodiesterase, GDE5, controls skeletal muscle development via a non-enzymatic mechanism.* J Biol Chem, 2010. **285**(36): p. 27652-63.
99. Corda, D., et al., *The developmentally regulated osteoblast phosphodiesterase GDE3 is glycerophosphoinositol-specific and modulates cell growth.* J Biol Chem, 2009. **284**(37): p. 24848-56.
100. Gallazzini, M., J.D. Ferraris, and M.B. Burg, *GDPD5 is a glycerophosphocholine phosphodiesterase that osmotically regulates the osmoprotective organic osmolyte GPC.* Proc Natl Acad Sci U S A, 2008. **105**(31): p. 11026-31.
101. Ohshima, N., et al., *New members of the mammalian glycerophosphodiester phosphodiesterase family: GDE4 and GDE7 produce lysophosphatidic acid by lysophospholipase D activity.* J Biol Chem, 2015. **290**(7): p. 4260-71.
102. van Meeteren, L.A., et al., *Spider and bacterial sphingomyelinases D target cellular lysophosphatidic acid receptors by hydrolyzing lysophosphatidylcholine.* J Biol Chem, 2004. **279**(12): p. 10833-6.
103. Tsuboi, K., et al., *Glycerophosphodiesterase GDE4 as a novel lysophospholipase D: a possible involvement in bioactive N-acylethanolamine biosynthesis.* Biochim Biophys Acta, 2015. **1851**(5): p. 537-48.
104. Chang, P.A., et al., *Isolation, characterization and molecular 3D model of human GDE4, a novel membrane protein containing glycerophosphodiester phosphodiesterase domain.* Mol Membr Biol, 2008. **25**(6-7): p. 557-66.
105. Nogusa, Y., et al., *Isolation and characterization of two serpentine membrane proteins containing glycerophosphodiester phosphodiesterase, GDE2 and GDE6.* Gene, 2004. **337**: p. 173-9.
106. Cao, M.D., et al., *Targeting choline phospholipid metabolism: GDPD5 and GDPD6 silencing decrease breast cancer cell proliferation, migration, and invasion.* NMR Biomed, 2016. **29**(8): p. 1098-107.
107. Yanaka, N., et al., *Involvement of membrane protein GDE2 in retinoic acid-induced neurite formation in Neuro2A cells.* FEBS Lett, 2007. **581**(4): p. 712-8.
108. Rao, M. and S. Sockanathan, *Transmembrane protein GDE2 induces motor neuron differentiation in vivo.* Science, 2005. **309**(5744): p. 2212-5.
109. Sabharwal, P., et al., *GDE2 regulates subtype-specific motor neuron generation through inhibition of Notch signaling.* Neuron, 2011. **71**(6): p. 1058-70.
110. Park, S., et al., *GDE2 promotes neurogenesis by glycosylphosphatidylinositol-anchor cleavage of RECK.* Science, 2013. **339**(6117): p. 324-8.
111. Muraguchi, T., et al., *RECK modulates Notch signaling during cortical neurogenesis by regulating ADAM10 activity.* Nat Neurosci, 2007. **10**(7): p. 838-45.

112. van Ree, J.W., *Changing world, changing doctors, changing education!* Sante Publique, 2003. **15 Spec No**: p. 151-5.
113. Cave, C., et al., *GDE2 is essential for neuronal survival in the postnatal mammalian spinal cord.* Mol Neurodegener, 2017. **12**(1): p. 8.
114. Sudo, H., et al., *In vitro differentiation and calcification in a new clonal osteogenic cell line derived from newborn mouse calvaria.* J Cell Biol, 1983. **96**(1): p. 191-8.
115. Yanaka, N., et al., *Novel membrane protein containing glycerophosphodiester phosphodiesterase motif is transiently expressed during osteoblast differentiation.* J Biol Chem, 2003. **278**(44): p. 43595-602.
116. van Veen, M., et al., *Negative regulation of urokinase receptor activity by a GPI-specific phospholipase C in breast cancer cells.* Elife, 2017. **6**.
117. Periz, G., et al., *GDP-bound Galphai2 regulates spinal motor neuron differentiation through interaction with GDE2.* Dev Biol, 2010. **341**(1): p. 213-21.
118. Yan, Y., et al., *The antioxidant enzyme Prdx1 controls neuronal differentiation by thiol-redox-dependent activation of GDE2.* Cell, 2009. **138**(6): p. 1209-21.
119. Yan, Y., et al., *Prdx4 is a compartment-specific H2O2 sensor that regulates neurogenesis by controlling surface expression of GDE2.* Nat Commun, 2015. **6**: p. 7006.
120. Smith, H.W. and C.J. Marshall, *Regulation of cell signalling by uPAR.* Nat Rev Mol Cell Biol, 2010. **11**(1): p. 23-36.
121. Ferraris, G.M. and N. Sidenius, *Urokinase plasminogen activator receptor: a functional integrator of extracellular proteolysis, cell adhesion, and signal transduction.* Semin Thromb Hemost, 2013. **39**(4): p. 347-55.
122. Boonstra, M.C., et al., *Clinical applications of the urokinase receptor (uPAR) for cancer patients.* Curr Pharm Des, 2011. **17**(19): p. 1890-910.
123. Madsen, C.D., et al., *uPAR-induced cell adhesion and migration: vitronectin provides the key.* J Cell Biol, 2007. **177**(5): p. 927-39.
124. Ferraris, G.M., et al., *The interaction between uPAR and vitronectin triggers ligand-independent adhesion signalling by integrins.* EMBO J, 2014. **33**(21): p. 2458-72.
125. Persson, M., et al., *First-in-human uPAR PET: Imaging of Cancer Aggressiveness.* Theranostics, 2015. **5**(12): p. 1303-16.
126. Ploug, M., et al., *A soluble form of the glycolipid-anchored receptor for urokinase-type plasminogen activator is secreted from peripheral blood leukocytes from patients with paroxysmal nocturnal hemoglobinuria.* Eur J Biochem, 1992. **208**(2): p. 397-404.
127. Pedersen, N., et al., *A ligand-free, soluble urokinase receptor is present in the ascitic fluid from patients with ovarian cancer.* J Clin Invest, 1993. **92**(5): p. 2160-7.
128. Haupt, T.H., et al., *Plasma suPAR levels are associated with mortality, admission time, and Charlson Comorbidity Index in the acutely admitted medical patient: a prospective observational study.* Crit Care, 2012. **16**(4): p. R130.
129. Sidenius, N., et al., *Serum level of soluble urokinase-type plasminogen activator receptor is a strong and independent predictor of survival in human immunodeficiency virus infection.* Blood, 2000. **96**(13): p. 4091-5.
130. Hayek, S.S., A.A. Quyyumi, and J. Reiser, *Soluble Urokinase Receptor and Chronic Kidney Disease.* N Engl J Med, 2016. **374**(9): p. 891.
131. Stephens, R.W., et al., *Plasma urokinase receptor levels in patients with colorectal cancer: relationship to prognosis.* J Natl Cancer Inst, 1999. **91**(10): p. 869-74.
132. Shariat, S.F., et al., *Association of the circulating levels of the urokinase system of plasminogen activation with the presence of prostate cancer and invasion, progression, and metastasis.* J Clin Oncol, 2007. **25**(4): p. 349-55.
133. Mustjoki, S., et al., *Soluble urokinase receptor levels correlate with number of circulating tumor cells in acute myeloid leukemia and decrease rapidly during chemotherapy.* Cancer Res, 2000. **60**(24): p. 7126-32.
134. Montuori, N. and P. Ragno, *Multiple activities of a multifaceted receptor: roles of cleaved and soluble uPAR.* Front Biosci (Landmark Ed), 2009. **14**: p. 2494-503.
135. Scallon, B.J., et al., *Primary structure and functional activity of a phosphatidylinositol-glycan-specific phospholipase D.* Science, 1991. **252**(5004): p. 446-8.

136. Mann, K.J., et al., *Effect of glycosylphosphatidylinositol (GPI)-phospholipase D overexpression on GPI metabolism.* Biochem J, 2004. **378**(Pt 2): p. 641-8.
137. Matas-Rico, E., et al., *Glycerophosphodiesterase GDE2 Promotes Neuroblastoma Differentiation through Glypican Release and Is a Marker of Clinical Outcome.* Cancer Cell, 2016. **30**(4): p. 548-562.
138. Matas-Rico, E., M. van Veen, and W.H. Moolenaar, *Neuronal differentiation through GPI-anchor cleavage* Cell Cycle, 2016. **in press**.
139. Maeda, Y. and T. Kinoshita, *Structural remodeling, trafficking and functions of glycosylphosphatidylinositol-anchored proteins.* Prog Lipid Res, 2011. **50**(4): p. 411-24.
140. Cunningham, O., et al., *Dimerization controls the lipid raft partitioning of uPAR/CD87 and regulates its biological functions.* EMBO J, 2003. **22**(22): p. 5994-6003.
141. Yang, J., et al., *The I-TASSER Suite: protein structure and function prediction.* Nat Methods, 2015. **12**(1): p. 7-8.
142. Kjoller, L. and A. Hall, *Rac mediates cytoskeletal rearrangements and increased cell motility induced by urokinase-type plasminogen activator receptor binding to vitronectin.* J Cell Biol, 2001. **152**(6): p. 1145-57.
143. LeBeau, A.M., et al., *Targeting uPAR with antagonistic recombinant human antibodies in aggressive breast cancer.* Cancer Res, 2013. **73**(7): p. 2070-81.
144. Barretina, J., et al., *The Cancer Cell Line Encyclopedia enables predictive modelling of anticancer drug sensitivity.* Nature, 2012. **483**(7391): p. 603-7.
145. Hoyer-Hansen, G., et al., *Urokinase plasminogen activator cleaves its cell surface receptor releasing the ligand-binding domain.* J Biol Chem, 1992. **267**(25): p. 18224-9.
146. Paulick, M.G. and C.R. Bertozzi, *The glycosylphosphatidylinositol anchor: a complex membrane-anchoring structure for proteins.* Biochemistry, 2008. **47**(27): p. 6991-7000.
147. Kinoshita, T. and M. Fujita, *Biosynthesis of GPI-anchored proteins: special emphasis on GPI lipid remodeling.* J Lipid Res, 2016. **57**(1): p. 6-24.
148. Furlan, F., et al., *Urokinase plasminogen activator receptor affects bone homeostasis by regulating osteoblast and osteoclast function.* J Bone Miner Res, 2007. **22**(9): p. 1387-96.
149. Munch, E.M., et al., *Differentially expressed genes in preimplantation human embryos: potential candidate genes for blastocyst formation and implantation.* J Assist Reprod Genet, 2016. **33**(8): p. 1017-25.
150. Pierleoni, C., et al., *Immunohistochemical identification of the receptor for urokinase plasminogen activator associated with fibrin deposition in normal and ectopic human placenta.* Placenta, 1998. **19**(7): p. 501-8.
151. Multhaupt, H.A., et al., *Expression of urokinase receptors by human trophoblast. A histochemical and ultrastructural analysis.* Lab Invest, 1994. **71**(3): p. 392-400.
152. Zhao, B., et al., *Mapping the topographic epitope landscape on the urokinase plasminogen activator receptor (uPAR) by surface plasmon resonance and X-ray crystallography.* Data Brief, 2015. **5**: p. 107-13.
153. Caiolfa, V.R., et al., *Monomer dimer dynamics and distribution of GPI-anchored uPAR are determined by cell surface protein assemblies.* J Cell Biol, 2007. **179**(5): p. 1067-82.
154. Cong, L., et al., *Multiplex genome engineering using CRISPR/Cas systems.* Science, 2013. **339**(6121): p. 819-23.
155. Blomen, V.A., et al., *Gene essentiality and synthetic lethality in haploid human cells.* Science, 2015. **350**(6264): p. 1092-6.
156. Mehlert, A. and M.A. Ferguson, *Proteomic scale high-sensitivity analyses of GPI membrane anchors.* Glycoconj J, 2009. **26**(8): p. 915-21.
157. Doering, T.L., P.T. Englund, and G.W. Hart, *Detection of glycophospholipid anchors on proteins.* Curr Protoc Protein Sci, 2001. **Chapter 12**: p. Unit 12 5.
158. Brinkman, E.K., et al., *Easy quantitative assessment of genome editing by sequence trace decomposition.* Nucleic Acids Res, 2014. **42**(22): p. e168.

159. Jiang, M., J. Stanke, and J.M. Lahti, *The connections between neural crest development and neuroblastoma.* Curr Top Dev Biol, 2011. **94**: p. 77-127.
160. Louis, C.U. and J.M. Shohet, *Neuroblastoma: molecular pathogenesis and therapy.* Annu Rev Med, 2015. **66**: p. 49-63.
161. Maris, J.M., *Recent advances in neuroblastoma.* N Engl J Med, 2010. **362**(23): p. 2202-11.
162. Brodeur, G.M. and R. Bagatell, *Mechanisms of neuroblastoma regression.* Nat Rev Clin Oncol, 2014. **11**(12): p. 704-13.
163. Molenaar, J.J., et al., *Sequencing of neuroblastoma identifies chromothripsis and defects in neuritogenesis genes.* Nature, 2012. **483**(7391): p. 589-93.
164. Pugh, T.J., et al., *The genetic landscape of high-risk neuroblastoma.* Nat Genet, 2013. **45**(3): p. 279-84.
165. van Nes, J., et al., *A NOTCH3 transcriptional module induces cell motility in neuroblastoma.* Clin Cancer Res, 2013. **19**(13): p. 3485-94.
166. Matthay, K.K., et al., *Long-term results for children with high-risk neuroblastoma treated on a randomized trial of myeloablative therapy followed by 13-cis-retinoic acid: a children's oncology group study.* J Clin Oncol, 2009. **27**(7): p. 1007-13.
167. Ganeshan, V.R. and N.F. Schor, *Pharmacologic management of high-risk neuroblastoma in children.* Paediatr Drugs, 2011. **13**(4): p. 245-55.
168. Holzel, M., et al., *NF1 is a tumor suppressor in neuroblastoma that determines retinoic acid response and disease outcome.* Cell, 2010. **142**(2): p. 218-29.
169. Brodeur, G.M., et al., *Therapeutic targets for neuroblastomas.* Expert Opin Ther Targets, 2014. **18**(3): p. 277-92.
170. Brodeur, G.M., *Neuroblastoma: biological insights into a clinical enigma.* Nat Rev Cancer, 2003. **3**(3): p. 203-16.
171. Welz, T., J. Wellbourne-Wood, and E. Kerkhoff, *Orchestration of cell surface proteins by Rab11.* Trends Cell Biol, 2014. **24**(7): p. 407-15.
172. Grant, B.D. and J.G. Donaldson, *Pathways and mechanisms of endocytic recycling.* Nat Rev Mol Cell Biol, 2009. **10**(9): p. 597-608.
173. Ridley, A.J., *Rho GTPase signalling in cell migration.* Curr Opin Cell Biol, 2015. **36**: p. 103-112.
174. Hall, A. and G. Lalli, *Rho and Ras GTPases in axon growth, guidance, and branching.* Cold Spring Harb Perspect Biol, 2010. **2**(2): p. a001818.
175. Govek, E.E., S.E. Newey, and L. Van Aelst, *The role of the Rho GTPases in neuronal development.* Genes Dev, 2005. **19**(1): p. 1-49.
176. Hall, A., *Rho family GTPases.* Biochem Soc Trans, 2012. **40**(6): p. 1378-82.
177. Spuul, P., et al., *Importance of RhoGTPases in formation, characteristics, and functions of invadosomes.* Small GTPases, 2014. **5**: p. e28195.
178. Hirose, M., et al., *Molecular dissection of the Rho-associated protein kinase (p160ROCK)-regulated neurite remodeling in neuroblastoma N1E-115 cells.* J Cell Biol, 1998. **141**(7): p. 1625-36.
179. Kranenburg, O., et al., *Activation of RhoA by lysophosphatidic acid and Galpha12/13 subunits in neuronal cells: induction of neurite retraction.* Mol Biol Cell, 1999. **10**(6): p. 1851-7.
180. Moolenaar, W.H., *Lysophosphatidic acid, a multifunctional phospholipid messenger.* J Biol Chem, 1995. **270**(22): p. 12949-52.
181. Frisca, F., et al., *Rho/ROCK pathway is essential to the expansion, differentiation, and morphological rearrangements of human neural stem/progenitor cells induced by lysophosphatidic acid.* J Lipid Res, 2013. **54**(5): p. 1192-206.
182. Jalink, K., et al., *Inhibition of lysophosphatidate- and thrombin-induced neurite retraction and neuronal cell rounding by ADP ribosylation of the small GTP-binding protein Rho.* J Cell Biol, 1994. **126**(3): p. 801-10.
183. Leeuwen, F.N., et al., *The guanine nucleotide exchange factor Tiam1 affects neuronal morphology; opposing roles for the small GTPases Rac and Rho.* J Cell Biol, 1997. **139**(3): p. 797-807.
184. Sander, E.E., et al., *Rac downregulates Rho activity: reciprocal balance between both GTPases determines cellular morphology and migratory behavior.* J Cell Biol, 1999. **147**(5): p. 1009-22.

185. Guilluy, C., R. Garcia-Mata, and K. Burridge, *Rho protein crosstalk: another social network?* Trends Cell Biol, 2011. **21**(12): p. 718-26.
186. Nakamura, F., *FilGAP and its close relatives: a mediator of Rho-Rac antagonism that regulates cell morphology and migration.* Biochem J, 2013. **453**(1): p. 17-25.
187. Kedziora, K.M., et al., *Rapid Remodeling of Invadosomes by Gi-coupled Receptors: DISSECTING THE ROLE OF Rho GTPases.* J Biol Chem, 2016. **291**(9): p. 4323-33.
188. Filmus, J., M. Capurro, and J. Rast, *Glypicans.* Genome Biol, 2008. **9**(5): p. 224.
189. Allen, N.J., et al., *Astrocyte glypicans 4 and 6 promote formation of excitatory synapses via GluA1 AMPA receptors.* Nature, 2012. **486**(7403): p. 410-4.
190. Veugelers, M., et al., *Glypican-6, a new member of the glypican family of cell surface heparan sulfate proteoglycans.* J Biol Chem, 1999. **274**(38): p. 26968-77.
191. Filmus, J. and M. Capurro, *Glypican-3: a marker and a therapeutic target in hepatocellular carcinoma.* FEBS J, 2013. **280**(10): p. 2471-6.
192. Han, S., et al., *Identification of Glypican-3 as a potential metastasis suppressor gene in gastric cancer.* Oncotarget, 2016.
193. Peters, M.G., et al., *Inhibition of invasion and metastasis by glypican-3 in a syngeneic breast cancer model.* Breast Cancer Res Treat, 2003. **80**(2): p. 221-32.
194. Raghupathy, R., et al., *Transbilayer lipid interactions mediate nanoclustering of lipid-anchored proteins.* Cell, 2015. **161**(3): p. 581-594.
195. Filmus, J. and M. Capurro, *The role of glypicans in Hedgehog signaling.* Matrix Biol, 2014. **35**: p. 248-52.
196. Capurro, M.I., et al., *Glypican-3 promotes the growth of hepatocellular carcinoma by stimulating canonical Wnt signaling.* Cancer Res, 2005. **65**(14): p. 6245-54.
197. Yiu, G.K., et al., *NFAT promotes carcinoma invasive migration through glypican-6.* Biochem J, 2011. **440**(1): p. 157-66.
198. Capurro, M., et al., *Glypican-3 binds to Frizzled and plays a direct role in the stimulation of canonical Wnt signaling.* J Cell Sci, 2014. **127**(Pt 7): p. 1565-75.
199. Coles, C.H., E.Y. Jones, and A.R. Aricescu, *Extracellular regulation of type IIa receptor protein tyrosine phosphatases: mechanistic insights from structural analyses.* Semin Cell Dev Biol, 2015. **37**: p. 98-107.
200. Coles, C.H., et al., *Proteoglycan-specific molecular switch for RPTPsigma clustering and neuronal extension.* Science, 2011. **332**(6028): p. 484-8.
201. Chagnon, M.J., et al., *Receptor tyrosine phosphatase sigma (RPTPsigma) regulates, p250GAP, a novel substrate that attenuates Rac signaling.* Cell Signal, 2010. **22**(11): p. 1626-33.
202. Novitch, B.G. and S.J. Butler, *Reducing the mystery of neuronal differentiation.* Cell, 2009. **138**(6): p. 1062-4.
203. Topanurak, S., et al., *High NaCl- and urea-induced posttranslational modifications that increase glycerophosphocholine by inhibiting GDPD5 phosphodiesterase.* Proc Natl Acad Sci U S A, 2013. **110**(18): p. 7482-7.
204. Bewick, V., L. Cheek, and J. Ball, *Statistics review 12: survival analysis.* Crit Care, 2004. **8**(5): p. 389-94.
205. Slaymaker, I.M., et al., *Rationally engineered Cas9 nucleases with improved specificity.* Science, 2016. **351**(6268): p. 84-8.
206. Folling, J., et al., *Fluorescence nanoscopy by ground-state depletion and single-molecule return.* Nat Methods, 2008. **5**(11): p. 943-5.
207. Hoogendoorn, E., et al., *The fidelity of stochastic single-molecule super-resolution reconstructions critically depends upon robust background estimation.* Sci Rep, 2014. **4**: p. 3854.
208. Price, L.S., et al., *Activation of Rac and Cdc42 by integrins mediates cell spreading.* Mol Biol Cell, 1998. **9**(7): p. 1863-71.
209. Trapnell, C., L. Pachter, and S.L. Salzberg, *TopHat: discovering splice junctions with RNA-Seq.* Bioinformatics, 2009. **25**(9): p. 1105-11.
210. Anders, S., P.T. Pyl, and W. Huber, *HTSeq--a Python framework to work with high-throughput sequencing data.* Bioinformatics, 2015. **31**(2): p. 166-9.
211. Law, C.W., et al., *voom: Precision weights unlock linear model analysis tools for RNA-seq read counts.* Genome Biol, 2014. **15**(2): p. R29.

212. Krawitz, P.M., et al., *Identity-by-descent filtering of exome sequence data identifies PIGV mutations in hyperphosphatasia mental retardation syndrome.* Nat Genet, 2010. **42**(10): p. 827-9.
213. Krawitz, P.M., et al., *Mutations in PIGO, a member of the GPI-anchor-synthesis pathway, cause hyperphosphatasia with mental retardation.* Am J Hum Genet, 2012. **91**(1): p. 146-51.
214. Bosse, K.R. and J.M. Maris, *Advances in the translational genomics of neuroblastoma: From improving risk stratification and revealing novel biology to identifying actionable genomic alterations.* Cancer, 2016. **122**(1): p. 20-33.
215. Hayashi, Y., et al., *Glypicans regulate JAK/STAT signaling and distribution of the Unpaired morphogen.* Development, 2012. **139**(22): p. 4162-71.
216. Jen, Y.H., M. Musacchio, and A.D. Lander, *Glypican-1 controls brain size through regulation of fibroblast growth factor signaling in early neurogenesis.* Neural Dev, 2009. **4**: p. 33.
217. O'Callaghan, P., et al., *Heparan sulfate accumulation with Abeta deposits in Alzheimer's disease and Tg2576 mice is contributed by glial cells.* Brain Pathol, 2008. **18**(4): p. 548-61.
218. van Horssen, J., et al., *Heparan sulfate proteoglycan expression in cerebrovascular amyloid beta deposits in Alzheimer's disease and hereditary cerebral hemorrhage with amyloidosis (Dutch) brains.* Acta Neuropathol, 2001. **102**(6): p. 604-14.
219. Dwivedi, P.P., N. Lam, and B.C. Powell, *Boning up on glypicans--opportunities for new insights into bone biology.* Cell Biochem Funct, 2013. **31**(2): p. 91-114.
220. de Wit, J., et al., *Unbiased discovery of glypican as a receptor for LRRTM4 in regulating excitatory synapse development.* Neuron, 2013. **79**(4): p. 696-711.
221. Ko, J.S., et al., *PTPsigma functions as a presynaptic receptor for the glypican-4/LRRTM4 complex and is essential for excitatory synaptic transmission.* Proc Natl Acad Sci U S A, 2015. **112**(6): p. 1874-9.
222. Farhy-Tselnicker, I., et al., *Astrocyte-Secreted Glypican 4 Regulates Release of Neuronal Pentraxin 1 from Axons to Induce Functional Synapse Formation.* Neuron, 2017. **96**(2): p. 428-445 e13.
223. Horn, K.E., et al., *Receptor protein tyrosine phosphatase sigma regulates synapse structure, function and plasticity.* J Neurochem, 2012. **122**(1): p. 147-61.
224. Dagdanova, A., et al., *Characterization of the prion protein in human urine.* J Biol Chem, 2010. **285**(40): p. 30489-95.
225. Chesebro, B., et al., *Anchorless prion protein results in infectious amyloid disease without clinical scrapie.* Science, 2005. **308**(5727): p. 1435-9.
226. Wykosky, J., et al., *Soluble monomeric EphrinA1 is released from tumor cells and is a functional ligand for the EphA2 receptor.* Oncogene, 2008. **27**(58): p. 7260-73.
227. Egea, J. and R. Klein, *Bidirectional Eph-ephrin signaling during axon guidance.* Trends Cell Biol, 2007. **17**(5): p. 230-8.
228. Cramer, K.S. and I.J. Miko, *Eph-ephrin signaling in nervous system development.* F1000Res, 2016. **5**.
229. Stockli, K.A., et al., *Regional distribution, developmental changes, and cellular localization of CNTF-mRNA and protein in the rat brain.* J Cell Biol, 1991. **115**(2): p. 447-59.
230. Masu, Y., et al., *Disruption of the CNTF gene results in motor neuron degeneration.* Nature, 1993. **365**(6441): p. 27-32.
231. Dutta, R., et al., *Activation of the ciliary neurotrophic factor (CNTF) signalling pathway in cortical neurons of multiple sclerosis patients.* Brain, 2007. **130**(Pt 10): p. 2566-76.
232. Davis, S., et al., *Released form of CNTF receptor alpha component as a soluble mediator of CNTF responses.* Science, 1993. **259**(5102): p. 1736-9.
233. Lin, H.W., et al., *Ciliary neurotrophic factor (CNTF) plus soluble CNTF receptor alpha increases cyclooxygenase-2 expression, PGE2 release and interferon-gamma-induced CD40 in murine microglia.* J Neuroinflammation, 2009. **6**: p. 7.
234. He, W., et al., *Membrane distal cytokine binding domain of LIFR interacts with soluble CNTFR in vitro.* FEBS Lett, 2002. **514**(2-3): p. 214-8.
235. Hase, A., et al., *Characterization of glial cell line-derived neurotrophic factor family receptor alpha-1 in peripheral nerve Schwann cells.* J Neurochem, 2005. **95**(2): p. 537-43.

236. Peterziel, H., K. Unsicker, and K. Krieglstein, *TGFbeta induces GDNF responsiveness in neurons by recruitment of GFRalpha1 to the plasma membrane.* J Cell Biol, 2002. **159**(1): p. 157-67.
237. Compton, A.G., et al., *Mutations in contactin-1, a neural adhesion and neuromuscular junction protein, cause a familial form of lethal congenital myopathy.* Am J Hum Genet, 2008. **83**(6): p. 714-24.
238. Gennarini, G., et al., *Transfected F3/F11 neuronal cell surface protein mediates intercellular adhesion and promotes neurite outgrowth.* Neuron, 1991. **6**(4): p. 595-606.
239. Durbec, P., et al., *A soluble form of the F3 neuronal cell adhesion molecule promotes neurite outgrowth.* J Cell Biol, 1992. **117**(4): p. 877-87.
240. Lamprianou, S., et al., *A complex between contactin-1 and the protein tyrosine phosphatase PTPRZ controls the development of oligodendrocyte precursor cells.* Proc Natl Acad Sci U S A, 2011. **108**(42): p. 17498-503.
241. Ninov, N., M. Borius, and D.Y. Stainier, *Different levels of Notch signaling regulate quiescence, renewal and differentiation in pancreatic endocrine progenitors.* Development, 2012. **139**(9): p. 1557-67.
242. Tehrani, Z. and S. Lin, *Endocrine pancreas development in zebrafish.* Cell Cycle, 2011. **10**(20): p. 3466-72.
243. Wang, Z., et al., *Targeting notch to eradicate pancreatic cancer stem cells for cancer therapy.* Anticancer Res, 2011. **31**(4): p. 1105-13.
244. Zecchin, E., et al., *Distinct delta and jagged genes control sequential segregation of pancreatic cell types from precursor pools in zebrafish.* Dev Biol, 2007. **301**(1): p. 192-204.
245. Apelqvist, A., et al., *Notch signalling controls pancreatic cell differentiation.* Nature, 1999. **400**(6747): p. 877-81.
246. Esni, F., et al., *Notch inhibits Ptf1 function and acinar cell differentiation in developing mouse and zebrafish pancreas.* Development, 2004. **131**(17): p. 4213-24.
247. Matas-Rico, E., M. van Veen, and W.H. Moolenaar, *Neuronal differentiation through GPI-anchor cleavage.* Cell Cycle, 2016: p. 1-2.
248. Nasevicius, A. and S.C. Ekker, *Effective targeted gene 'knockdown' in zebrafish.* Nat Genet, 2000. **26**(2): p. 216-20.
249. Field, H.A., et al., *Formation of the digestive system in zebrafish. II. Pancreas morphogenesis.* Dev Biol, 2003. **261**(1): p. 197-208.
250. Appel, B., et al., *Motoneuron fate specification revealed by patterned LIM homeobox gene expression in embryonic zebrafish.* Development, 1995. **121**(12): p. 4117-25.
251. Dasen, J.S. and T.M. Jessell, *Hox networks and the origins of motor neuron diversity.* Curr Top Dev Biol, 2009. **88**: p. 169-200.
252. Uhlen, M., et al., *Proteomics. Tissue-based map of the human proteome.* Science, 2015. **347**(6220): p. 1260419.
253. Lang, Q., et al., *Cloning and characterization of a human GDPD domain-containing protein GDPD5.* Mol Biol Rep, 2008. **35**(3): p. 351-9.
254. Gupta, M. and M. Brand, *Identification and expression analysis of zebrafish glypicans during embryonic development.* PLoS One, 2013. **8**(11): p. e80824.
255. Strate, I., F. Tessadori, and J. Bakkers, *Glypican4 promotes cardiac specification and differentiation by attenuating canonical Wnt and Bmp signaling.* Development, 2015. **142**(10): p. 1767-76.
256. High, F.A. and J.A. Epstein, *The multifaceted role of Notch in cardiac development and disease.* Nat Rev Genet, 2008. **9**(1): p. 49-61.
257. Zhao, L., et al., *Notch signaling regulates cardiomyocyte proliferation during zebrafish heart regeneration.* Proc Natl Acad Sci U S A, 2014. **111**(4): p. 1403-8.
258. Kimmel, C.B., et al., *Stages of embryonic development of the zebrafish.* Dev Dyn, 1995. **203**(3): p. 253-310.
259. Thisse, C. and B. Thisse, *High-resolution in situ hybridization to whole-mount zebrafish embryos.* Nat Protoc, 2008. **3**(1): p. 59-69.
260. Zhang, Y., U. Werling, and W. Edelmann, *Seamless Ligation Cloning Extract (SLiCE) cloning method.* Methods Mol Biol, 2014. **1116**: p. 235-44.
261. Bessler, M., A. Schaefer, and P. Keller, *Paroxysmal nocturnal hemoglobinuria: insights from recent advances in molecular biology.* Transfus Med Rev, 2001. **15**(4): p. 255-67.

262. Takeda, J., et al., *Deficiency of the GPI anchor caused by a somatic mutation of the PIG-A gene in paroxysmal nocturnal hemoglobinuria.* Cell, 1993. **73**(4): p. 703-11.
263. Sharom, F.J. and G. Radeva, *GPI-anchored protein cleavage in the regulation of transmembrane signals.* Subcell Biochem, 2004. **37**: p. 285-315.
264. Kakugawa, S., et al., *Notum deacylates Wnt proteins to suppress signalling activity.* Nature, 2015. **519**(7542): p. 187-192.
265. Muller, A., et al., *Selective and programmed cleavage of GPI-anchored proteins from the surface membrane by phospholipase C.* Biochim Biophys Acta, 2012. **1818**(1): p. 117-24.
266. Cortes, L.K., et al., *Proteomic identification of mammalian cell surface derived glycosylphosphatidylinositol-anchored proteins through selective glycan enrichment.* Proteomics, 2014. **14**(21-22): p. 2471-84.
267. Nicholson, T.B. and C.P. Stanners, *Specific inhibition of GPI-anchored protein function by homing and self-association of specific GPI anchors.* J Cell Biol, 2006. **175**(4): p. 647-59.
268. Saha, S., A.A. Anilkumar, and S. Mayor, *GPI-anchored protein organization and dynamics at the cell surface.* J Lipid Res, 2016. **57**(2): p. 159-75.
269. Barbieri, E., P.P. Di Fiore, and S. Sigismund, *Endocytic control of signaling at the plasma membrane.* Curr Opin Cell Biol, 2016. **39**: p. 21-7.
270. Irannejad, R., et al., *Effects of endocytosis on receptor-mediated signaling.* Curr Opin Cell Biol, 2015. **35**: p. 137-43.
271. Simons, K. and G. van Meer, *Lipid sorting in epithelial cells.* Biochemistry, 1988. **27**(17): p. 6197-202.
272. Simons, K. and E. Ikonen, *Functional rafts in cell membranes.* Nature, 1997. **387**(6633): p. 569-72.
273. Edidin, M., *The state of lipid rafts: from model membranes to cells.* Annu Rev Biophys Biomol Struct, 2003. **32**: p. 257-83.
274. Simons, K. and W.L. Vaz, *Model systems, lipid rafts, and cell membranes.* Annu Rev Biophys Biomol Struct, 2004. **33**: p. 269-95.
275. Mayor, S. and F.R. Maxfield, *Insolubility and redistribution of GPI-anchored proteins at the cell surface after detergent treatment.* Mol Biol Cell, 1995. **6**(7): p. 929-44.
276. Heerklotz, H., *Triton promotes domain formation in lipid raft mixtures.* Biophys J, 2002. **83**(5): p. 2693-701.
277. van Zanten, T.S., et al., *Hotspots of GPI-anchored proteins and integrin nanoclusters function as nucleation sites for cell adhesion.* Proc Natl Acad Sci U S A, 2009. **106**(44): p. 18557-62.
278. Zhang, F., et al., *Lateral diffusion of membrane-spanning and glycosylphosphatidylinositol-linked proteins: toward establishing rules governing the lateral mobility of membrane proteins.* J Cell Biol, 1991. **115**(1): p. 75-84.
279. Dietrich, C., et al., *Relationship of lipid rafts to transient confinement zones detected by single particle tracking.* Biophys J, 2002. **82**(1 Pt 1): p. 274-84.
280. Kusumi, A., et al., *Paradigm shift of the plasma membrane concept from the two-dimensional continuum fluid to the partitioned fluid: high-speed single-molecule tracking of membrane molecules.* Annu Rev Biophys Biomol Struct, 2005. **34**: p. 351-78.
281. Lenne, P.F., et al., *Dynamic molecular confinement in the plasma membrane by microdomains and the cytoskeleton meshwork.* EMBO J, 2006. **25**(14): p. 3245-56.
282. Chiantia, S. and E. London, *Acyl chain length and saturation modulate interleaflet coupling in asymmetric bilayers: effects on dynamics and structural order.* Biophys J, 2012. **103**(11): p. 2311-9.
283. Polley, A., S. Mayor, and M. Rao, *Bilayer registry in a multicomponent asymmetric membrane: dependence on lipid composition and chain length.* J Chem Phys, 2014. **141**(6): p. 064903.
284. Rao, M. and S. Mayor, *Active organization of membrane constituents in living cells.* Curr Opin Cell Biol, 2014. **29**: p. 126-32.
285. Legler, D.F., et al., *Differential insertion of GPI-anchored GFPs into lipid rafts of live cells.* FASEB J, 2005. **19**(1): p. 73-5.
286. Gordon, V.M., et al., *Clostridium septicum alpha toxin uses glycosylphosphatidylinositol-anchored protein receptors.* J Biol Chem, 1999. **274**(38): p. 27274-80.
287. Dolezal, S., et al., *Elevated levels of glycosylphosphatidylinositol (GPI) anchored proteins in plasma from human cancers detected by C. septicum alpha toxin.* Cancer Biomark, 2014. **14**(1): p. 55-62.

288. Parkin, E.T., et al., *Dual mechanisms for shedding of the cellular prion protein.* J Biol Chem, 2004. **279**(12): p. 11170-8.
289. Ieguchi, K., et al., *ADAM12-cleaved ephrin-A1 contributes to lung metastasis.* Oncogene, 2014. **33**(17): p. 2179-90.
290. Taylor, D.R., et al., *Role of ADAMs in the ectodomain shedding and conformational conversion of the prion protein.* J Biol Chem, 2009. **284**(34): p. 22590-600.
291. Mann, K.J. and D. Sevlever, *1,10-Phenanthroline inhibits glycosylphosphatidylinositol anchoring by preventing phosphoethanolamine addition to glycosylphosphatidylinositol anchor precursors.* Biochemistry, 2001. **40**(5): p. 1205-13.
292. Sevlever, D., K.J. Mann, and M.E. Medof, *Differential effect of 1,10-phenanthroline on mammalian, yeast, and parasite glycosylphosphatidylinositol anchor synthesis.* Biochem Biophys Res Commun, 2001. **288**(5): p. 1112-8.
293. Huang, J., et al., *A sandwich ELISA for detection of soluble GPI-80, a glycosylphosphatidyl-inositol (GPI)-anchored protein on human leukocytes involved in regulation of neutrophil adherence and migration--its release from activated neutrophils and presence in synovial fluid of rheumatoid arthritis patients.* Microbiol Immunol, 2001. **45**(6): p. 467-71.
294. Piec, G. and M. Le Hir, *The soluble 'low-Km' 5'-nucleotidase of rat kidney represents solubilized ecto-5'-nucleotidase.* Biochem J, 1991. **273(Pt 2)**: p. 409-13.
295. Vogel, M., et al., *Soluble low-Km 5'-nucleotidase from electric-ray (Torpedo marmorata) electric organ and bovine cerebral cortex is derived from the glycosyl-phosphatidylinositol-anchored ectoenzyme by phospholipase C cleavage.* Biochem J, 1992. **284 (Pt 3)**: p. 621-4.
296. Park, S.W., et al., *Endogenous glycosylphosphatidylinositol-specific phospholipase C releases renal dipeptidase from kidney proximal tubules in vitro.* Biochem J, 2001. **353**(Pt 2): p. 339-44.
297. Almqvist, P. and S.R. Carlsson, *Characterization of a hydrophilic form of Thy-1 purified from human cerebrospinal fluid.* J Biol Chem, 1988. **263**(25): p. 12709-15.
298. Movahedi, S. and N.M. Hooper, *Insulin stimulates the release of the glycosyl phosphatidylinositol-anchored membrane dipeptidase from 3T3-L1 adipocytes through the action of a phospholipase C.* Biochem J, 1997. **326 (Pt 2)**: p. 531-7.
299. Park, S.W., et al., *Spontaneous release of glycosylphosphatidylinositol (GPI)-anchored renal dipeptidase from porcine renal proximal tubules.* Arch Pharm Res, 2002. **25**(1): p. 80-5.
300. Elortza, F., et al., *Modification-specific proteomics of plasma membrane proteins: identification and characterization of glycosylphosphatidylinositol-anchored proteins released upon phospholipase D treatment.* J Proteome Res, 2006. **5**(4): p. 935-43.
301. Ueda, Y., et al., *Regulation of the transbilayer movement of diacylglycerol in the plasma membrane.* Biochimie, 2014. **107 Pt A**: p. 43-50.
302. Creaney, J., I.M. Dick, and B.W. Robinson, *Discovery of new biomarkers for malignant mesothelioma.* Curr Pulmonol Rep, 2015. **4**(1): p. 15-21.
303. Wu, G., et al., *Overexpression of glycosylphosphatidylinositol (GPI) transamidase subunits phosphatidylinositol glycan class T and/or GPI anchor attachment 1 induces tumorigenesis and contributes to invasion in human breast cancer.* Cancer Res, 2006. **66**(20): p. 9829-36.
304. Jiang, W.W., et al., *Alterations of GPI transamidase subunits in head and neck squamous carcinoma.* Mol Cancer, 2007. **6**: p. 74.
305. Nagpal, J.K., et al., *Profiling the expression pattern of GPI transamidase complex subunits in human cancer.* Mod Pathol, 2008. **21**(8): p. 979-91.
306. Zhao, P., et al., *Proteomic identification of glycosylphosphatidylinositol anchor-dependent membrane proteins elevated in breast carcinoma.* J Biol Chem, 2012. **287**(30): p. 25230-40.
307. Dangaj, D., et al., *Mannose receptor (MR) engagement by mesothelin GPI anchor polarizes tumor-associated macrophages and is blocked by anti-MR human recombinant antibody.* PLoS One, 2011. **6**(12): p. e28386.

308. Huber, M.C., et al., *uPAR enhances malignant potential of triple-negative breast cancer by directly interacting with uPA and IGF1R.* BMC Cancer, 2016. **16**: p. 615.
309. Sidenius, N., C.F. Sier, and F. Blasi, *Shedding and cleavage of the urokinase receptor (uPAR): identification and characterisation of uPAR fragments in vitro and in vivo.* FEBS Lett, 2000. **475**(1): p. 52-6.
310. Grisaru, S., et al., *Glypican-3 modulates BMP- and FGF-mediated effects during renal branching morphogenesis.* Dev Biol, 2001. **231**(1): p. 31-46.
311. Paine-Saunders, S., et al., *glypican-3 controls cellular responses to Bmp4 in limb patterning and skeletal development.* Dev Biol, 2000. **225**(1): p. 179-87.
312. Song, H.H., et al., *The loss of glypican-3 induces alterations in Wnt signaling.* J Biol Chem, 2005. **280**(3): p. 2116-25.
313. Pilia, G., et al., *Mutations in GPC3, a glypican gene, cause the Simpson-Golabi-Behmel overgrowth syndrome.* Nat Genet, 1996. **12**(3): p. 241-7.
314. Veugelers, M., et al., *GPC4, the gene for human K-glypican, flanks GPC3 on xq26: deletion of the GPC3-GPC4 gene cluster in one family with Simpson-Golabi-Behmel syndrome.* Genomics, 1998. **53**(1): p. 1-11.
315. Filmus, J., *Glypicans in growth control and cancer.* Glycobiology, 2001. **11**(3): p. 19R-23R.
316. Shirakawa, H., et al., *Glypican-3 is a useful diagnostic marker for a component of hepatocellular carcinoma in human liver cancer.* Int J Oncol, 2009. **34**(3): p. 649-56.
317. Kirkpatrick, C.A., et al., *Spatial regulation of Wingless morphogen distribution and signaling by Dally-like protein.* Dev Cell, 2004. **7**(4): p. 513-23.
318. Franch-Marro, X., et al., *Glypicans shunt the Wingless signal between local signalling and further transport.* Development, 2005. **132**(4): p. 659-66.
319. Nybakken, K. and N. Perrimon, *Heparan sulfate proteoglycan modulation of developmental signaling in Drosophila.* Biochim Biophys Acta, 2002. **1573**(3): p. 280-91.
320. Fico, A., F. Maina, and R. Dono, *Fine-tuning of cell signaling by glypicans.* Cell Mol Life Sci, 2011. **68**(6): p. 923-9.
321. Capurro, M., et al., *Glypican-6 promotes the growth of developing long bones by stimulating Hedgehog signaling.* J Cell Biol, 2017. **216**(9): p. 2911-2926.
322. Chen, Y., et al., *Retinoic acid signaling is essential for pancreas development and promotes endocrine at the expense of exocrine cell differentiation in Xenopus.* Dev Biol, 2004. **271**(1): p. 144-60.
323. Huang, W., et al., *Retinoic acid plays an evolutionarily conserved and biphasic role in pancreas development.* Dev Biol, 2014. **394**(1): p. 83-93.
324. Zertal-Zidani, S., A. Bounacer, and R. Scharfmann, *Regulation of pancreatic endocrine cell differentiation by sulphated proteoglycans.* Diabetologia, 2007. **50**(3): p. 585-95.
325. Dotti, C.G., R.G. Parton, and K. Simons, *Polarized sorting of glypiated proteins in hippocampal neurons.* Nature, 1991. **349**(6305): p. 158-61.
326. Matas-Rico, E., M. van Veen, and W.H. Moolenaar, *Neuronal differentiation through GPI-anchor cleavage.* Cell Cycle, 2017. **16**(5): p. 388-389.

Nederlandse samenvatting voor leken

Cel signalering, een land als metafoor

Om te begrijpen hoe het menselijk lichaam functioneert kan men een land als metafoor gebruiken. Een land is opgebouwd uit compleet verschillende en autonome steden die met elkaar moeten communiceren om als natie te kunnen functioneren. Deze communicatie verloopt via verschillende kanalen (o.a. snelweg, vliegtuig, trein en per schip) en kan zowel uitgaand als inkomend zijn. Externe communicatie wordt aan de stadsgrens gecontroleerd, opgenomen en doorgegeven via interne routes met als doel adequaat te reageren. Het hart van de stad, het stadhuis, heeft de blauwdruk van de stad en zorgt voor de continuïteit van haar infrastructuur. Wanneer een stad de communicatie met andere steden stopt, onstaat onbegrip wat uiteindelijk kan leiden tot oorlog en overname.

Hoewel vereenvoudigd, functioneert het menselijk lichaam vergelijkbaar. In deze vergelijking zijn de verschillende typen cellen, zoals steden, beschermd door een stadsgrens bestaande uit een fluïde lipide membraan. Cellen comuniceren met elkaar via verschillende externe signaalmoleculen (o.a. hormonen, neurotransmitters en groeifactoren) die worden opgevangen door receptoren (de stadspoorten) die het membraan overbruggen (transmembraaneiwitten). Via een opeenvolging van intracellulaire biochemische reacties geven deze receptoren signalen door die uitmonden in een respons, bijvoorbeeld het aflezen van genen of het aansturen van diezelfde transmembraaneiwitten. Vergelijkbaar met de expansie van een stad ten koste van een andere, kan een verstoring van celsignalering door mutaties zorgen voor een maligne cel met uiteindelijk een ongeremde groei als gevolg, de aanzet van kanker.

Het GPI anker

Naast transmembraan eiwitten bestaan er ook membraaneiwitten die, buiten de cel, verankerd zitten in het membraan (GPI-verankerde eiwitten). Door middel van een complexe moleculaire structuur, bestaande uit een lipide dat is verbonden door suikergroepen aan de C-terminus, blijft het eiwit verankerd in het membraan zonder deze te overbruggen. De functies van GPI-verankerde eiwitten lopen uiteen van die van enzymen (uPAR) tot die van celadhesie moleculen (NCAM) en het reguleren van het complementsysteem (CD55). Derhalve spelen GPI-verankerde eiwitten een fundamentele rol in allerlei (patho-)fysiologische processen in het lichaam en zijn ze noodzakelijk voor de ontwikkeling van een embryo. Juist omdat dit type eiwitten niet door het membraan steken is de functie en regulatie van een GPI-anker, vanuit dezelfde cel (celautonoom), lang een mysterie geweest. Een duidelijke aanwijzing voor een vorm van regulatie van deze eiwitten op het membraan, is de observatie van circulerende GPI-

verankerde eiwitten door het lichaam. In deze circulerende vorm is het GPI-anker niet meer aanwezig wat erop duidt dat de eiwitten van het membraan zijn geknipt. Enzymen die hiertoe in staat zijn hebben een duale rol en zorgen niet alleen voor depletie op het membraan (en de bijbehorende adaptatie van de cel) maar ook voor een potentieel circulerend signaalmolecuul. Hoewel verschillende enzymen geïdentificeerd zijn die GPI-verankerde eiwitten *in vitro* kunnen knippen, is de fysiologische relevantie van deze enzymen voor de productie van een circulerend eiwit tot nog toe onbekend.

In dit proefschrift wordt een familie van enzymen beschreven, glycerofosfodiester fosfodiesterases (GDEs of GDPDs) die een rol spelen in het knippen van GPI-verankerde eiwitten. Doormiddel van functionele en biochemische studies wordt het inzicht in de regulatie van GPI-verankerde eiwitten vergroot en draagt de verkregen kennis bij aan het begrijpen van bepaalde ziekteprocessen.

Dit proefschrift

Hoofdstuk 1 van dit proefschrift geeft een algemene inleiding over de synthese, structuur, lokalisatie en functie van GPI ankers en de daarmee verbonden eiwitten. Daarnaast worden enzymen met een vermeende GPIase activiteit besproken evenals de familie van GDPDs en de enzymatische activiteit zoals die tot nu toe, in de literatuur, bekend is.

In **Hoofdstuk 2** wordt GDE3, een specifiek GDPD familielid onderzocht. GDE3 knipt een GPI-verankerde eiwit genaamd uPAR van het membraan. uPAR is een receptor eiwit dat een belangrijke rol speelt in weefselregeneratie en wondheling, een proces dat vaak wordt gekaapt door kankercellen. Door uPAR expressie te verhogen, worden enzymen geactiveerd die de extracellulair matrix kunnen afbreken, met als gevolg dat kankercellen makkelijker migreren en metastaseren in omliggend gezond weefsel. Net als andere GPI-verankerde eiwitten wordt uPAR geknipt teruggevonden in de circulatie en omdat de expressie veelal hoger is in kankercellen, dient circulerend uPAR vaak als tumor marker. Hoewel veelvuldig gebruikt als marker, is het precieze mechanisme van uPAR afgifte aan de circulatie en de functie daarvan onbekend. In dit hoofdstuk laten we zien dat GDE3 en niet het nauw verwante GDE2, uPAR knipt van het membraan. We demonstreren dat GDE3 in de structuur van het GPI-anker knipt en identificeren GDE3 als het eerste GPI specifieke enzym dat knipt volgens het zogenoemde PLC mechanisme. Door uPAR op specifieke plaatsen van het membraan te knippen, verliest het zijn functie en wordt de signalering geremd. Hoge GDE3 expressie in borstkankercellen resulteert in minder maligniteit, waarschijnlijk doordat GDE3 uPAR van het membraan knipt. Daarnaast zorgt hoge GDE3 expressie voor een verminderde tumorgroei in een muismodel voor borstkanker en correleert het met een verlengde overleving in borstkanker patiënten.

Dit onderzoek laat niet alleen zien dat GDE3 tumorgroei onderdrukt maar demonstreert ook een nieuw mechanisme waarin extracellulair verankerd uPAR geknipt wordt door een transmembraan GPI-PLC specifiek enzym.

In **Hoofdstuk 3** wordt de rol van een ander GDPD familielid, GDE2, in neuroblastoma onderzocht. Omdat eerder onderzoek heeft laten zien dat GDE2 essentieel is voor de differentiatie van motorneuronen tijdens de embryonale ontwikkeling en in een later stadium voor neuronale overleving, hebben wij onderzocht wat de rol van GDE2 in neuroblastoma zou kunnen zijn. Neuroblastoma is een kinderkanker dat wordt gekenmerkt door een defecte neuronale differentiatie tijdens de embryonale ontwikkeling. Voor de behandeling van neuroblastoma wordt onder andere gebruik gemaakt van retinoic acid met als doel de cellen alsnog te laten differentieren. Helaas zijn deze behandelingen erg gelimiteerd en de resultaten teleurstellend. Een beter begrip van deze ziekte en neuronale differentiatie in het algemeen is daarom vereist. In hoofdstuk 3 laten wij zien dat GDE2 neuroblastoma cellen aanzet tot differentiëren. Door gebruik te maken van verschillende *in vitro* technieken demonstreren wij dat GDE2 zorgt voor een verhoogde neuriet uitgroei, een proces dat gepaard gaat met de activatie en inhibitie van intracellulaire signaleringsroutes, Rac en Rho respectievelijk. In lijn met deze *in vitro* data, kan in neuroblastoma patienten, GDE2 worden gebruikt als prognostische marker voor een beter ziekteverloop. Mechanistisch hebben wij gevonden dat GDE2 specifiek het GPI-verankerde eiwit Glypican 6 van het membraan knipt en zodoende cellen aanzet tot differentieren. Omdat het eiwit Glypican 6 zelf niet goed onderzocht is weten we nog niet precies hoe Glypican 6, dat aan de buitenkant van de cell verankerd zit, cel differentiatie van binnenuit de cel reguleert. Waarschijnlijk spelen andere, nog onbekende transmembraan co-receptoren hier een rol en verder onderzoek zou dit moeten uitwijzen. Afrondend demonstreert ons werk een nieuwe signaleringsroute waarbij het knippen van een extracellulair eiwit zorgt voor neuroblastoma differentiatie, door een cel-autonoom mechanisme.

Omdat meerdere GPI-verankerde eiwitten een belangrijke rol spelen in neuronale differentiatie en omdat veel van deze eiwitten worden teruggevonden in de circulatie, is een bredere rol voor GDE's niet uitgesloten. In **Addendum Hoofdstuk 3** wordt de mogelijke rol van GDE2 en het bijbehorende knippen van GPI-verankerde eiwitten tijdens neuronale differentiatie besproken.

GDE2 komt niet uitsluitend in neuronale cellen tot expressie en zou daarom ook andere fysiologische functies kunnen vervullen. Om deze potentiële functies tijdens de embryonale ontwikkeling te onderzoeken hebben we gebruik gemaakt van het modelorganisme *Danio Rerio* (zebravis). Er zijn vele redenen waarom juist dit organisme veelvuldig wordt gebruikt in

ontwikkelingsstudies; zebravissen leggen 300 eieren en de embryonale ontwikkeling verloopt snel en vindt buiten de moeder plaats. Misschien wel de belangrijkste reden is dat de embryo's doorzichtig zijn, waardoor het ontwikkelingsproces non-invasief gevolgd kan worden. In **Hoofdstuk 4** identificeren we de zebravis-ortholoog van humaan GDE2 en analyseren we de rol tijdens de embryonale ontwikkeling. Zebravis embryo's waarin de expressie van GDE2 is onderdrukt door specifieke morpholino's (MO's), vertonen afwijkingen in motiliteit en pancreas differentiatie. Evenals muismodellen gebruikt in eerder onderzoek, hebben GDE2-deficiënte zebravissen (motor) neuronale afwijkingen, zoals een korter en gebogen lichaam dat met moeite uit het ei breekt. Nieuw is echter dat GDE2 depletie ook zorgt voor specifieke defecten aan het hart en de pancreas. Kleuringen voor insuline en trypsine, die de exocrine cellen van de pancreas markeren, zijn gereduceerd in GDE2 deficiënte MO's. Aan de andere kant zorgt geforceerde overexpressie van humaan GDE2 ook voor malformaties van de lichaamsas evenals vasculaire en hartdefecten. Uit dit onderzoek blijkt dat de rol van GDE2 ook in lagere organismen functioneel geconserveerd is en dat de zebravis een goed model is gebleken voor ontwikkelingsstudies naar GDE2. Verder onderzoek zal moeten uitwijzen wat de exacte rol van GDE2 tijdens de ontwikkeling van de pancreas is en welke GPI-verankerde eiwitten hierbij een rol spelen.

Tot slot hebben wij GDE2 en GDE3 met elkaar vergeleken, de resultaten hiervan staan beschreven in **Hoofdstuk 5**. In eerdere hoofdstukken hebben we laten zien dat zowel GDE2 als GDE3 de GPI-anker van Glypican 6 hydrolyseren. Daarmee karakteriseren wij beide enzymen als GPI specifiek. Wij laten echter ook zien dat alleen GDE3 en niet het nauw verwante GDE2, uPAR knipt. Dit is verassend omdat deze familie van enzymen hiermee specificiteit vertoont voor verschillende GPI-verankerde eiwitten. Met andere woorden, modificaties van het GPI-anker of het verbonden eiwit dragen bij aan de substraatherkenning van GDE's. In dit hoofdstuk demonstreren wij dat beide enzymen co-lokaliseren in dezelfde membraandomeinen, maar dat alleen GDE2 aanwezig is in intracellulaire vesicles. GDE2 wordt dus op andere wijze gereguleerd maar de substraat specificiteit wordt daar niet door bepaald. Door het ecto-domein van GDE2 te vervangen met dat van GDE3 verandert de specificiteit maar niet de lokalisatie. Andersom verandert de lokalisatie maar niet de specificiteit door het uitwisselen van de N-terminus. GDE2 glycosylering speelt hierbij geen rol. Omdat modificaties in het GPI-anker de substraat specificiteit zou kunnen bepalen, hebben wij de GPI-ankers van uPAR en Glypican 6 uitgewisseld en getest op GDE activiteit. Verassend genoeg had dit geen effect waaruit wij concluderen dat behalve het GPI-anker ook het eiwit van belang is in substraatherkenning door GDE's.

In de algemene discussie, **Hoofdstuk 6**, plaatsen we onze bevindingen in een bredere context en proberen we de rol en functie van de familie van GDE's te duiden.

Curriculum Vitae

Michiel van Veen was born on September 10th 1985 in Amsterdam, The Netherlands. In 2004 he completed his secondary education at the Willem Lodewijk Gymnasium in Groningen. In the same year, he started his bachelor Life Science and Technology at the University of Groningen. During his first internship at the Pathology department, University Medical Centre Groningen under the supervision of dr. Lydia Visser, he worked on setting up a high throughput calcium measurement protocol to test leukocyte activation. After finishing his bachelor, he enrolled in the Medical Pharmaceutical Science master programme. During his first 9-month research training in the laboratory of Prof dr Ody Sibon and Prof dr Harry van Goor at the Cell Biology department of the University Medical Centre Groningen, he studied the protective effects of hydrogen sulfide on a drosophila animal model with increased oxidative stress. He performed his second master internship in the laboratory of dr. Ben Giepmans, Groningen university and Prof. dr. Moolenaar, Netherlands Cancer Institute in Amsterdam where he started to work on the recently identified enzyme GDE2 and its role in neuroblastoma differentiation. In 2011, Michiel obtained his Master of Science degree and continued his research on the GDE family of proteins as a PhD student in the laboratory of Prof dr Moolenaar at the Division of Cell Biology. The project was funded by a NWO top grant and the results of his research are described in this thesis.

List of Publications

Van Veen M[&]., Matas-Rico E[&]., Van de Wetering K., Leyton-Puig D., Kedziora KM., De Lorenzi V., Bultsma Y., Van den Broek B., Jalink K., Sidenius N., Perrakis A., Moolenaar WH. *Negative regulation of urokinase receptor activity by a GPI-specific phospholipase C in breast cancer cells.* eLife 2017;6:e23649

Van Veen M[&], Mans L.[&], Matas-Rico E., Van Pelt J., Perrakis A., Moolenaar WH, Haramis A. *Glycerophosphodiesterase GDE2/GDPD5 affects pancreas differentiation in zebrafish.* Int J Biochem Cell Biol. 2018; 94:71-78.

Matas-Rico E., **Van Veen M.**, Moolenaar WH. *GDE2/GDPD5 in neuroblastoma.* Oncotarget 2017;8:5672–5673.

Matas-Rico E., **Van Veen M.**, Moolenaar WH. *Neuronal differentiation through GPI-anchor cleavage*. Cell Cycle 2017;16:388-389.

Matas-Rico E, **Van Veen M**, Leyton-Puig D, Van den Berg J, Koster J, Kedziora KM, Molenaar B, Weerts MJ, De Rink I, Medema RH, Giepmans BN, Perrakis A, Jalink K, Versteeg R, Moolenaar WH. *Glycerophosphodiesterase GDE2 promotes neuroblastoma differentiation through glypican release and is a marker of clinical outcome*. Cancer Cell 2016;30:548-562.

[&] These authors contributed equally

Acknowledgments

I wish to express my gratitude to all those who contributed to this thesis.
Mijn dank gaat uit naar allen die hebben bijgedragen aan de totstandkoming van dit proefschrift